Shear Flow Visualization at High Reynolds Numbers

by

Danielle Ames

Submitted to the Department of Ocean Engineering
in partial fulfillment of the requirements for the degree of

Master of Science in Ocean Engineering

at the

MASSACHUSETTS INSTITUTE OF TECHNOLOGY

June 1998

Author .....
Department of Ocean Engineering
May 8, 1998

Certified by .....
Michael S. Triantafyllou
Professor of Ocean Engineering
Thesis Supervisor

Accepted by .....
J. Kim Vandiver
Chairman, Department Committee on Graduate Students

Shear Flow Visualization at High Reynolds Numbers

by

Danielle Ames

Submitted to the Department of Ocean Engineering
on May 8, 1998, in partial fulfillment of the
requirements for the degree of
Master of Science in Ocean Engineering

Abstract

The mechanisms responsible for various disturbances in the wakes of ships have been investigated for some time. Efforts to define and characterize the contributing factors and resulting turbulent wake manifestations conclude that ship length, speed and geometry play integral and interdependant roles. Previous experimentation in the Ocean Engineering Towing Tank at MIT on small scale model ships supplied data for Reynold's Numbers upto $\sim$ O(10^6). The work included in this thesis represents a continuation of those efforts up to $\mathcal{R}e$ O(10^7) using a model DDG51 (5514) Destroyer. Through endeavors to identify wake phenomena and closely examine possible sources, previously unvisualized charicteristics were revealed and the calibration, comparison and validation of numerical simulations were made possible. Experimental efforts were concentrated on the study of flow in the wake and near the bow of the model DDG-51 Destroyer (5514). Qualitative and quantitative flow visualization methods were adapted, designed and implimented including ship-fixed and tank fixed streak videography and Digital Particle Image Velocimetry (DPIV). In addition, the experimental apparatus was modified for similar flow visualization near live fish, and a description of this endeavor and its progress are included.

Thesis Supervisor: Michael S. Triantafyllou
Title: Professor of Ocean Engineering

Acknowledgments

I would like to pay sincere gratitude to my advisors Michael S. Triantafyllou and Dick K.P. Yue who offered the support and guidance that made this project possible, and the freedom that made it truly valuable. In addition, my appreciation for the faith and friendship of Dr. Thomas Consi cannot compare with the debt that he is owed. He has been both a mentor and confrere, who helped carve my path through MIT and make it amusing and enlightening.

Additional thanks go to Leonard Imas, Kelli Hendrickson, Alexandra Techet, Ryan Cleary, Drew Mutch, Franz Hover, Wade McGillis, and all my cohorts in the Vorticle Flow Research Laboratory and Ocean Engineering Towing Tank, for teaching me what I did not know, helping fix what I broke, understanding my evolving plans, and making this crazy place colorful.

I am grateful to my parents and grandmother for their love and support and to all the friends who know how I love a good party and that I'm only a little bit crazy.

Finally, no sucess would be possible or fullfilling without the love, support and encouragement of Meldon Wolfgang. I cherish his understanding and confidence through these personal and academic challenges and look forward to putting MIT behind us both and a lifetime happiness.

Contents

List of Figures

List of Tables

Chapter 1

Introduction

Flow visualization is a complex and multi-disciplinary experimental technique used to build an understanding of the flow near or in the wake of a solid body. It can be used to prove the existence of theoretical phenomena or to closely examine specific features complex flows. A multitude of flow visualization techniques have been implemented for applications in physics, aeronautics, mechanics, architecture and ocean engineering. Implementation, however, is complicated by the difficulty of examining a flow without disturbing it.

Relatively unintrusive methods of visualization involve seeding the flow with highly visible, neutrally buoyant particles. The presence of such particles has been shown to contribute negligibly to the motion of the fluid. [16] A seeded flow can subsequently be imaged through various means to extract qualitative and/or qualitative data. Imaging methods include qualitative streak photography and quantitative particle tracking methods.

Streak imagery involves the illumination of a single plane of particles exposed over for enough time to show streak-lines of particle paths. Velocities are determined from the length of the streaks, but the direction of particle travel is uncertain, particularly in complex or rotating flows. Although the extraction of quantitative data from these methods is possible, it can be tedious and uncertain. Streak photography methods are therefore generally used to gain qualitative illustration of fluid motion. Furthermore, sequences of streak photographs lend directional and evolutional information to this

technique in sufficiently slow flows.

Digital photography and videography have made quantitative visualization simpler through the use of image processing techniques. Successive images of a particle field can be digitally characterized and compared to determine displacement and subsequent fluid dynamical properties with a high degree of accuracy. The directional uncertainties characteristic of double exposed images and traditional Particle Image Velocimetry (PIV) techniques, are averted with digital methods and resolution and processing times are continuously improved with updates in technology.

Digital Particle Image Velocimetry (DPIV) [3] has been used extensively in the Department of Ocean Engineering at MIT for a variety of experimental applications with a high rate of success. This quantitative flow visualization method is comprised of two steps; (1) sequential imaging of a single plane of particles in the flow and (2) Digital processing of successive images using the DPIV algorithm.

The DPIV algorithm divides the particle field in to smaller windows of pixels which are then characterized by their fast-Fourier transform. The next image in sequence is then searched for the pixel window which correlates best with the first FFT. The distance from the first pixel window to its 'closest match' in the second image is the displacement of the particles contained in that window, and the process is repeated until a complete grid of displacements has been determined for the image pair.

Accurate DPIV analysis of a flow depends upon careful experimental techniques. Any background noise or streaked particle images will compromise the certainty of DPIV calculations. This makes DPIV difficult to implement near the surface and close to objects. Complexities in DPIV implementation also arise from the delicacy and expense of necessary equipment. For these reasons, qualitative methods remain valuable in the investigation of many flow fields.

1.1 The Focus of this Thesis

This thesis explores select extensions and limitations of the DPIV method in the visualization of shear flow at relatively high Reynolds Number, as well as modifications

to this technique for visualization near live fish. The work included herein represents an extension of previous work at MIT in the nature of ship wake turbulence and fish swimming. Extensive theoretic study and numerical simulations including Direct Numerical Simulation (DNS) and Large Eddy Simulation (LES) are complimented by these experiments.

The majority of this thesis will discuss experimental visualization of the flow in the wake and near the bow of a DDG-51 model destroyer hull (model #5514). Previous, low Reynolds Number ship wake experiments focused on small scale model hulls 0.5m and 1.75m in length. The study of the DDG51 model (3m) extends our data and capabilities in these areas and also exhibits interesting characteristics specific to the geometry of the ship.

The work in this thesis compliments previous hull studies in the compilation of an empirical data-set spanning a range of Reynolds Numbers from $\sim 10^4$ to $\sim 10^7$ and proving invaluable for numeric and theoretic comparisons. In addition, near-hull flows were studied using qualitative flow visualization techniques and compared to theoretical and computational models.

These empirical studies serve to:

- **Test theory**

  Through these DPIV experiments we tested the method of flow visualization as well as the existing hydrodynamic understanding of wake features.

- **Introduce the existence of new phenomena**

  Wake features such meandering and the 'double wake' were evidenced in these tests.

- **Compare, calibrate and validate numerical simulations (DNS/LES)**

  The DPIV experiments were conducted at the MIT Towing tank and performed in conjunction with DNS and LES computational methods implemented in the Vorticle Flow Research Laboratory at MIT.

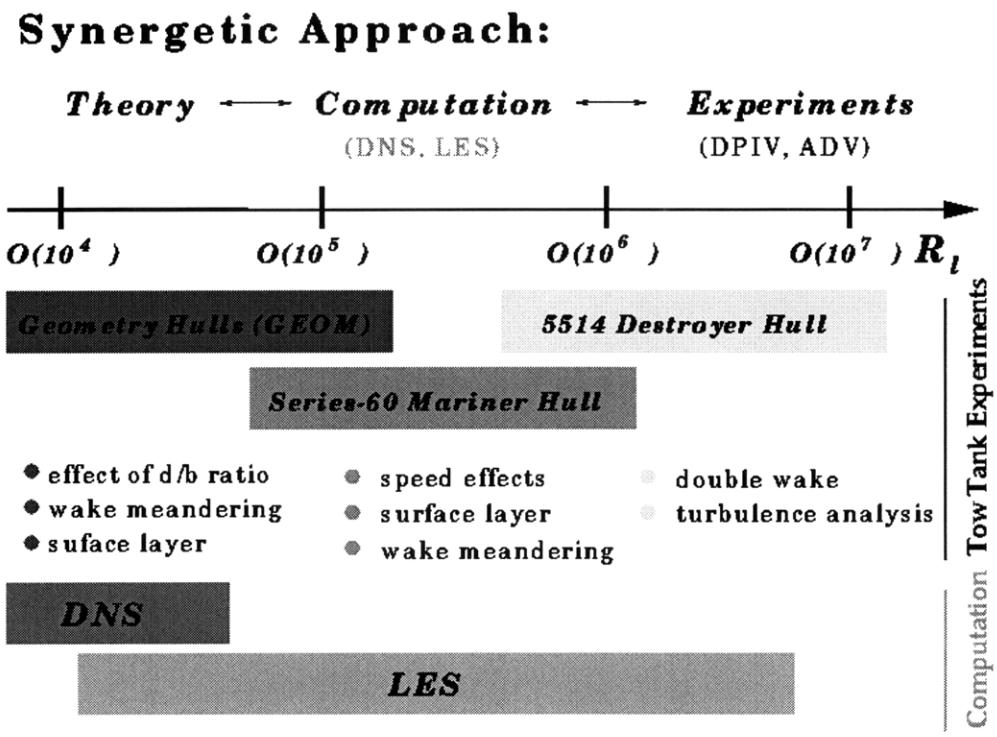

Figure 1-1: Schematic of relationship between experiment, theory and computation

1.2 This Paper

The following chapters will illustrate flow visualization experimentation, (including background, procedure and results) on the 5514 as well as select technical modifications to the method to facilitate live fish flow visualization. Chapter 2 will present an overview of prior model ship studies including select DPIV "wake mapping" experiments". Chapter 3 will discuss the DPIV experimental technique implemented in preliminary "wake mapping" of the 5514 model. Chapter 4 will present the improved DPIV apparatus and follow-up experiments to the initial wake mapping. Chapter 5 describes alternate flow visualization techniques implemented on the 5414 as well as cross-sectional DPIV images which were taken just behind the stern of the moving ship. Finally, Chapter 6 is a discussion of similar flow visualizations and necessary modifications for applications involving live fish.

Chapter 2

DPIV Wake Mapping at Low Reynolds Numbers

2.1 Background on Method and Hulls

Seeded flow methods of visualization such as Particle Image Velocimtry (PIV), DPIV and Particle Tracking Velocimetry (PTV) infer the motion of the fluid from the displacement of suspended particles. In DPIV, a single plane of particles is illuminated using a laser and line generating optics which is imaged by a camera positioned perpendicular to the plane. A sequence of images is recorded and image pairs are then digitally processed to return displacement, velocity and vorticity data.

The mapping of the wake of a model ship is accomplished by towing the hull past the field of view of the camera and then imaging and analyzing a sequence of frames. Initial tests were performed by Sean McKenna [14] on three simple geometry hulls to investigate the dependence of Draft/Beam ratio on wake turbulence. The length (L), beam (b), draft (d) and draft-to-beam ratio (d/b) of the models are listed in the following table. As shown in Figure 2-1, the three different geometries produced noticeably different wakes.

McKenna's results [14] show that Hull 1 (d/b=0.17) produced a narrow wake region on the order of 1-2 ship beams in breadth. As expected, the vortical regions on either side of the wake spun in opposite directions. Farther aft in the wake region the

hull	L (cm)	b (cm)	d (cm)	d/b
hull 1	50	4.0	0.67	0.17
hull 2	50	4.0	2.0	0.5
hull 3	50	2.0	2.0	1

Table 2.1: Dimensions of Small Hulls

flow was much less active. Fewer eddies were present, and their strength attenuated significantly. The far wake region was made up of a small number of turbulent structures which were marginally noticeable and, in general, not well defined.

The wake formed by the Hull 2 model was somewhat more energetic and spread out more drastically downstream. The width of the wake ranged from approximately 2 ship beams (near wake) to 4 ship beams (far wake), and vortical structures of larger diameter (on the order of 1 beam) were located in the wake of Hull 2. Similar to Hull 1, the wake intensity attenuated downstream where vorticies became less defined and frequent.

The most prominent feature in the Hull 3 wake was the significant amount of wake meandering present at all downstream locations. The wake width spanned a range of 4 beams (near wake) to approximately 8 beams (far wake), and as with the other two hulls, the intensity of the Hull 3 wake fell off with distance downstream.

General trends present for all three hull models included higher wake energy near the ship stern. Later in the wake, turbulent structures weakened and diffused, leaving only a few coherent areas of vorticity. These experiments indicated an increase in wake intensity for hulls of deeper draft, and increase in wake meandering with wider beam.

2.2 Dense Volume Whole Field Wake Mapping

Further tests were performed to characterize the full volume of the wake of Hull 2 [23] . Again, the model was towed past the field of view of the camera and the wake imaged perpendicularly. Tests were run with the laser plane oriented horizontally in the wake as well as vertically (perpendicular to the free-surface) at multiple depths

at multiple locations across the beam of the model. The compilation of these runs created a "dense-volume" profile (See Figure 2-2) of the wake. This "dense-volume wake mapping" technique was implemented on both Hull 2 of the small (0.5m) scale model hulls and a larger (1.75m) scale model Mariner Series 60 hull in the MIT Towing Tank.

The tow speed was left constant for all runs in the dense volume tests. Only the position and orientation of the laser plane were altered. The experimental results were used to quantify wake features and for comparison and validation of numerical simulations. In the range of $\mathcal{R}e \sim O(10^5)$, these results compared remarkably well to corresponding LES and DNS simulations.

The "wake meandering" feature uncovered in the first set of tests was more carefully examined in these results. This phenomena was pursued quantitatively using velocity data from the experiments. Figure 2-3 shows results for Hull 2 d/b=1 at a speed of 19.05 cm/s. Plotted here is the streamwise velocity, u*, across the wake for three downstream locations aft of the ship. The streamwise velocity is non-dimensionalized by the maximum u in the nearby wake field. Examining the three curves, it can be seen that at the station nearest the stern, the wake activity is roughly centered about the ship longitudinal axis. At the second station, the wake motion appears to have shifted to the port side of the ship. Finally, at the last station, the wake seems to have migrated back across the ship stern to starboard. This appears to confirm the observations of wake meandering in the flow visualization studies.

The wake of the small hulls is dominated by large-scale and persistent coherent structures which meandered in the streamwise direction (this co-incidentally corresponds with the numerical simulations). Figure 2-4 illustrates this meandering in contour plots of streamwise velocity u at three DPIV data stations away from the ship.

To continue the wake mapping through R_e $O(10^6)$, subsequent DPIV tests were performed on a Mariner Series 60 model hull, and similar results were found. Dense Volume wake mapping experiments revealed a meandering wake with similar variations with depth and tow speed, behind this model as well.

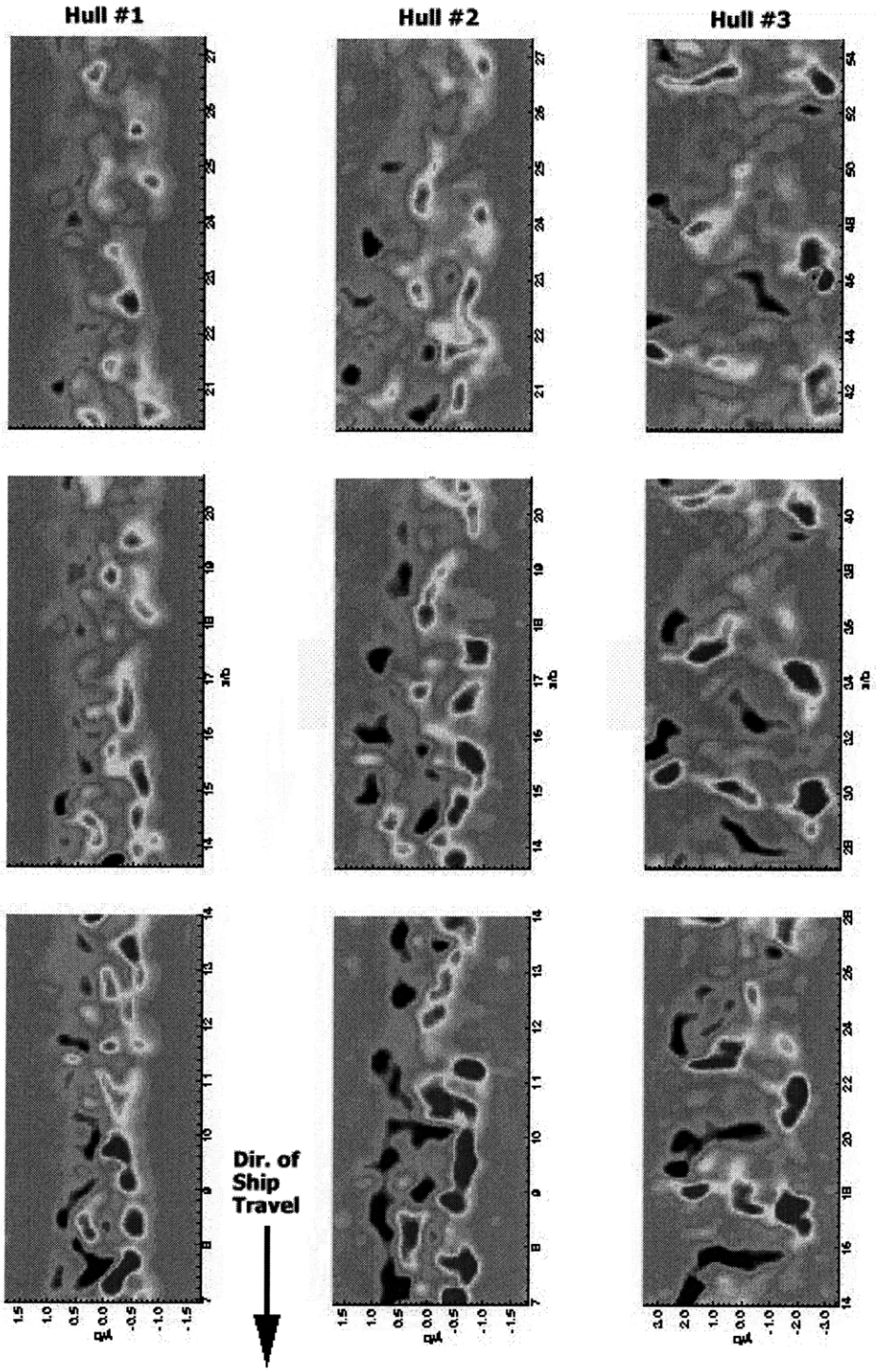

Figure 2-1: DPIV vorticity wake mapping of three hull geometries at u=190mm/s

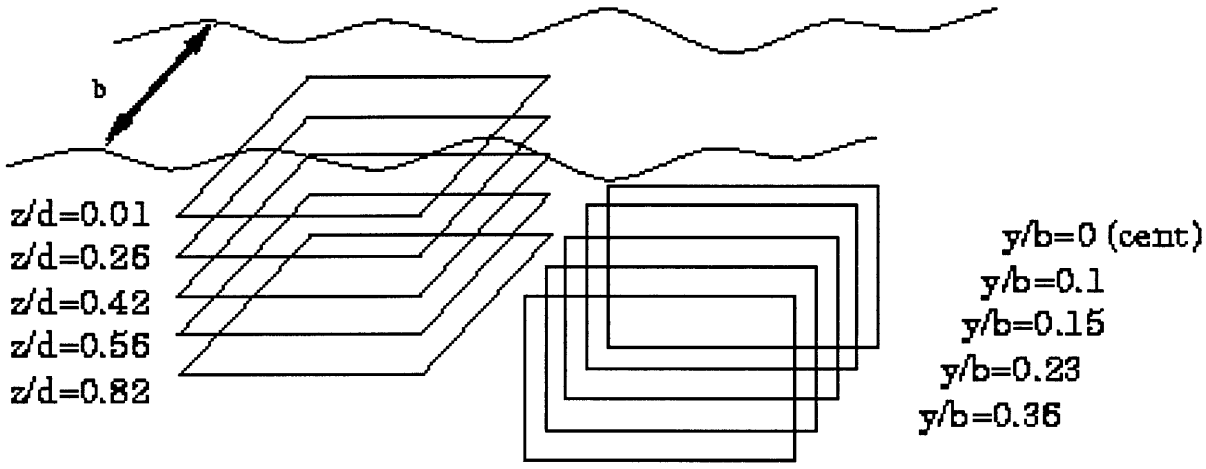

Figure 2-2: Dense-Volume, Whole field flow mapping as performed on Small hull and Mariner Models

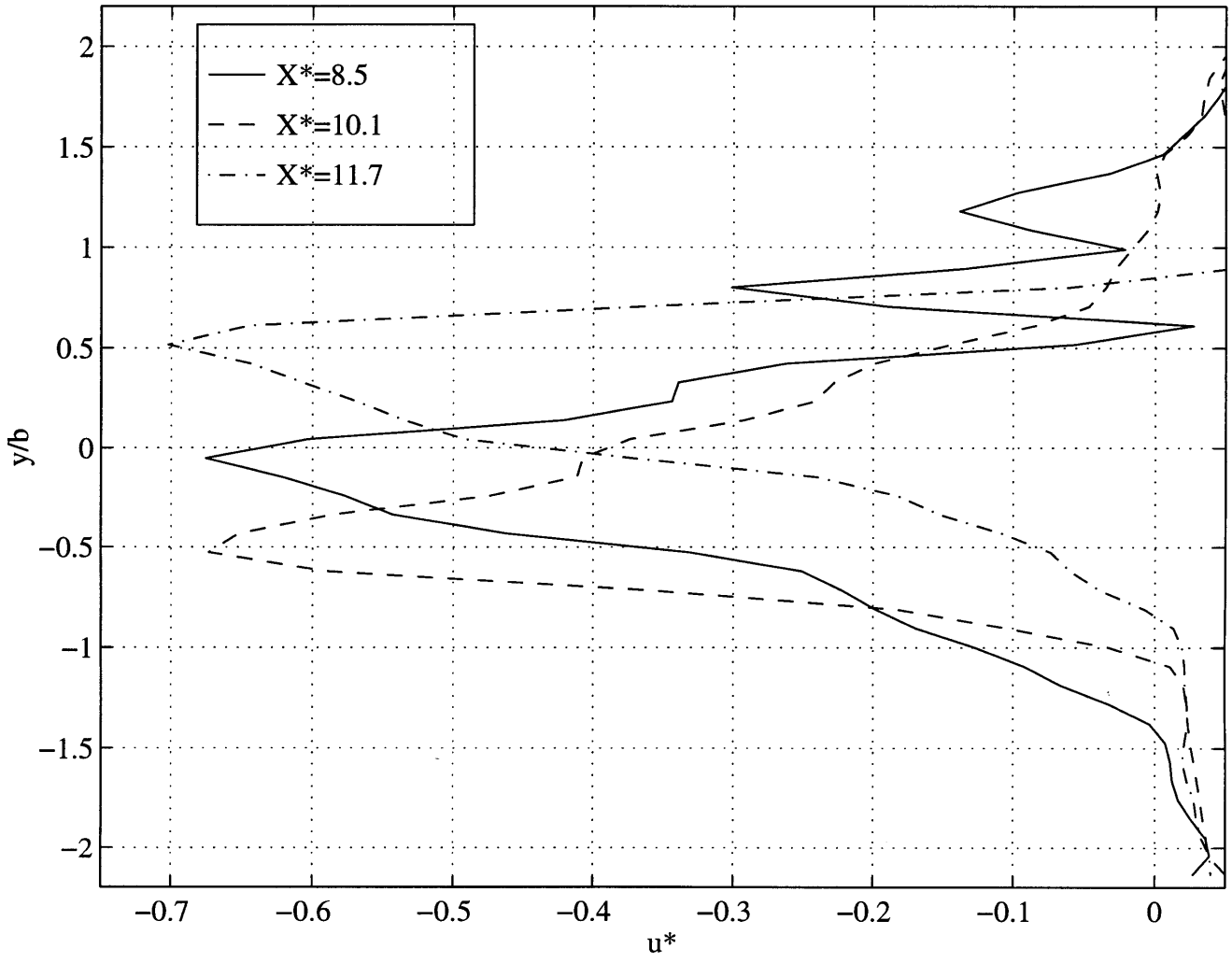

Figure 2-3: Streamwise Velocity as a function of wake location

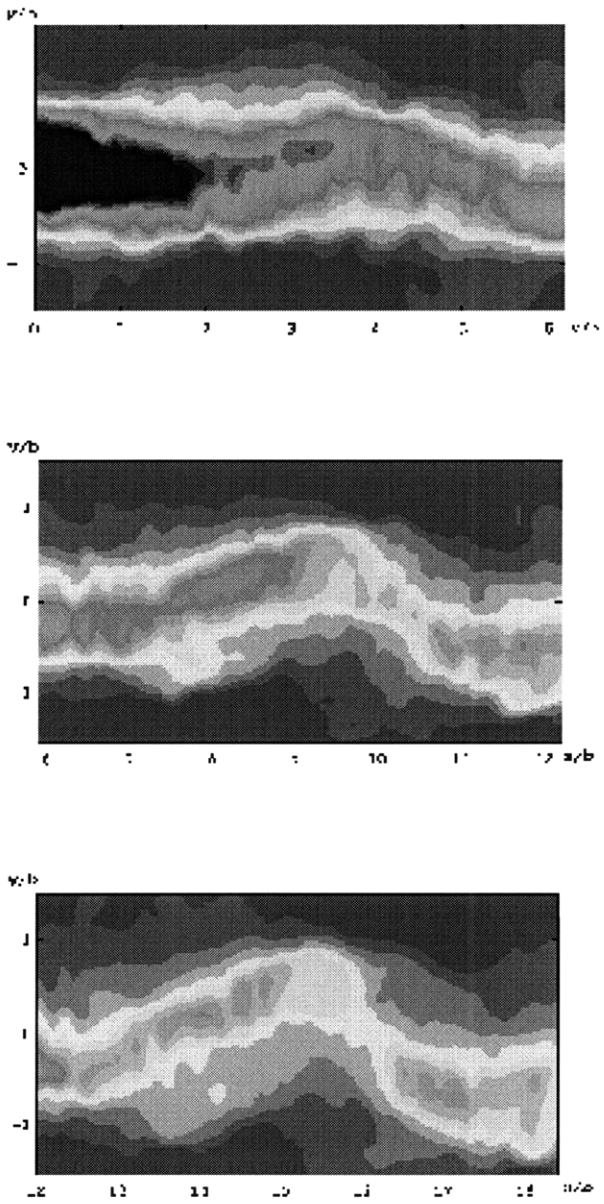

Figure 2-4: Streamwise velocity contours at three locations downstream

Chapter 3

Wake Mapping of the 5514

The model 5514 is a 3m scale model of the 505ft DDG-51, *Arleigh Burke* Class destroyer. The full scale model weighs approximately 8500 tons and is capable of speeds in excess of 30knots. Figure 3-1 is a photograph of the full-scale *USS Curtis Wilbur* (DDG-54).

Figure 3-1: Photograph of DDG-54 *(USS Curtis Wilbur)* from the Pacific Fleet web page

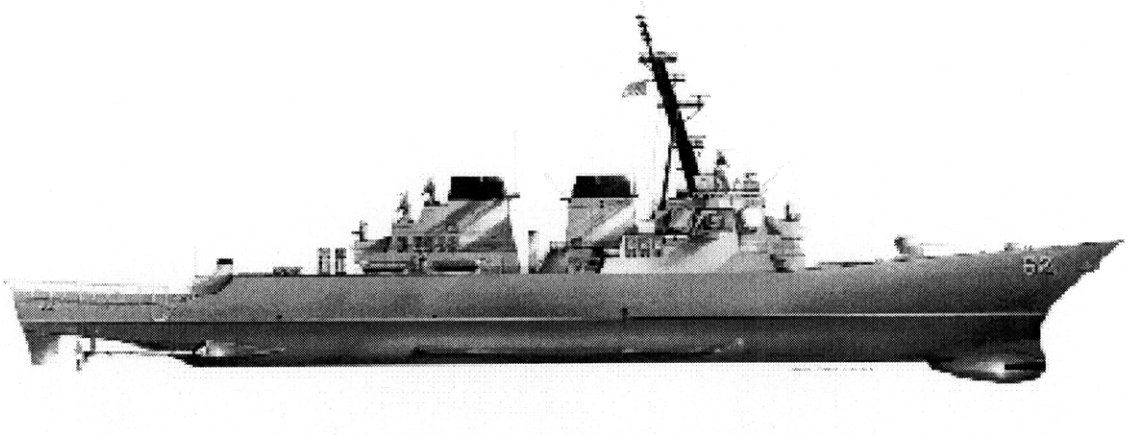

Figure 3-2: Rendition of the USS Fitzgerald (DDG-62) taken from www.surfpac.navy.mil

The DDG51 is unique in its design due to its bow mounted radar bulb. This large projecting bulb contributes interesting manifestations in the wake behind the ship. Figure 3-2 is a rendition of the *USS Fitzgerald* (DDG-62) and Figure 3-3 shows the 3 meter fiberglass scale model (5514) mounted on the towing carriage in the Ocean Engineering Towing Tank for flow visualization experiments.

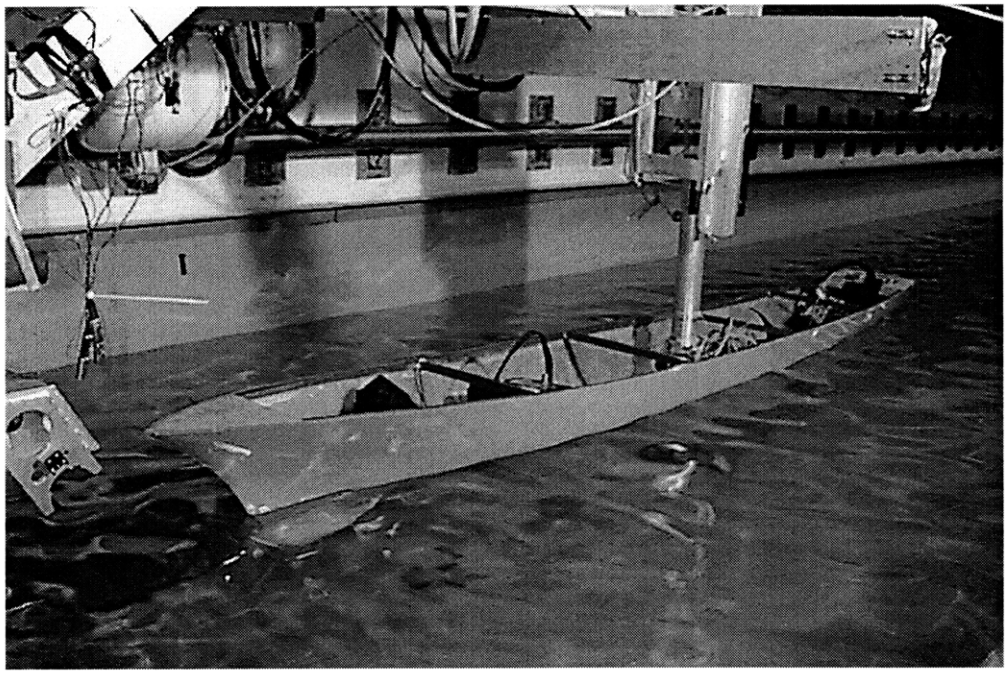

Figure 3-3: Model 5514 mounted to carriage in MIT Towing Tank

Wake mapping of the 5514 model extended the empirically mapped ship wake

data-set (from earlier work) into the range of $\mathcal{R}e\ O(10^7)$. In addition to exhibiting the meandering and surface layer phenomena associated with the simple geometry and Mariner Hulls, DPIV mapping of the DDG-51 revealed a novel and interesting "double wake" feature.

3.1 Experimental Methods

The wake study of the 5514 was performed in the MIT Ocean Engineering Towing Tank and was used to support numerical and theoretical analysis of similar flows. Digital Particle Image Velocimetry (DPIV) techniques were used to gain quantitative wake profiles at various towspeeds and depths.

3.1.1 DPIV Processing

The DPIV algorithm generates a vector field of displacements from a pair of sequential flow images and depends on crisp particle images (no streaking) and low background noise. The algorithm essentially divides the first image in a pair into small (e.g. 32x32 pixels) "processing windows", and characterizes the scattering of particles in a particular window by its Fast-Fourier Transform (FFT). The successive image is then interrogated to find the processing window's "closest match" using a cross-correlation function and Gaussian peak finding. (See Figure 3-4) The difference in position of the first window and its "closest match" is considered the average displacement of the particles contained therein. The processing window in the first image is successively stepped in both dimensions and the cross-correlation function repeated until the entire area of the images has been processed, a field of displacement vectors complete.

To assure accurate cross-correlations, camera position must be such that a single particle can be imaged by 2-3 pixels across its diameter. In addition, Willert and Gharib [22] determined that optimal seeding density occurs when 10-20 particles are imaged in each processing window.

Noise can be introduced to the data through any difference in appearance of particles and background from the first image to the second. In other words, if

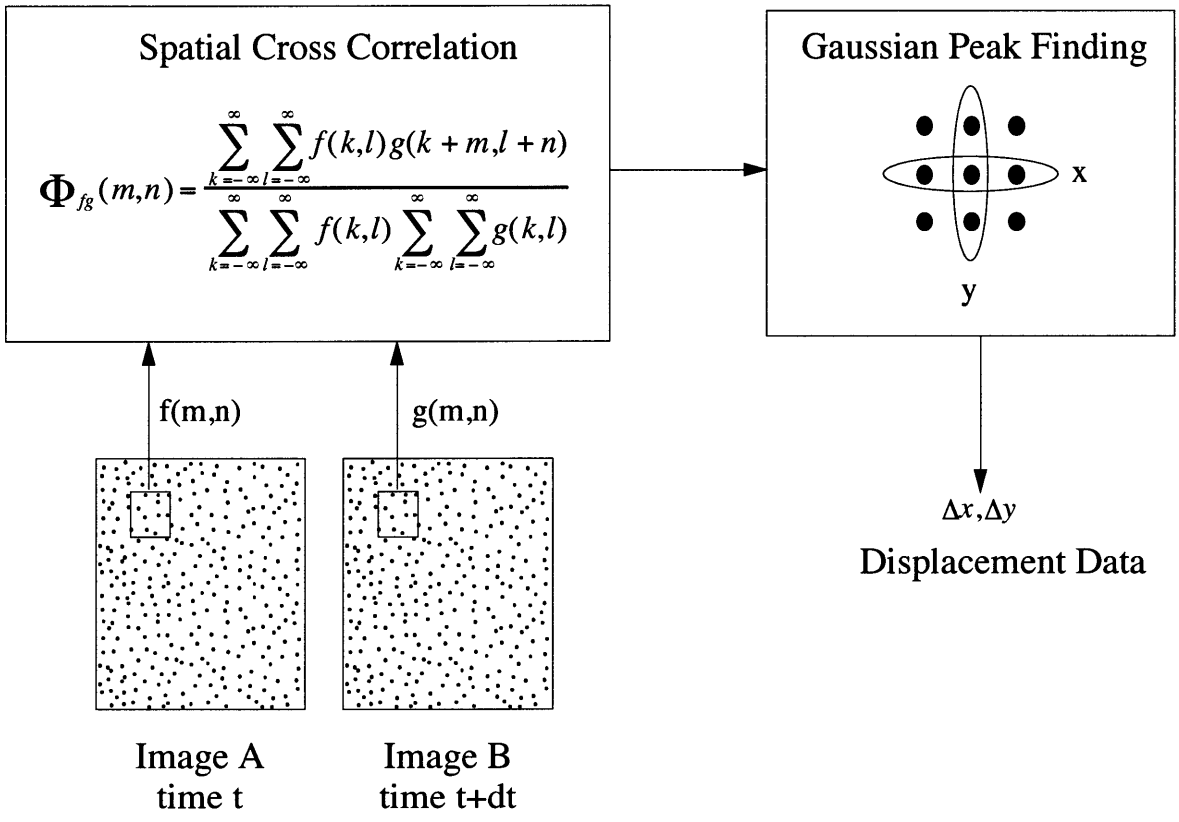

Figure 3-4: Diagram of DPIV processing algorithm

the particles in an interrogation window in Image 1 look different in Image 2, the algorithm will not likely correlate the two windows and therefore return inaccurate displacements.

Sources of error can include:

- Particles leaving or entering the plane or interrogation window.
- Relative particle displacements within the interrogation window.
- Streaking of particle images.
- Inconsistent background images and intensity gradients in the laser plane.

The time difference between images in an image pair, and interrogation window size are optimized to reduce the possibility of relative particle motion. The laser plane and camera are positioned such that the primary motion of the fluid is within the plane. Thus reducing the likelihood of a particle appearing in the first image and not in the second. Background inconsistencies, and illumination gradients in the images, however, are difficult to remove and can significantly degrade DPIV accuracy.

Reflections cause potential problems with processing as they alter the background of images from frame to frame. For instance, if a cluster of particles in an interrogation window in Image 1 moves from a region with a black background to a region in Image 2 in which there is a reflection from the ceiling, the DPIV algorithm is less likely to find accurate displacements from cross-correlation. Any inconsistencies in image background (including intensity fluctuations) from image to image or from interrogation window to interrogation window, introduce error into the processing algorithm. Data filters can be used to suppress these artifacts, but optical filters are a more reliable alternative. It is difficult, however to find a filter that eliminates background noise without also reducing the brightness of the particles.

3.1.2 Tow Tank Set-Up

The experimental set-up for DPIV testing of the model 5514 consisted of the following:

- A 6W Argon-ion laser (λ=488nm)
- A high-resolution Texas Instruments MC-1134p camera with stationary mount
- Fluorescent dye-injected polystyrene particles with absorption peak at 510 nm and emission peak at 560nm
- A Sony LVR-5000A/LVS-5000A video disk recorder with media
- An IBM compatible 486PC with DPIV software for frame-by-frame analysis

Neutrally buoyant, fluorescent particles were used to seed the flow, and a 2-D plane of illumination was created using the argon laser and lensed fiber optic cable. This plane was then reflected off a 45^o angled mirror and imaged from the side of the tank with the CCD camera. These images were stored on laser disk and later digitized and processed using the DPIV software. Figure 3-5 is a diagram of the experimental set-up and Figure 3-6 for a schematic representation of the DPIV Method.

3.1.3 Timing

Similar to photographic imaging, a CCD image is formed during the entire period over which the apparature is left open. At video rate, the equivalent shutter speed is $\sim$1/30s. To obtain crisp particle images, the argon laser was mechanically shuttered within each video frame. This produced the same effect as strobing or shuttering the camera. The time during which the shutter was open was optimized such that sufficient energy exposed the particles while minimizing streaking. The time between shutter releases was adjusted so that particle displacements fell within the measurable range of the DPIV algorithm. According to Willert and Gharib [22], this time separation should be such that particle displacement are at least twice the step size between sampling regions and no more that half the window size. Simillarly, J. Anderson [4], states that the time separation between images should be adjusted to maximize the displacement of particles. Increasing the time difference, however, increases the probability of particles leaving or entering the interrogation window

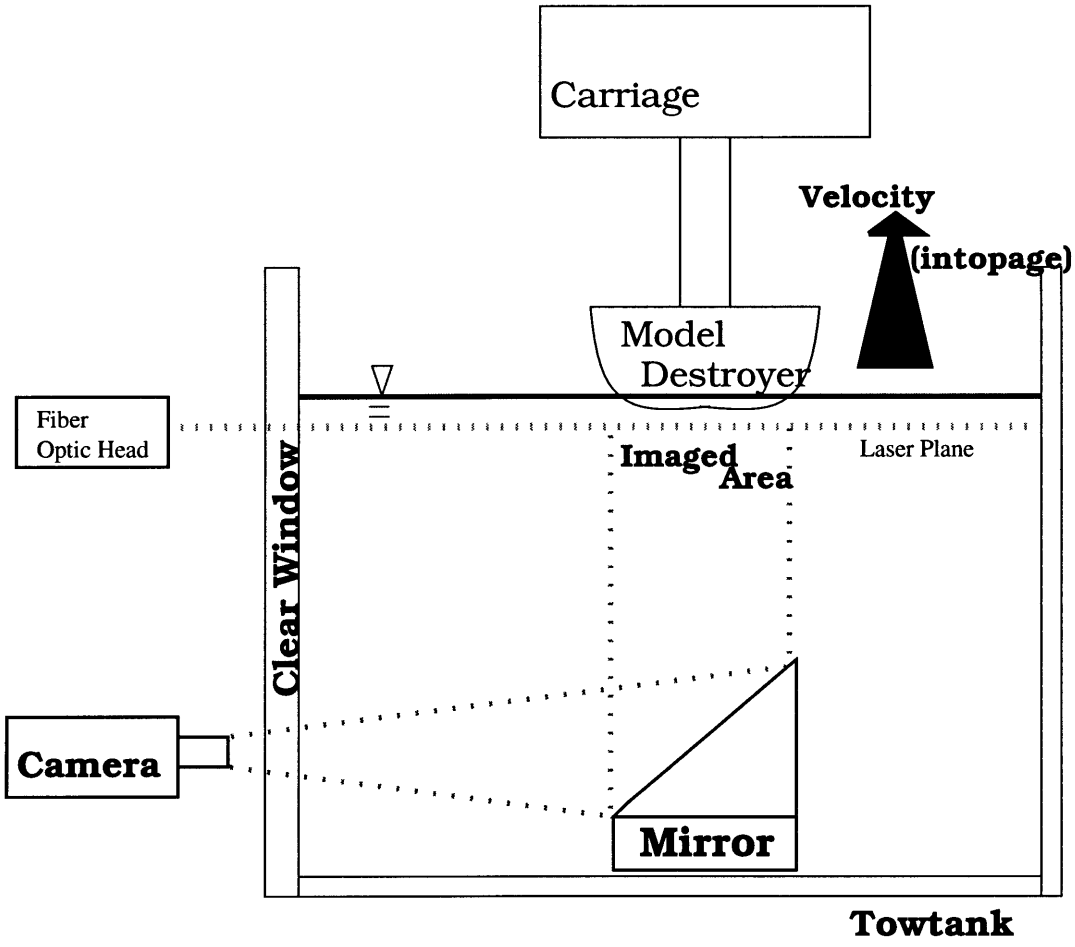

Figure 3-5: Diagram of the 5514 mounted on the towing carriage and towed past the plane of illumination

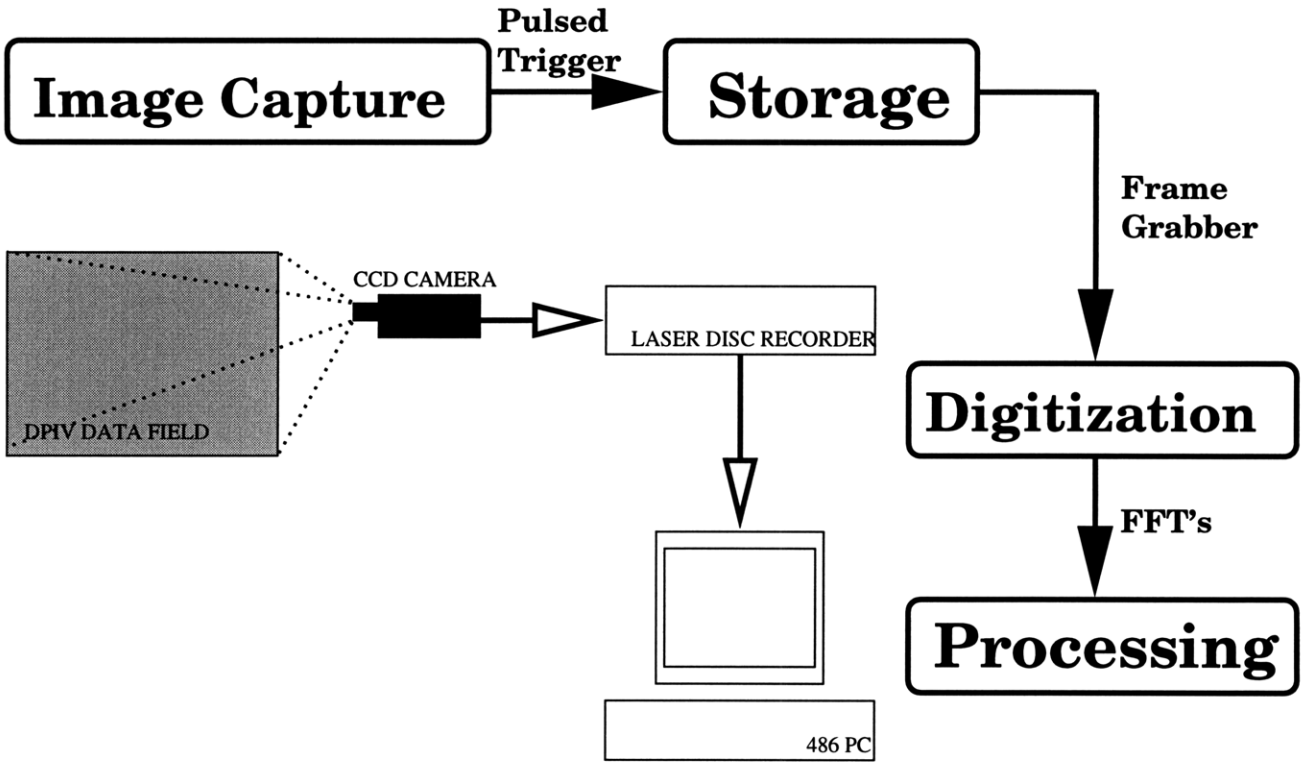

Figure 3-6: Schematic representation of DPIV Method

and adds noise. Generally, it is advantageous to minimize the temporal separation in image pairs, which can be accomplished by exposing the CCD array at the end of the first frame of an image pair and at the beginning of the next frame. (See Figure 3-7)

For these tests on the 5514, the shutter was timed such that the exposure time was 12.5ms, the time between images in an image pair (for DPIV analysis) was 1.7ms and the time between image pairs was 39.3ms.

3.2 Results

Attempts were made to investigate the wake as close to the free surface as 3mm. However, reflections and disturbances due to the height of the waves in the wake caused significant degradation of the data for these runs. We were able to obtain clear images for the z=-4mm, z=-5mm and z=-7mm runs at towspeeds of 0.75m/s and 1.0m/s. Table 3.1 illustrates the tests which were run and the corresponding

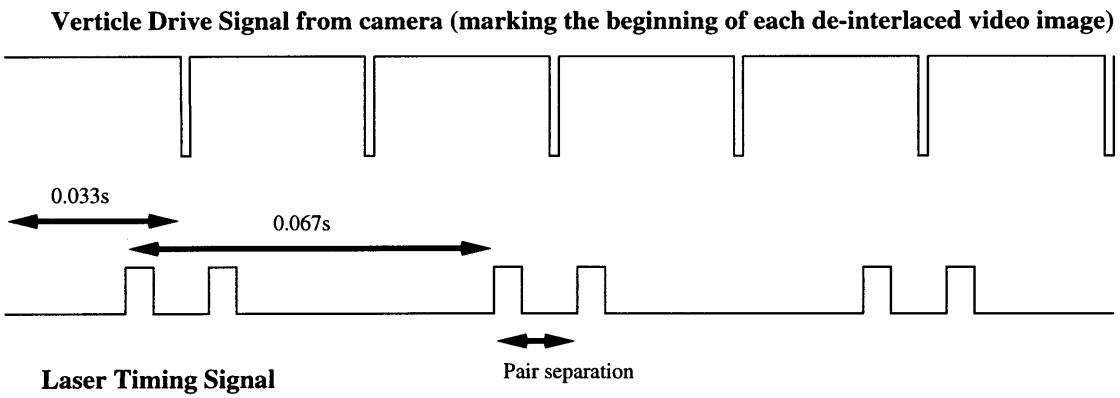

Figure 3-7: Diagram of shutter timing around video signal to minimize time between frames and particle dispersion

plots at the end of this chapter.

Figure	Towspeed(m/s)	$\mathcal{R}e$	Depth(z/d)
Figure 3-9	0.75	2.25×10^6	0.27
Figure 3-10	0.75	2.25×10^6	0.33
Figure 3-11	0.75	2.25×10^6	0.47
Figure 3-12	1.0	3.0×10^6	0.27
Figure 3-13	1.0	3.0×10^6	0.33
Figure 3-14	1.0	3.0×10^6	0.47

Table 3.1: DPIV plots located at the end of Chapter 3

3.2.1 Double Wake

The tests on the Destroyer Hull revealed the presence of the 'double wake'. The wake of this model was 'split' into a port and a starboard wake which were mirror images of each other. These smaller wakes exhibited the features associated with and described in the chapters on the smaller hulls. The double wake and its associated features were evident throughout the depths and speeds tested. The wake typically extended $\sim$0.2 beam-widths on either side of centerline.

The plot of streamwise velocity (Figure 3-8) exhibits the double wake in the two peeks that are shown. This plot shows the streamwise velocity at each y-location on a DPIV plot (made from an image-pair) .

The nature of the double wake, its turbulent structures and the mechanisms which contribute to its formation and characteristics were subsequently investigated. A more thorough study, however, required updating the experimental techniques to improve spatial and temporal resolution. Several equipment upgrades including the acquisition of a pulsed Nd:Yag laser facilitated higher resolution visualization. The implications of implementation of these upgrades, and a more detailed examination of the double wake, are discussed in Chapter 4.

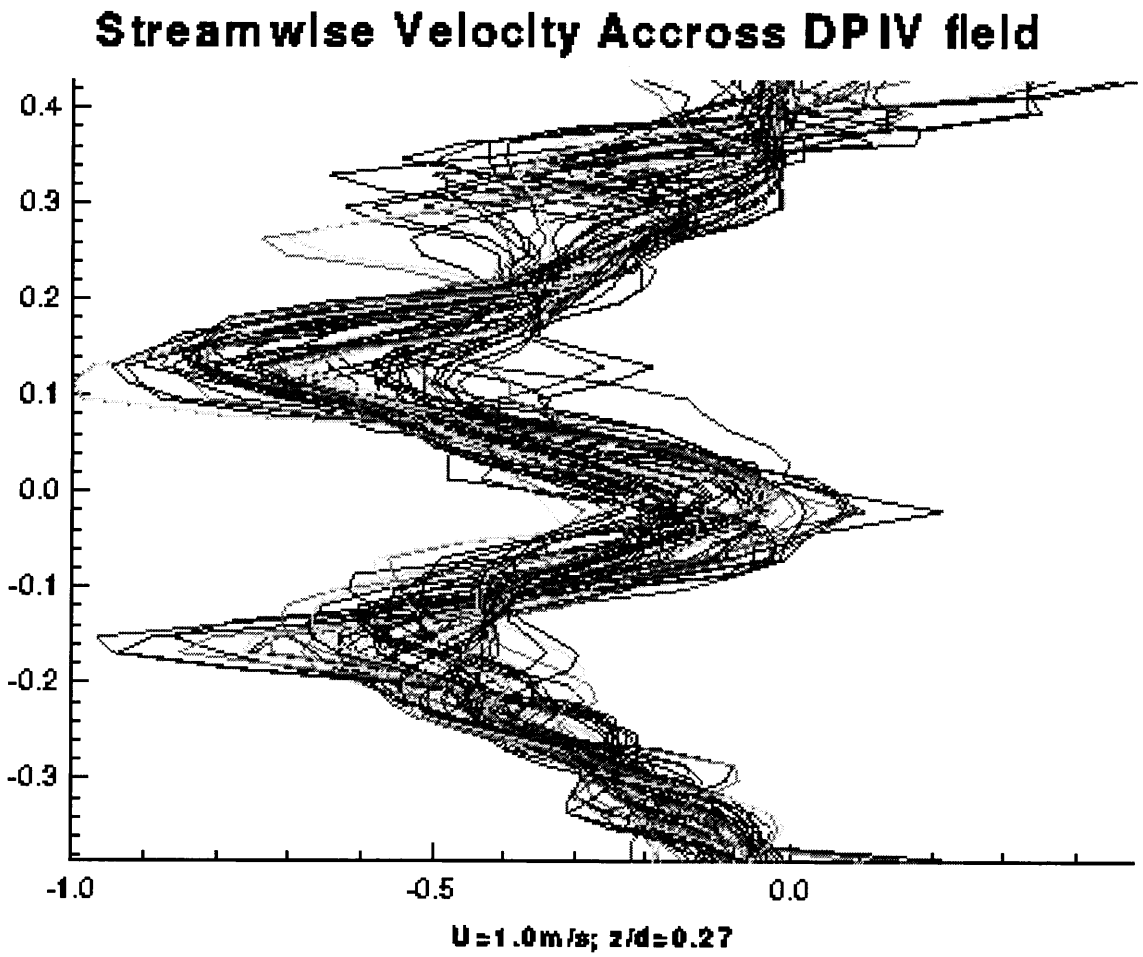

Figure 3-8: Streamwise Velocity across beam

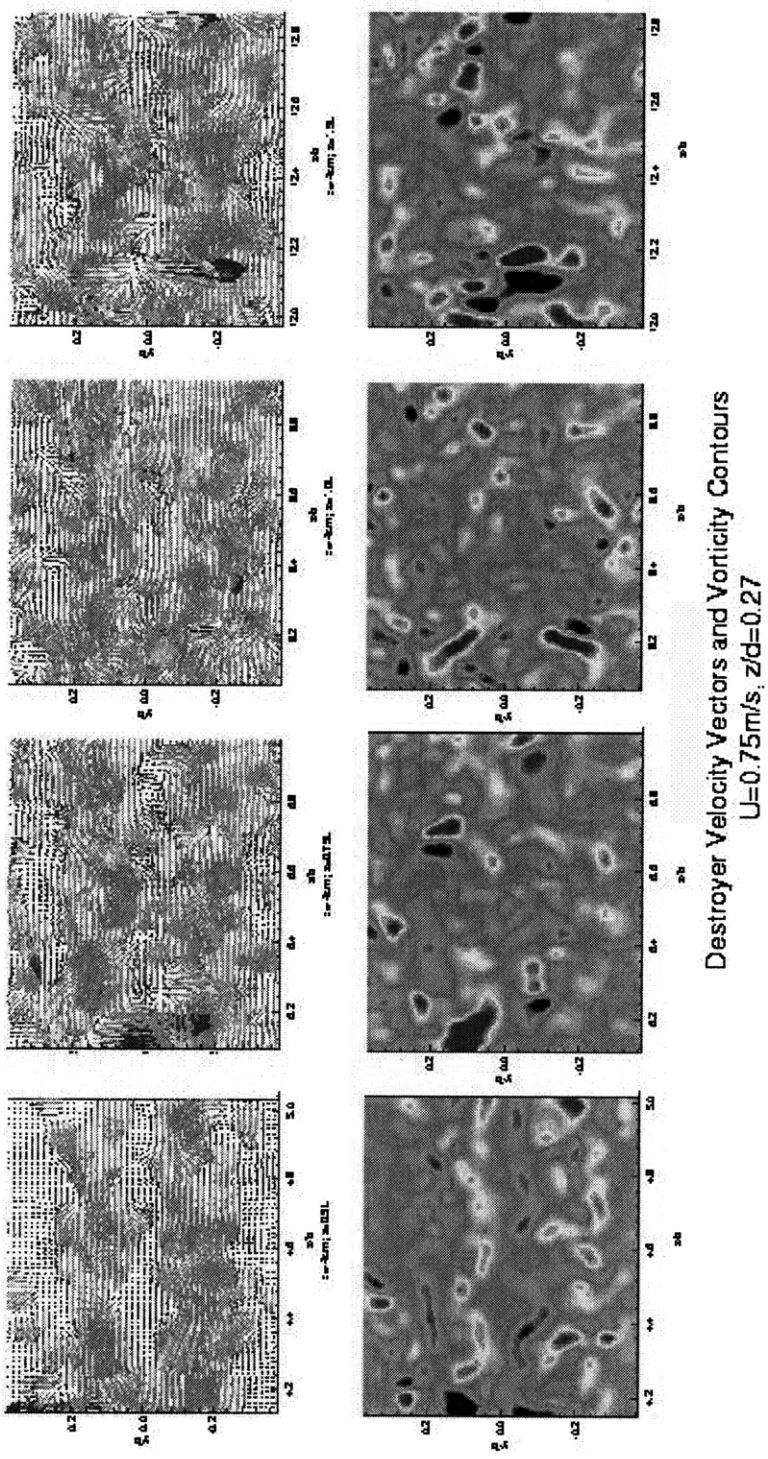

Figure 3-9: Velocity Vectors and Vorticity Contours in the wake of the 5514; u=0.75m/s; z/d=0.27

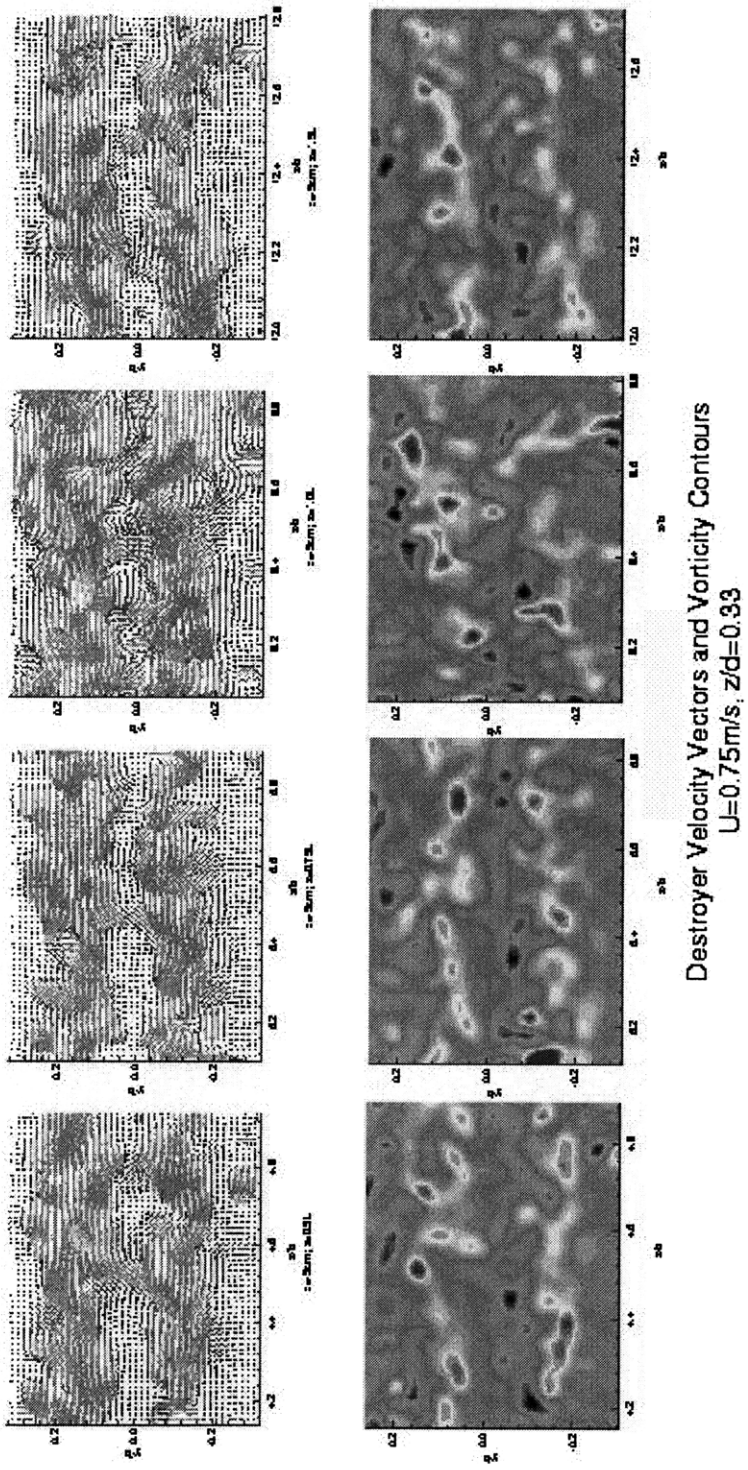

Figure 3-10: Velocity Vectors and Vorticity Contours in the wake of the 5514; u=0.75m/s; z/d=0.33

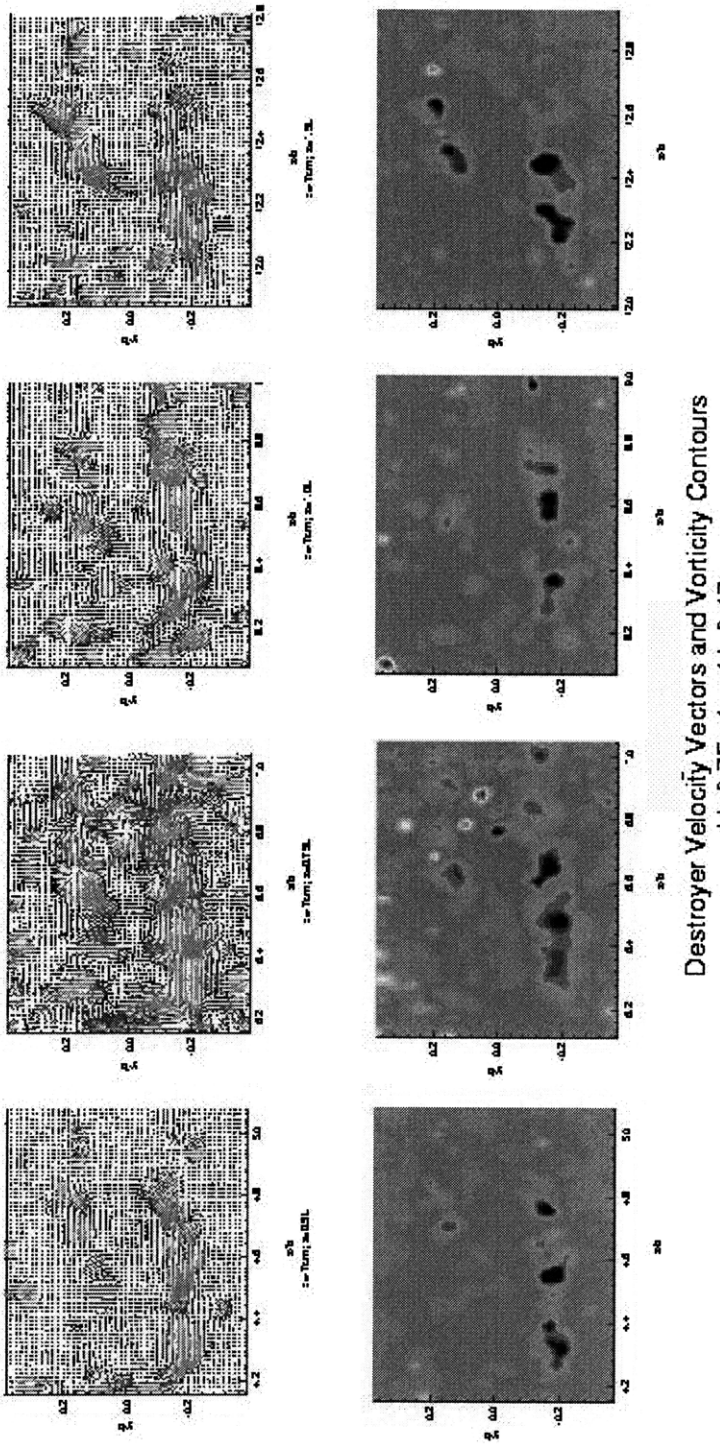

Figure 3-11: Velocity Vectors and Vorticity Contours in the wake of the 5514; u=0.75m/s; z/d=0.47

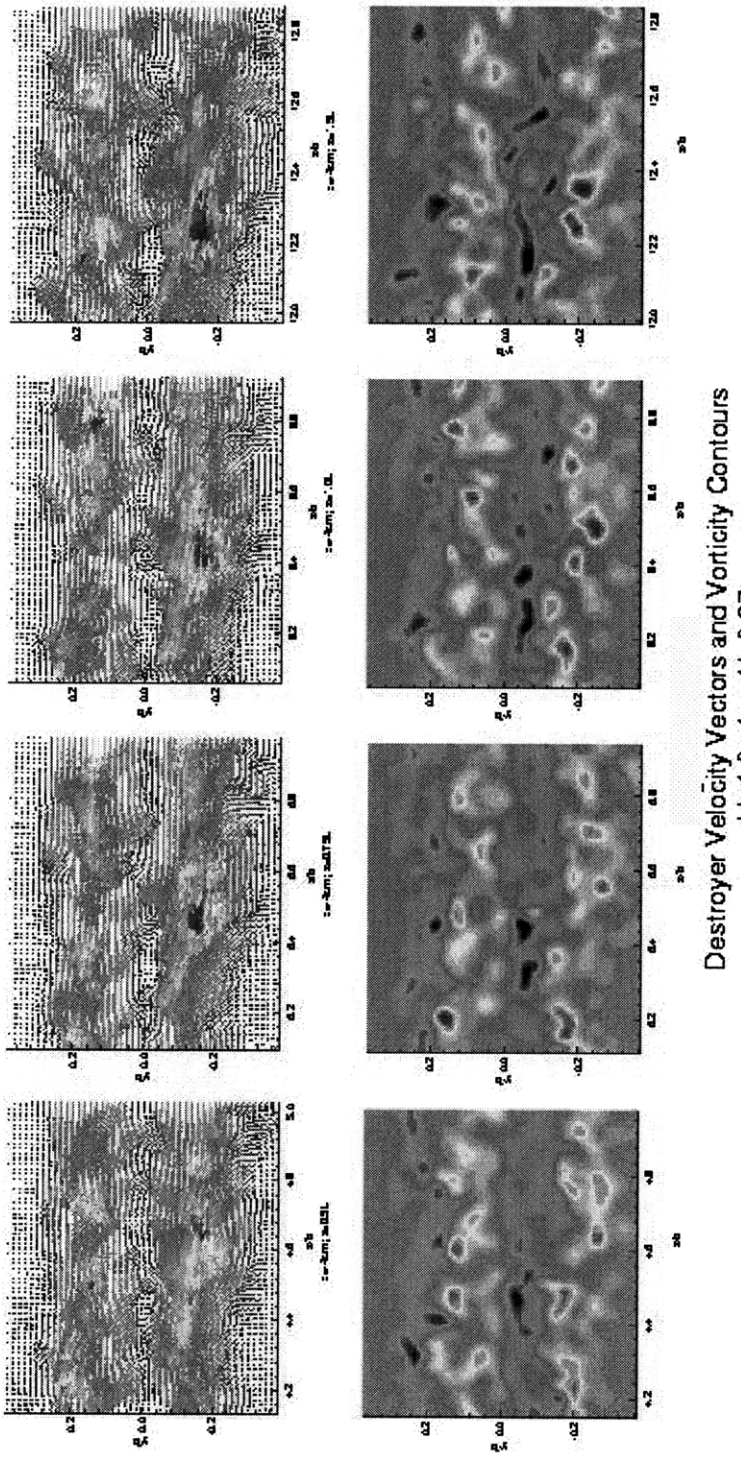

Figure 3-12: Velocity Vectors and Vorticity Contours in the wake of the 5514; u=1.0m/s; z/d=0.27

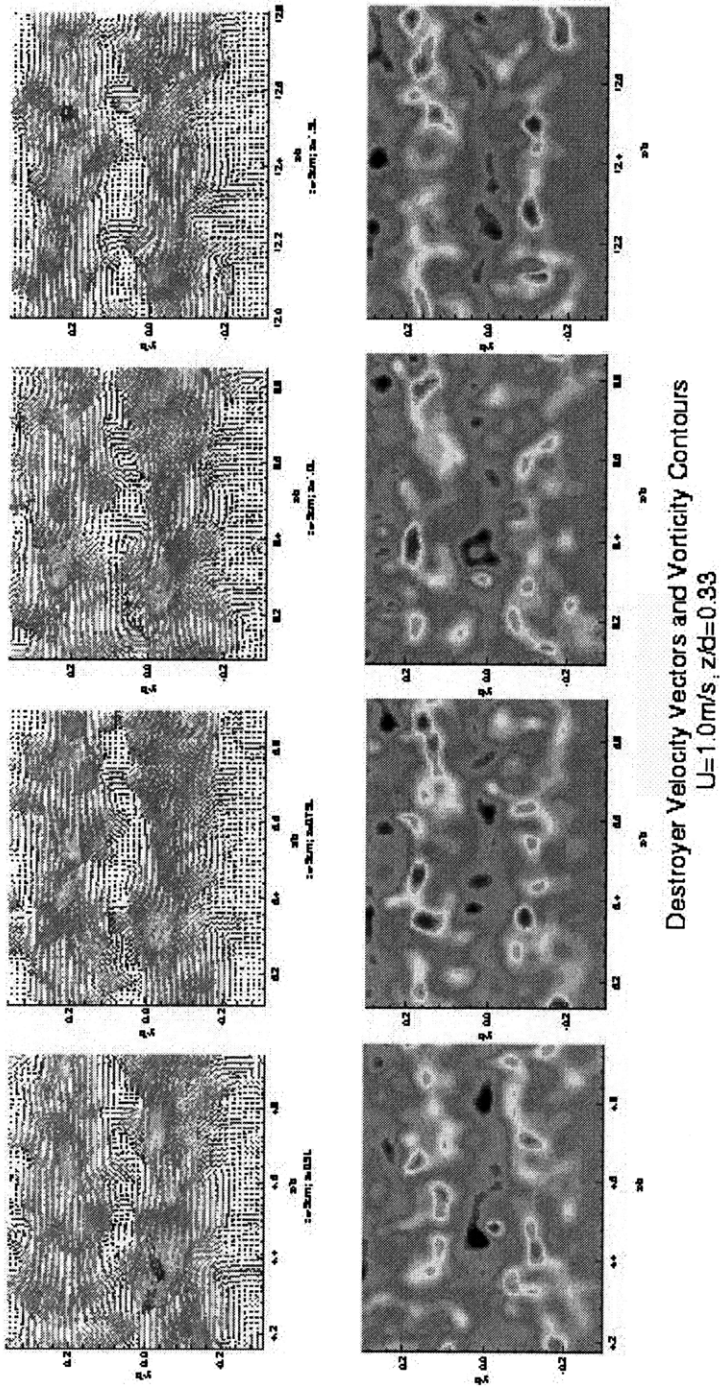

Figure 3-13: Velocity Vectors and Vorticity Contours in the wake of the 5514; u=1.0m/s; z/d=0.33

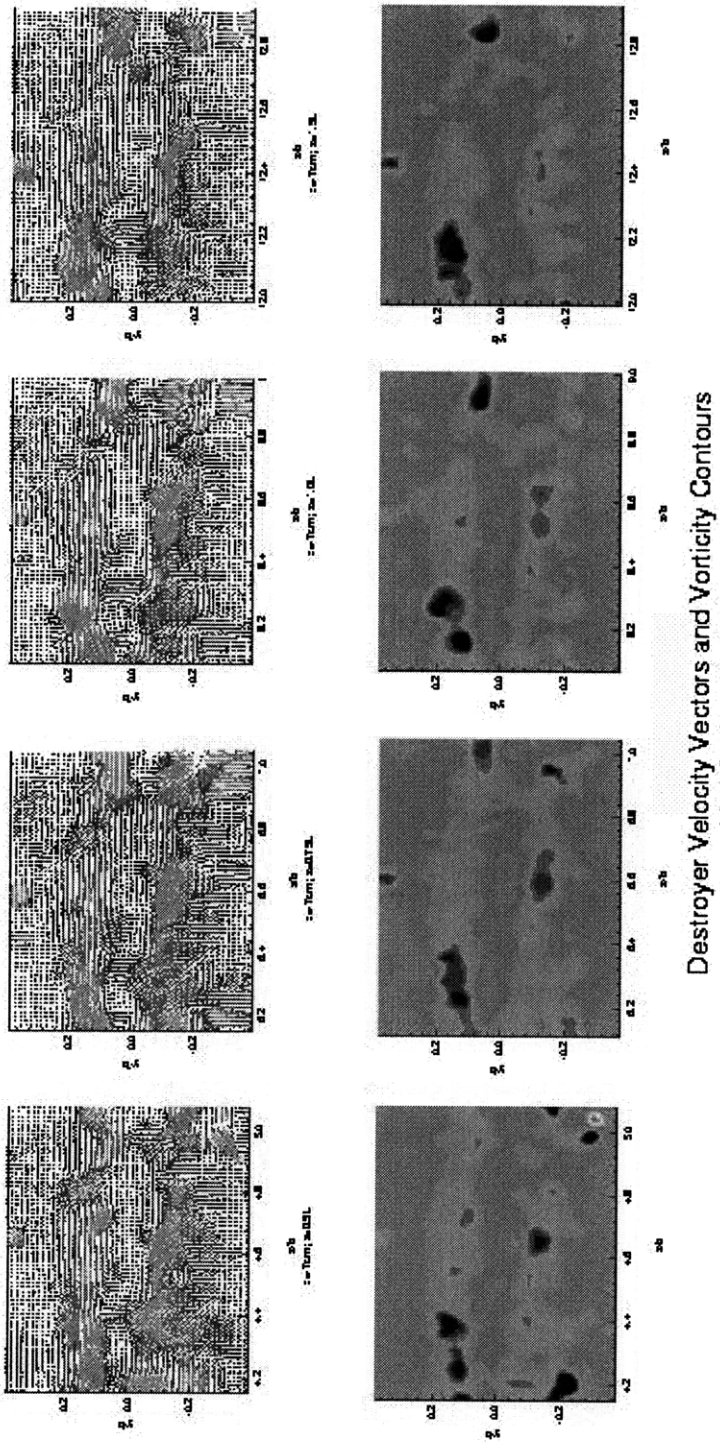

Figure 3-14: Velocity Vectors and Vorticity Contours in the wake of the 5514; u=1.0m/s; z/d=0.47

Chapter 4

Improved Apparatus and Further Wake Studies

The DPIV apparatus used for the tests in Chapter 3, was sufficient but non-optimal. Improvements in computer components and laser assemblies made significant enhancements to the apparatus possible which improved both the quality and certainty of our DPIV profiles. These improvements to the experimental system effected gains in spatial and temporal resolution, otherwise imposed by (1) the CW laser with fiber optic assembly, (2) the digitizing board used to grab the images for processing, and (3) the available particles. In rebuilding the apparatus for the next set of tests, we employed the following changes in technology:

- A 30Hz pulsed Nd:Yag laser
- A PCI-bus mastering frame grabber with enhanced resolution capabilities for digitizing sequences real-time
- An underwater camera housing and removing distortions and attenuations due to air-water, mirror, and glass interfaces
- Larger particles with similar buoyancy characteristics

4.1 Spectra Physics PIV-400-30 Nd:Yag Laser

The Coherent Argon-Ion, CW laser used for the tests described in Chapter 3, was rated for 6W of optical power. The available power for our DPIV experiments, however, was restricted by the use of the fiber optic assembly which could output no more than 2W. (Attempts to put more energy through the cable melted it.) 2W was sufficient to continuously illuminate the 4 meter, 30^o plane of particles, but, the source required modulation via a mechanical shutter to get crisp particle images (necessary for reliable cross-correlation calculations). The shutter was timed around the vertical drive of the CCD camera to expose the plane for just a fraction of the 0.033s (video rate) exposure time. Opening the shutter for no more than 0.002s produced acceptably crisp particle images. Longer exposure times caused streaking and shorter exposure times detrimentally attenuated the brightness of the particles. The 0.002s of light allowed to pass through the shutter, effectively illuminated the particles with only 7% of the available 2W. If the laser could store its energy while the shutter was closed and release all of it in the 0.002s exposure time, the brightness of the particles would be improved ten fold without streaking. This is effectively the benefit of pulsed lasers.

Although the modulated CW beam, provided sufficient energy for the tests described in the previous chapter, any degradation of the system, (i.e. slight misalignment of laser optics or fiber optic cable) significantly attenuated output. Furthermore, optical filters could not be employed to blocked reflections (including those from the free-surface and objects around the tank), due to the resulting attenuation of particle image brightness. An abundance of laser power could have fascillitated the use of filters and absorbers to reduce noise without degrading the signal (particle intensity).

A Spectra-Physics PIV-400-30 laser was purchased to increase available power in DPIV experimentation. This laser is capable of outputting pulsed light in 400mJ, 9ns bursts at frame rate. That is more than twenty times the energy in the CW exposures, in one-tenth the time. The 9ns bursts produce extremely crisp particle

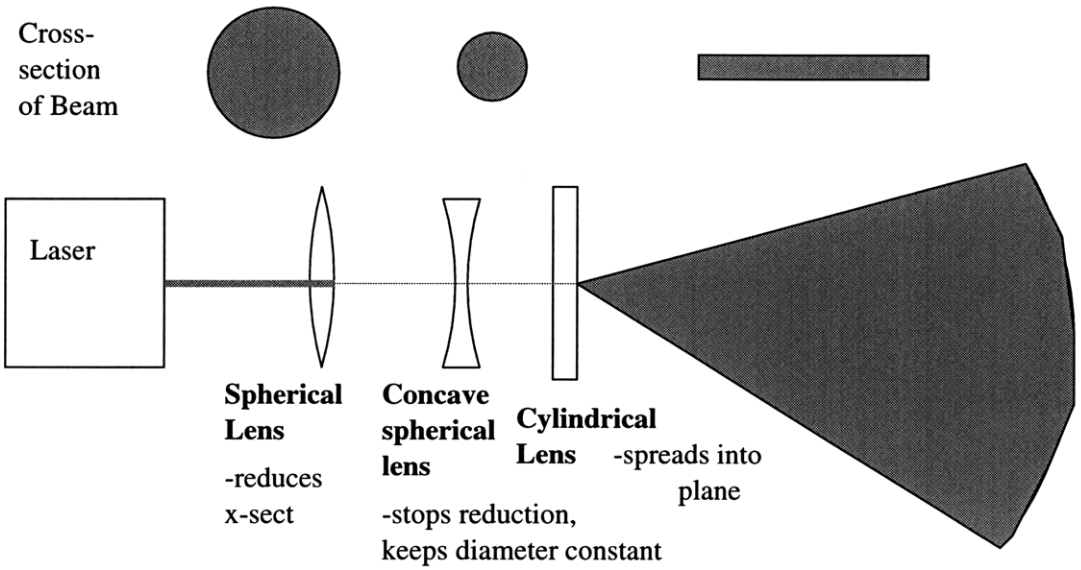

Figure 4-1: Diagram of spherical optics for focusing beam and making it into a plane

images with more than sufficient particle illumination.

Use of the fiber optic cable with this laser, however, was impossible. An optical bench with several mirrors and lenses (rated for extremely high power) was therefore set-up. This arrangement required more space and was slightly more clumsy, but easier to control and change.

4.2 Optics

The PIV-400-30 outputs a 10mm diameter beam which must be lensed into an horizontal plane with even intensity distribution and negligible thickness. This proved a difficult task. 400mJ over a $8mm^2$ area is enough energy to melt the coating from a conventional optical mirror. Focusing that energy to a smaller point, destroyed some very high quality lenses. Initial attempts to reduce the diameter of the beam using spherical lenses (one convex lens to focus the beam down and a concave lens to stop focusing and keep the diameter constant) (See Figure 4-1) destroyed several expensive lenses. This was because the cross-section of the beam into the concave and cylindrical lenses was extremely small with ten times the energy density of the 10mm beam.

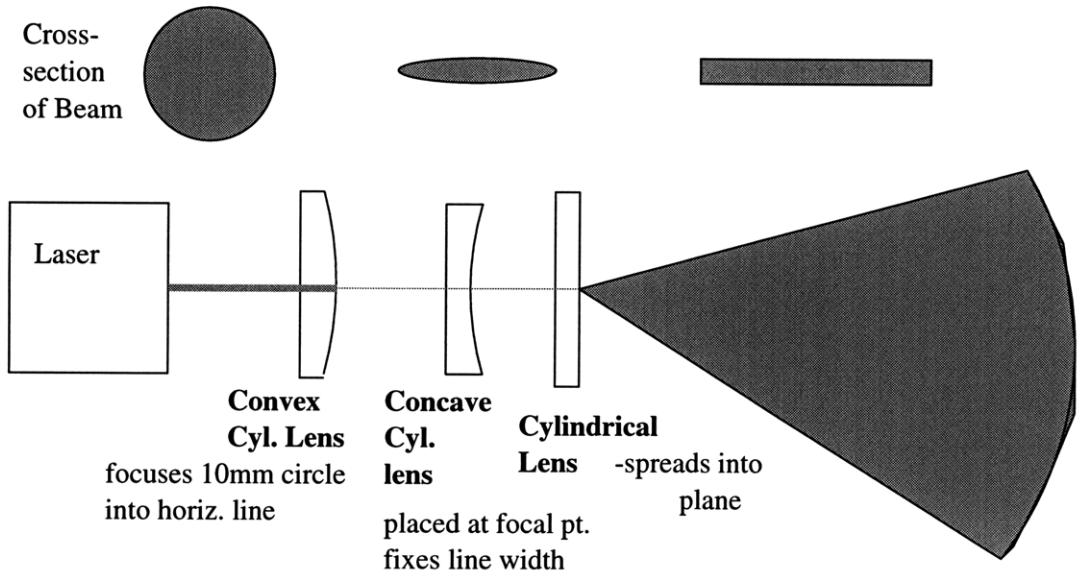

Figure 4-2: Diagram of cylindrical optics for focusing beam and making it into a plane

The incident energy density on the lenses was reduced with a system of cylindrical lenses rather than spherical lenses. The first lens was a horizontally (long axis of cylinder) oriented convex cylindrical lens which focused the beam to horizontal line. Then a horizontally oriented concave cylindrical lens placed at the focal point of the convex lens, stopped the focusing and fixed the width of the line. This horizontal line then passes through a vertically oriented cylindrical lens which expanded it to a 20^o fan angled DPIV plane. (See Figure 4-2)

4.3 Tuning and Firing the Laser

The Spectra Physics PIV 400-30 laser is an assembly of two laser tubes, each tuned to pulse at 15Hz. The light pulses from both tubes are steered with optics to exit from the same aperture and when alternately fired have an effective repetition rate of 30Hz. As mentioned in Section 3.1, it is extremely important to have similar laser intensity in both images of an image pair, therefore it is critical that the two tubes output co-incident beams of equal intensity. Minute path differences cause different planes of particles to be illuminated in successive images and thereby corrupt the

DPIV data.

Two controls ("Lamp Trigger" and "Q-Switch") excites the gas in the laser tube and open the acoustic shutter releasing the pulse. The four TTL laser controls were synched to the vertical drive from the CCD camera, for extremely accurate control of the laser timing as verified by an optical sensor. A Berkeley Nucleonics, Four-channel pulse generator input the v-drive from the camera and timed the laser via four output channels.

According to Spectra Physics, optimal delay between Lamp Trigger and Q-Switch is between 0.0015s and 0.0017s. By dynamically incrementing the delay and visually noting the change in light intensity, optimal delay was determined to be ~0.00165s. Similar to the method employed in shuttering the CW Argon-Ion Laser, the pulsing of the Nd:Yag laser was timed such that particle displacements were greater than the step size between interrogation windows but less than limited by the Nyquist criteria. Refer to Figure 3-7 for a depiction of laser timing.

4.4 Image Sequencing

The set-up in from Chapter 3 was further improved with the replacement of the Sony LDV recorder and Epix 4Mg video digitizer with a Mu-Tech MV-1000 PCI Bus Mastering Video sequencer. Where before, a sequence was recorded in NTSC on the Laser Disk Recorder and then digitized frame-by-frame using the Epix card, a sequence could now be digitally recorded, real-time on the Mu-Tech card in a Windows95 PC. The Mu-Tech card assumed control of the PC's PCI bus and wrote the frames to the computer's RAM. With this system, the maximum length of a sequence was determined by the amount of RAM in the computer. For the tests on the 5514, a Pentium processor with 128Mg of RAM was capable of recording more than 300 frames in a sequence (i.e. 10s of data). Sequences of more than ~250 frames, however, required significantly more overhead time). Sequenced images were archived on a recordable CD-Rom which can store up to 600Mg of data.

A Texas Instruments High-Resolution Black and White MC-1134mod Multi-cam

camera was used to image the DPIV plane. While most video cameras interlace images (i.e. transmit odd then even lines at 60Hz.), the MC-1134mod can operate in dual-field mode whereby it outputs each line sequentially at 30Hz. Furthermore, the TI camera has 2 CCD arrays (one which is shielded from light) and instantaneously shifts the entire image from the exposed array to the second which then feeds the data out in NTSC format (interlaced or de-interlaced) while the exposed array captures the next frame. This dual-field, double array method removes temporal differences common in typical CCD scanning cameras. It has the capability of functioning like a shuttered photographic camera, in that it can instantaneously capture a complete field of image data.

4.5 Positioning

A preliminary round of tests using the new laser, digitizing board and larger particles was conducted using a 25mm CCD camera lens (large field of view). In these tests, the camera was outside the tank and imaged the entire wake reflected off an angled mirror on the bottom of the tank. (Like the set-up employed for the tests described in Chapter 3.)

There were several problems with these tests that were resolved in future experiments. Firstly, the shorter focal length lens reduced the particle size beyond the 3 pixel/diameter processing constraint. In addition, reflections were greater with the more powerful laser and introduced significant noise to the data. Figure 4-3 shows the result of processing images with lots of background imagery and particles which are too small.

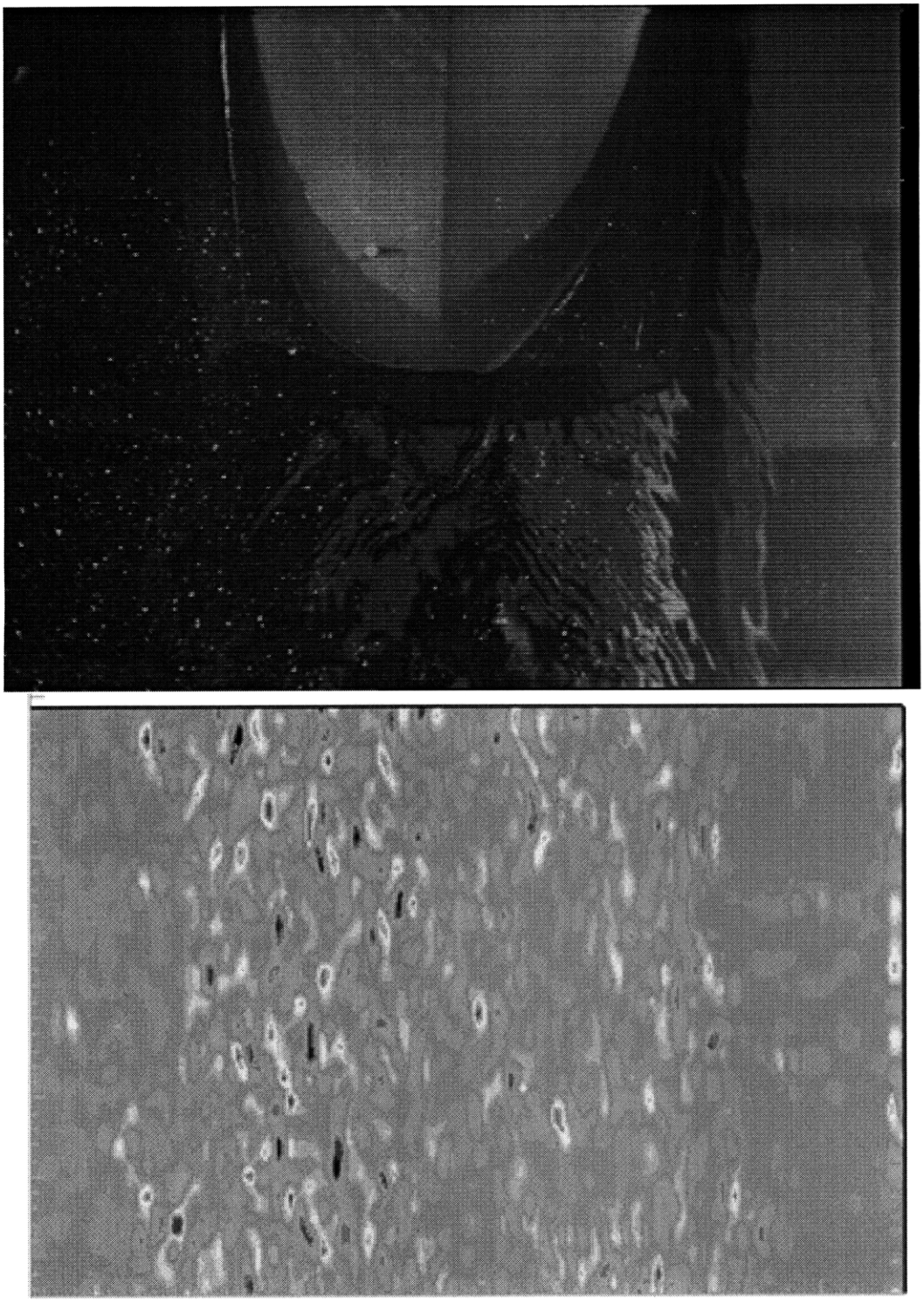

Figure 4-3: (TOP) Transom of 5514 passing camera (BOT) Vorticity contours from images 1 sec behind transom in sequence.

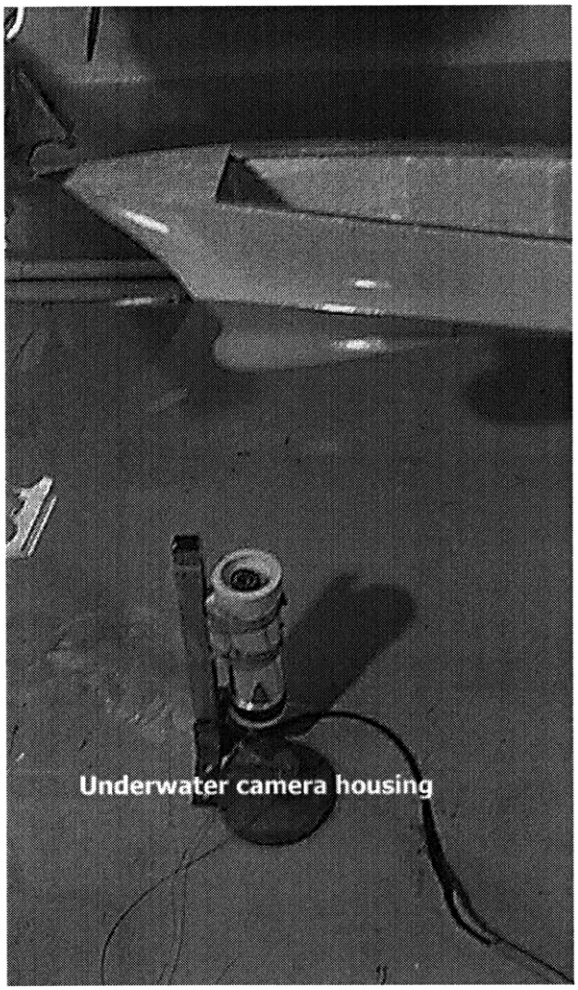

Figure 4-4: Camera in underwater housing aimed at surface to image half of the stern wake of the Model 5514

Improvements came with various filters, especially the Kodak Wratten Green filter, but the best results were obtained with the camera in an underwater housing aimed towards the surface from the bottom of the tank. (See Figure 4-4)

Further improvements resulted from the construction of a canopy which hung from the stern of the boat over the wake to shield the camera from reflections off the ceiling of the tank. (See Figure 4-5.) The canopy eliminated background inconsistencies as evidenced by the centralization of correlation peaks. In addition, the camera was placed underwater and aimed directly at the half-wake of the model with a 35mm (magnifying) lens. Adding the canopy and zooming in on half the wake, significantly improved the processing results which follow.

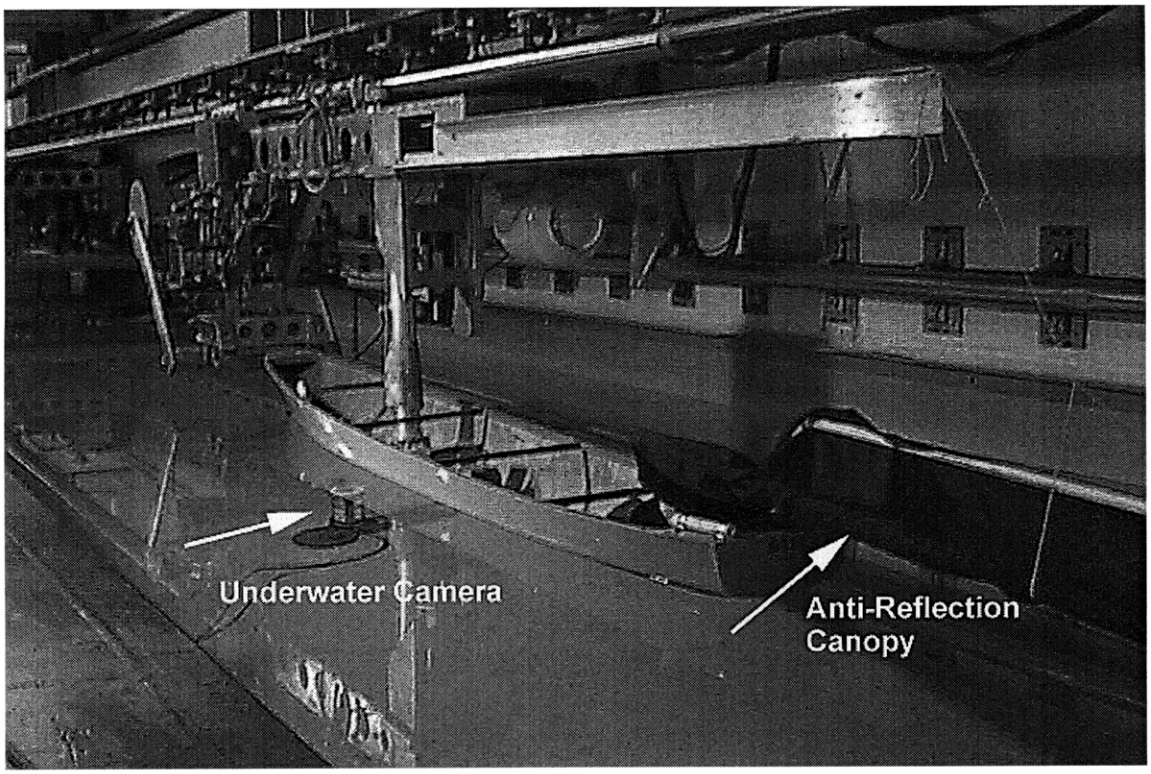

Figure 4-5: 5514 pictured with anti-reflection canopy extended into wake to protect camera from ceiling reflections

4.6 Processing Optimization

The DPIV software written by Willert and Gharib [22] at CalTech has two post-processing algorithms for removing possible errors inherent with the fast fourier transform/cross-correlation method. These post-processing algorithms can be turned on or off according to the user specified parameter file. These parameters are (1) smoothing and (2) outlier removal. The smoothing operation uses a spatial filter that is passed over the entire data field to remove high frequency jitter inherent to the DPIV processing algorithm. The second method removes outliers in the data field. Outliers are flagged by computing the velocity differences from eight surrounding data points for each data point in the field. If the differences exceed the threshold for four of the eight surrounding neighbors, the data point is considered an outlier and replaced by linear interpolation.

The inclusion or exclusion of either of these two post-processing operations yields

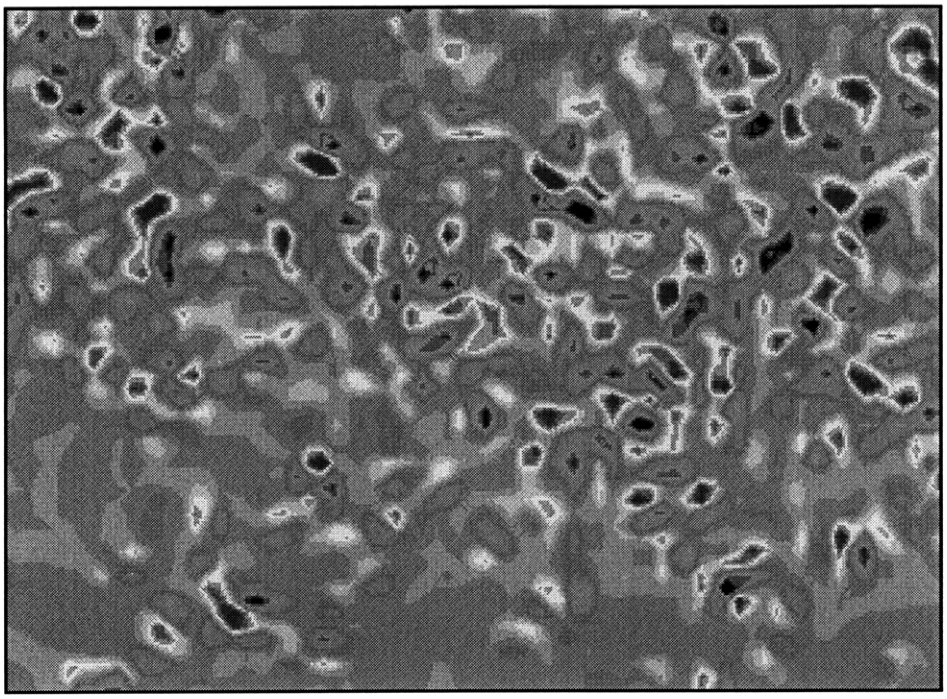

Figure 4-6: Vorticity contours of pair processed without smoothing or outlier removal

four possible processing methods with results that vary dramatically. To decide on a processing method, the same image pair was processed using the four possible combinations of post-processing algorithms (or lack there of). Figures 4-6 through 4-8 are contour plots of vorticity data from the same image pair processed with three different parameter sets.

Spectral analysis of the four different parameter options was performed by taking the two-dimensional fast-Fourier Transform of the velocity data and plotting the results vs. wave number. Figure 4-9 and Figure 4-10 show how the different methods affect the higher energy components of the field. Because the smoothing function altered the entirety of the energy spectrum, and outlier removal seemed to remove variations which could be logically due to random errors in the DPIV algorithm, processing with outlier removal and without smoothing was applied to the entirety of the DPIV data.

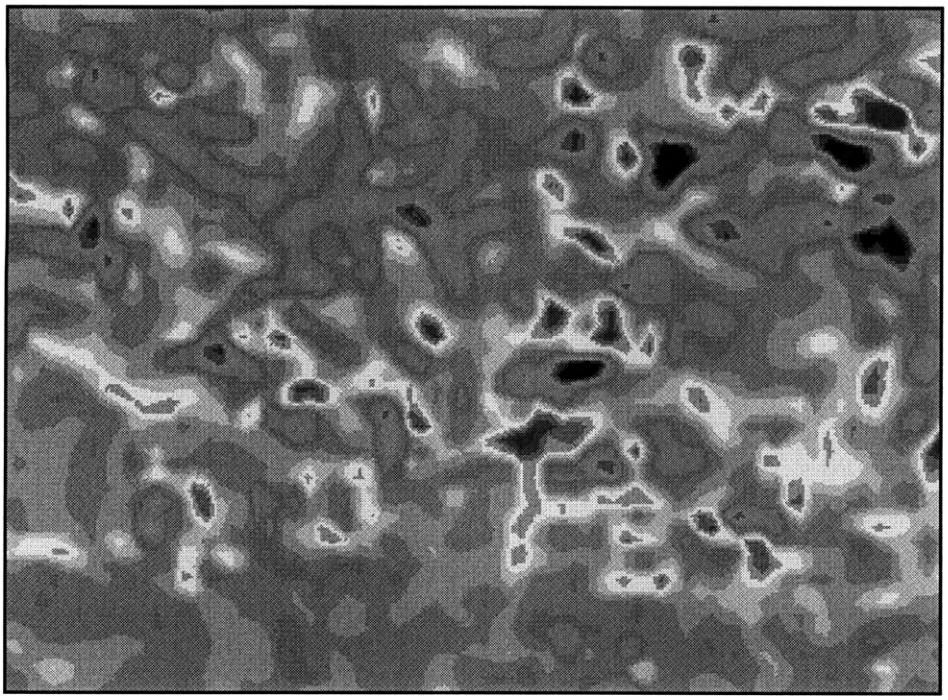

Figure 4-7: Vorticity contours of pair processed without smoothing and with outlier removal

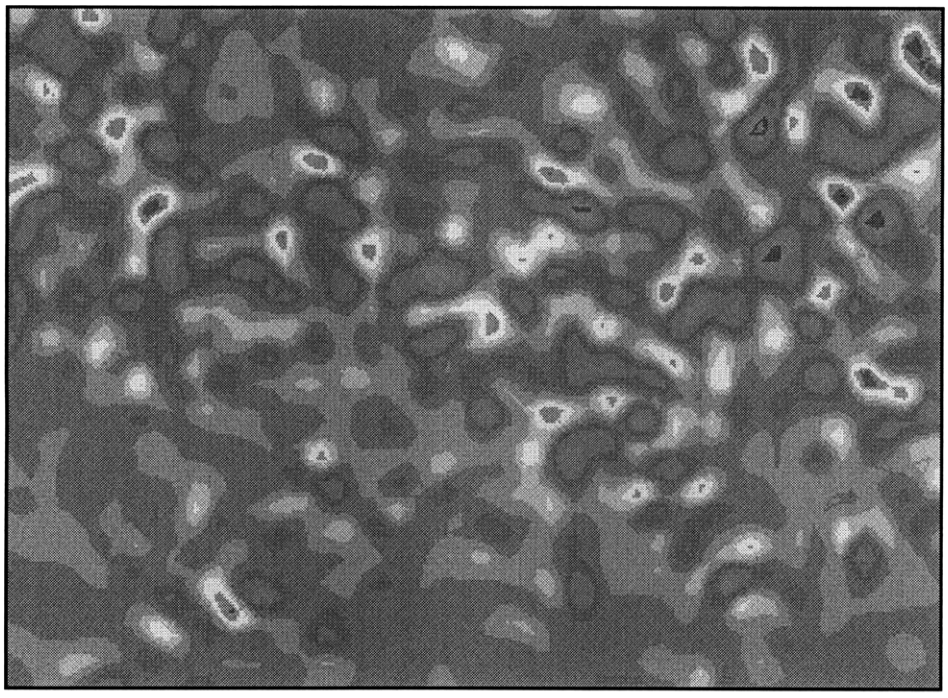

Figure 4-8: Vorticity contours of pair processed with smoothing and without outlier removal

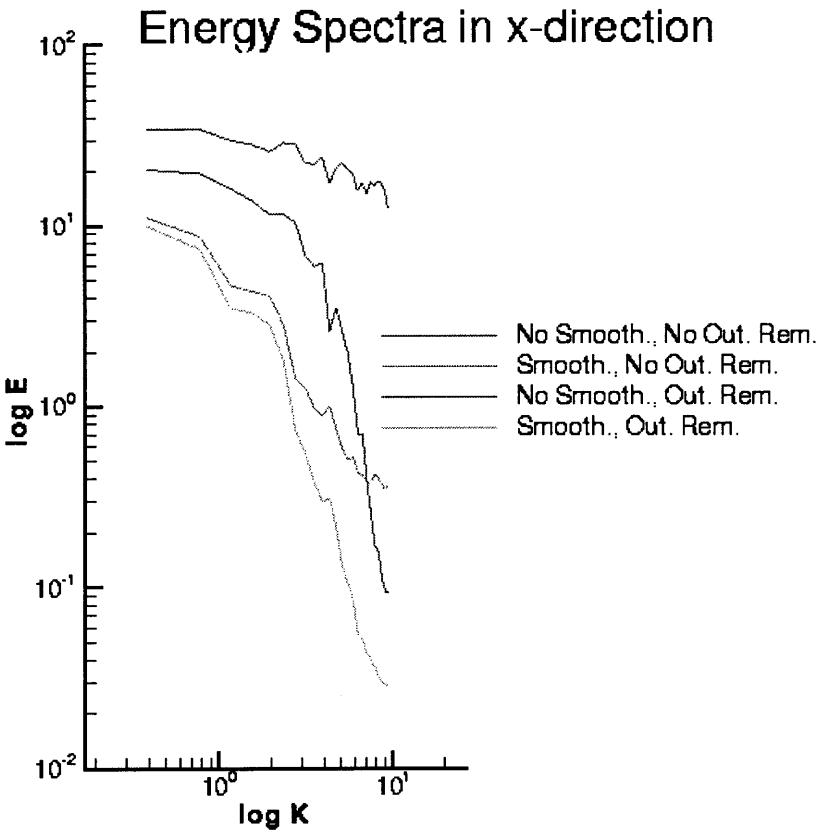

Figure 4-9: Streamwise Energy Distribution

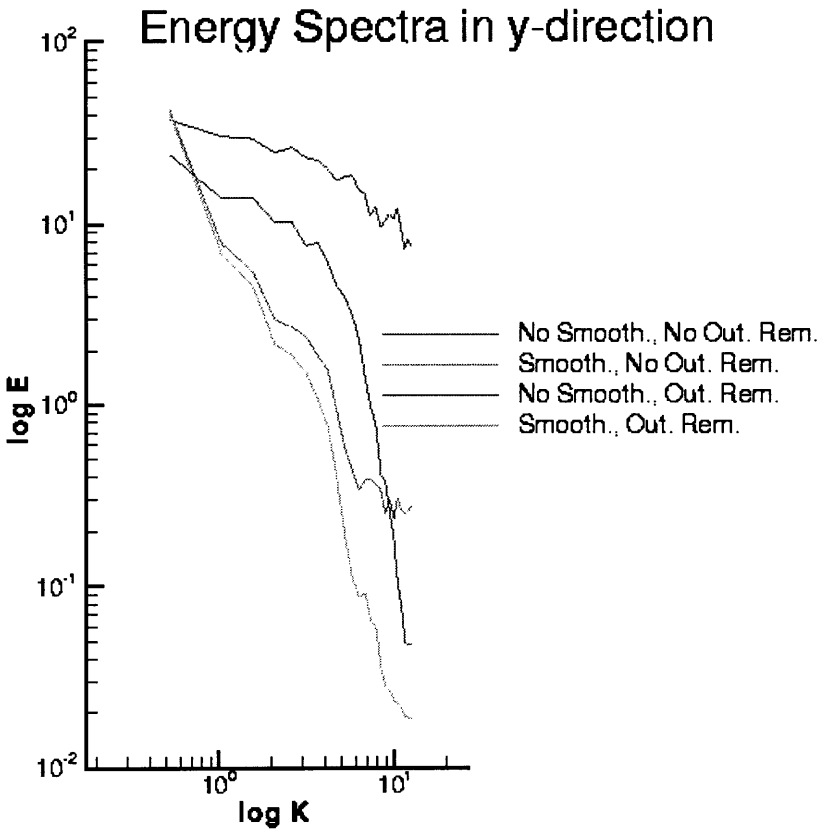

Figure 4-10: Transverse Energy Distribution

4.7 Double Wake Validation

An objective of these tests was to take multiple DPIV images of a single location in the wake for statistical analysis, and to more closely examine the "double wake" left by the 5514. The results of these tests re-confirm the production of a "double wake" by the model. Figure 4-11 shows the average streamwise velocity at seven locations downstream. This data was taken by averaging a DPIV velocity field from eighteen runs at the same depth, towspeed (0.75 m/s) and distance from the model (0.25m). This process will be discussed in depth in Section 4.8.

One half the wake (from centerline to 0.25b to port) was imaged in these DPIV experiments and Figure 4-11 shows the streamwise velocity goes to zero at centerline and peaks at ~0.17b, as was also shown in the full wake experiments in Chapter 3. (See Figure 3-8 for a similar plot of the full wake).

Figure 4-12 and Figure 4-13 show the evolution of half wake as it separates from the center of the hull. (In these figures the model is moving from left to right and the centerline of the hull is at the top of the plot) The right most plot of Figure 4-12 is quite close to the stern of the hull (.1m to the left of the hull) and is the only frame in the DPIV sequence in which there is noticeable activity near the center of the wake. At 1 beam-width downstream of the model (leftmost plot), the double wake is clearly established with the predominant activity more than 0.05b from centerline (2.4cm). It is also noted that the vortical activity is centered around 0.15b and remains at that location in the three successive downstream locations.

Figure 4-14 and 4-15 show the same six locations downstream with U=1.0m/s. Here we notice that the wake separates closer to the stern of the hull. We also see more vortical activity at this higher Reynolds Number.

4.8 Statistics

Eighteen identical runs were performed at U=0.75m/s and z=0.05m, to statistically analyze the wake. The average velocities at each point in the DPIV field at four

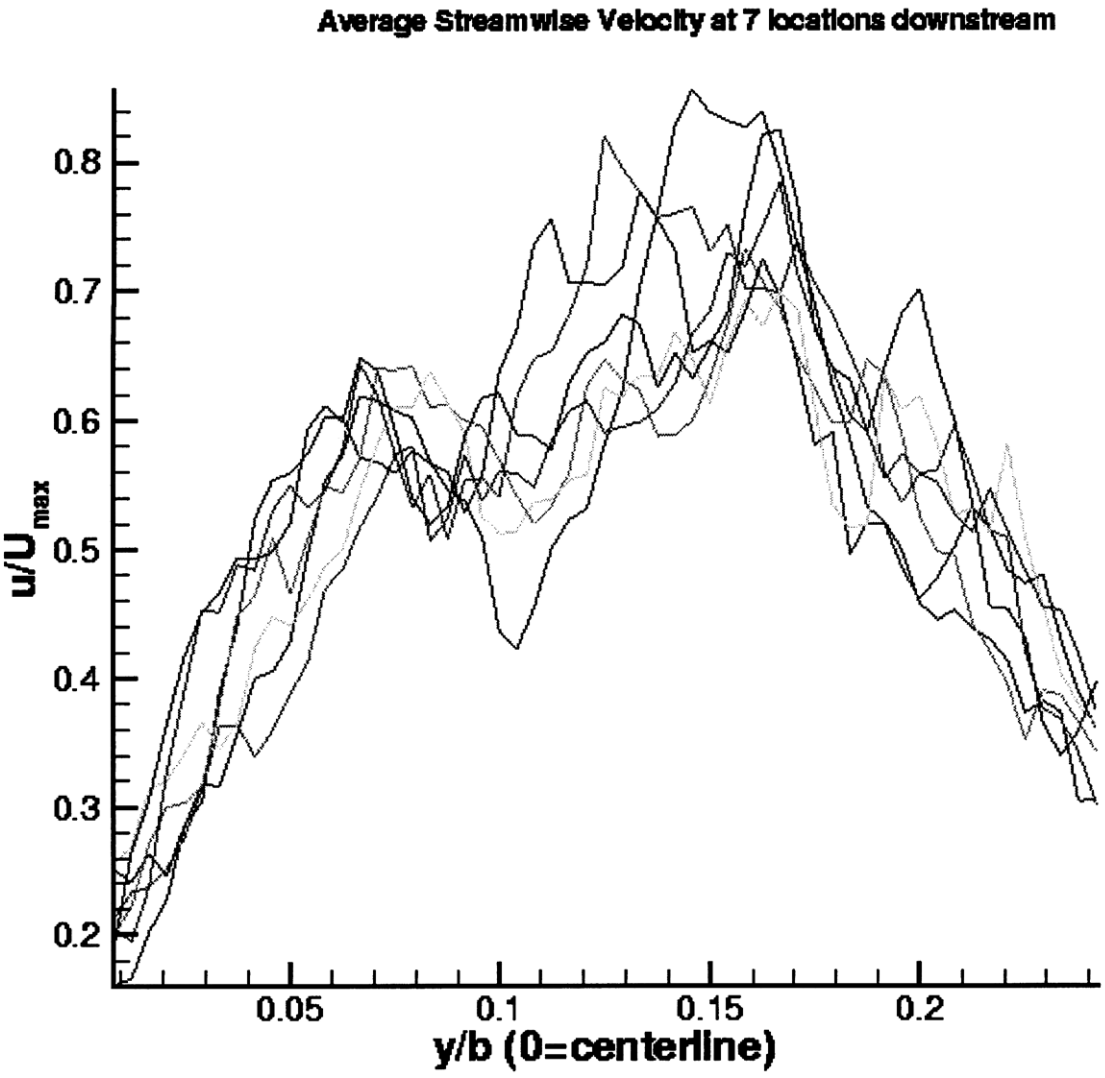

Figure 4-11: Streamwise veloctiy vs. y/b for half the wake

identical wake locations (x=0.075m, 0.25m, 0.5m, 0.76m) were calculated following Equation 4.1.

$$u_{nave} = \frac{1}{N}\sum_{n=1}^{N} u_n \tag{4.1}$$

Where u_{nave} is the average velocity at point n as calculted by summing u_n (the streamwise velocity at point n) in the eighteen (N) runs and dividing by eighteen.

Figure 4-16 through Figure 4-19 show the mean streamwise velocity from 18 DPIV velocity fields 0.075m, 0.25m, 0.5m and 0.76m downstream of the model.

Again, we see that the activity just past the stern, comes from the center of the

model and diverges, becoming centered around 0.15b at .25L. The mean streamwise velocity deteriorates near the center of the wake and falls to ~20% of maximum. Although spatial constraints prevented imaging of the full beam width, it can be seen that the streamwise velocity falls off outwards from 0.2b as was also noted in previous experiments.

Standard deviations were found for each point in the DPIV field following Equation 4.2.

$$\frac{1}{N}\sum_{n=1}^{N}(u_n - u_{nave})^2 \tag{4.2}$$

Where u_{nave} was found using Equation 4.1 and u_n is again the velocity at point n in each of the N (18) runs. The average differece between the average velocity at point n and the velocity at point n in the eighteen particular runs is by definition the standard deviation of the streamwise velocity at that point.

The areas of greatest velocity fluctuation over the eighteen runs, correspond to the largest standard deviations. Thus, the velocity in these regions is most difficult to statistically predict.

Contour plots of standard deviations from the average velocities calculated for Figures 4-16- 4-19 are shown in Figures 4-20 - 4-23.

The standard deviation information shows the largest velocity fluctuations at (0.25L downstream) centered around 0.15b. We see significantly fewer fluctuations around 0.1b where we also see relatively high mean streamwise velocities.

4.9 Conclusions

These tests validated the existence, and illustrated the evolution of the "double wake" behind the model 5514. Investigation of the mechanisms responsible for this double wake prompted further examination of flow around the model, including visualization of the flow near the bow-mounted sonar bulb.

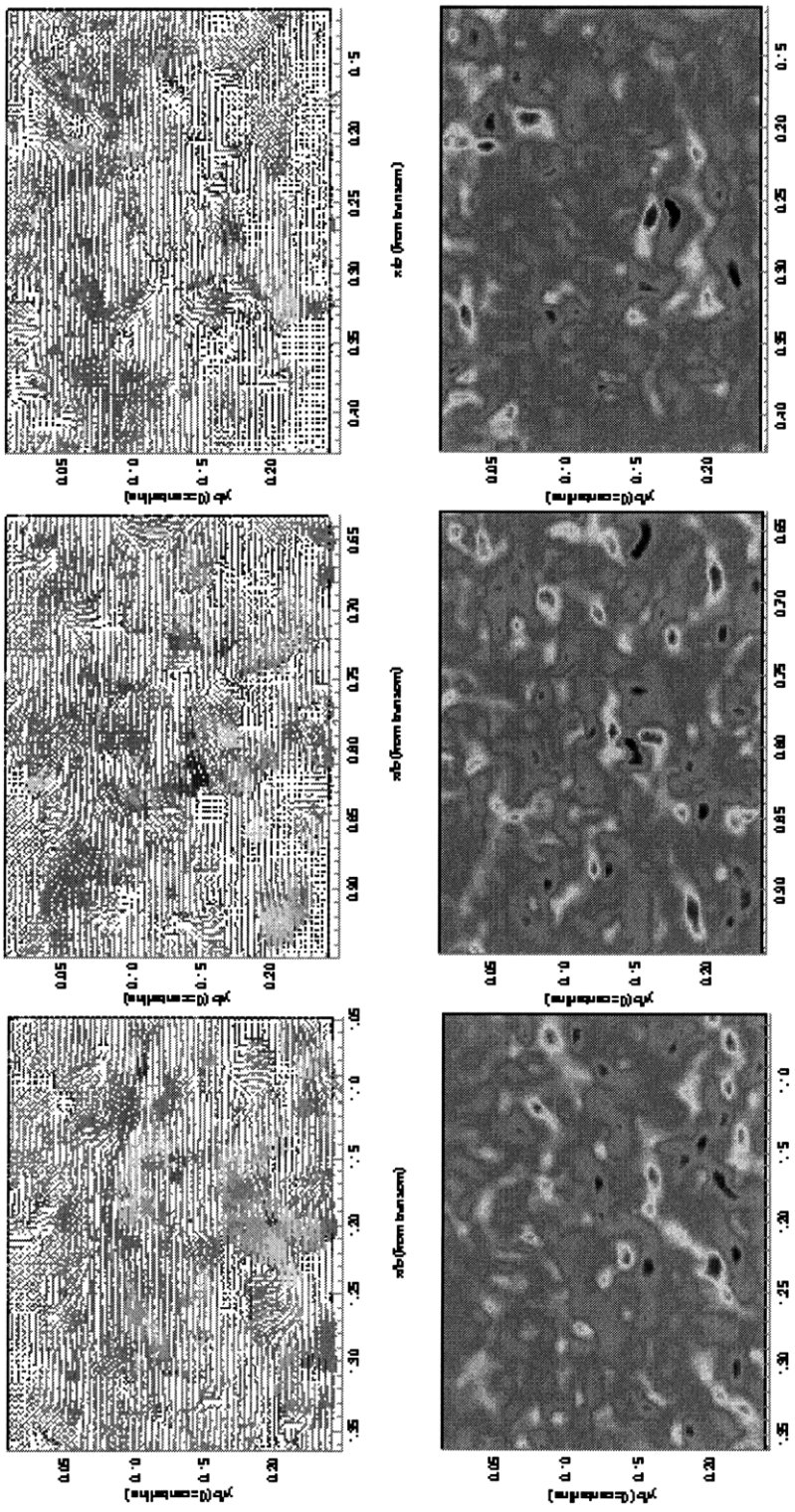

Figure 4-12: Velocity vectors and vorticity contours for three downstream wake locations.(0.01m-0.63m Model has moved from bottom to top of page.

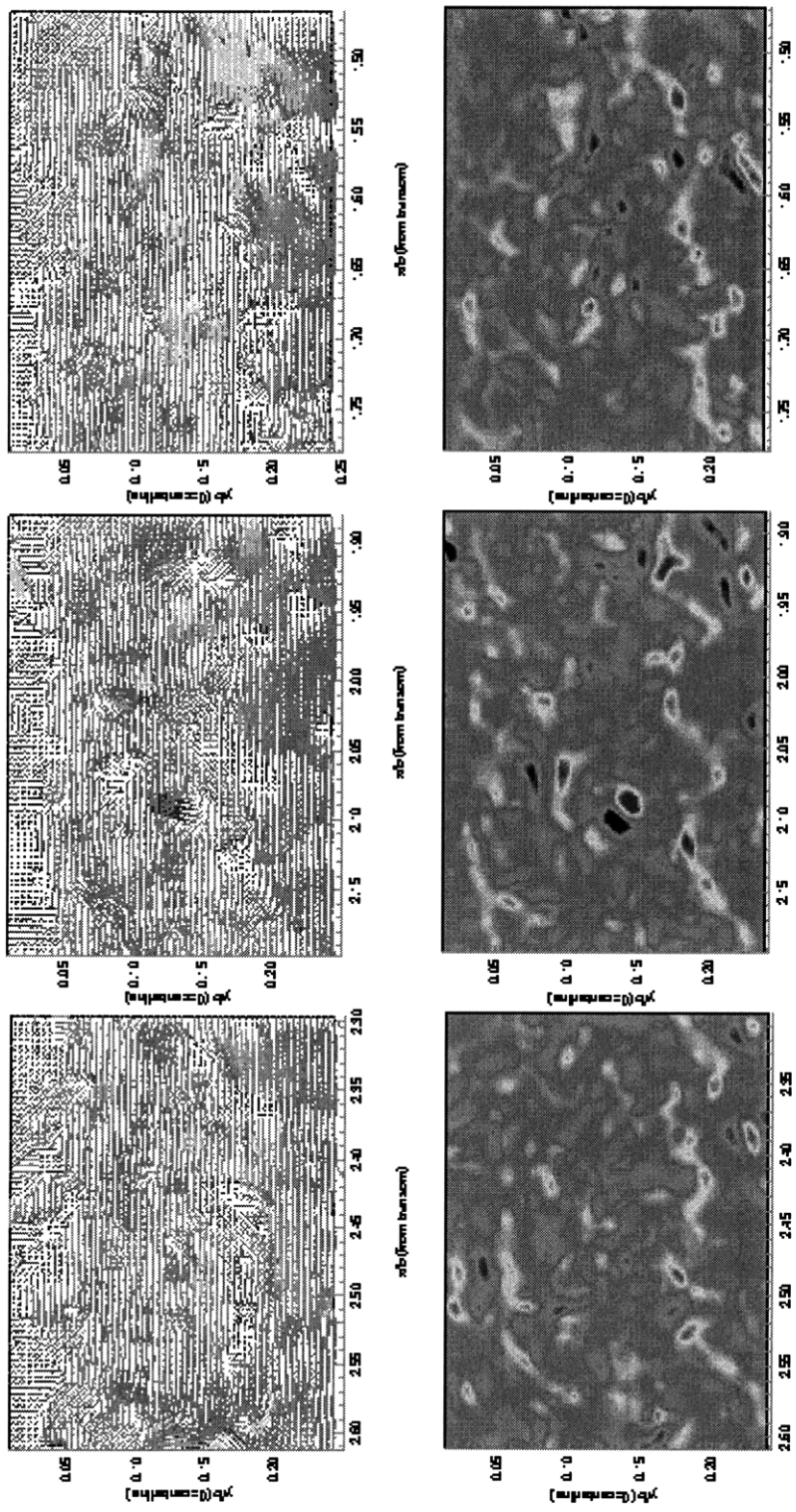

Figure 4-13: Velocity vectors and vorticity contours for three downstream wake locations (0.7m-1.25m) Model has moved from bottom to top of page.

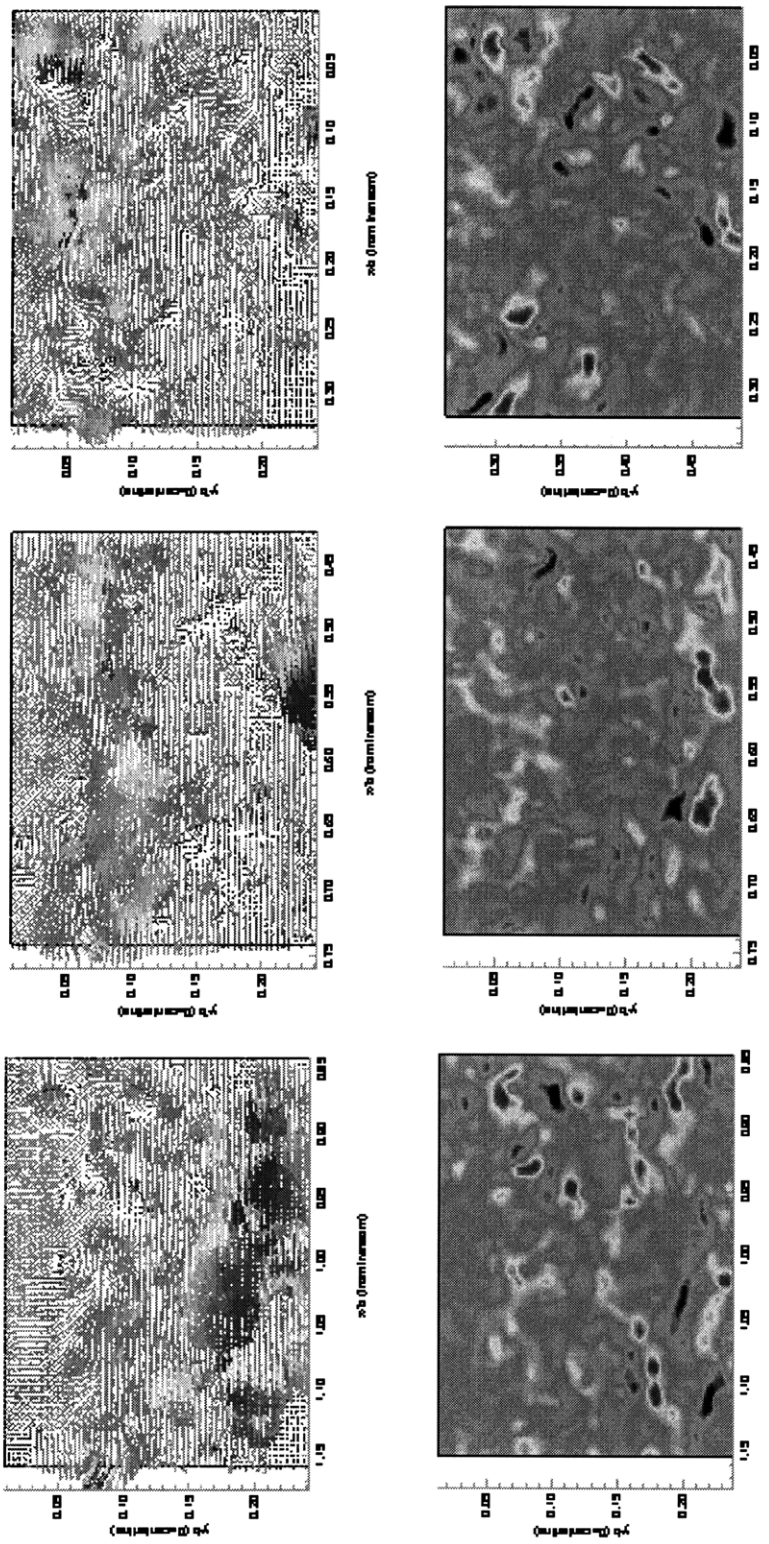

Figure 4-14: Velocity vectors and vorticity contours for three downstream wake locations (0.01m-0.63m). Model has moved from bottom to top of page.

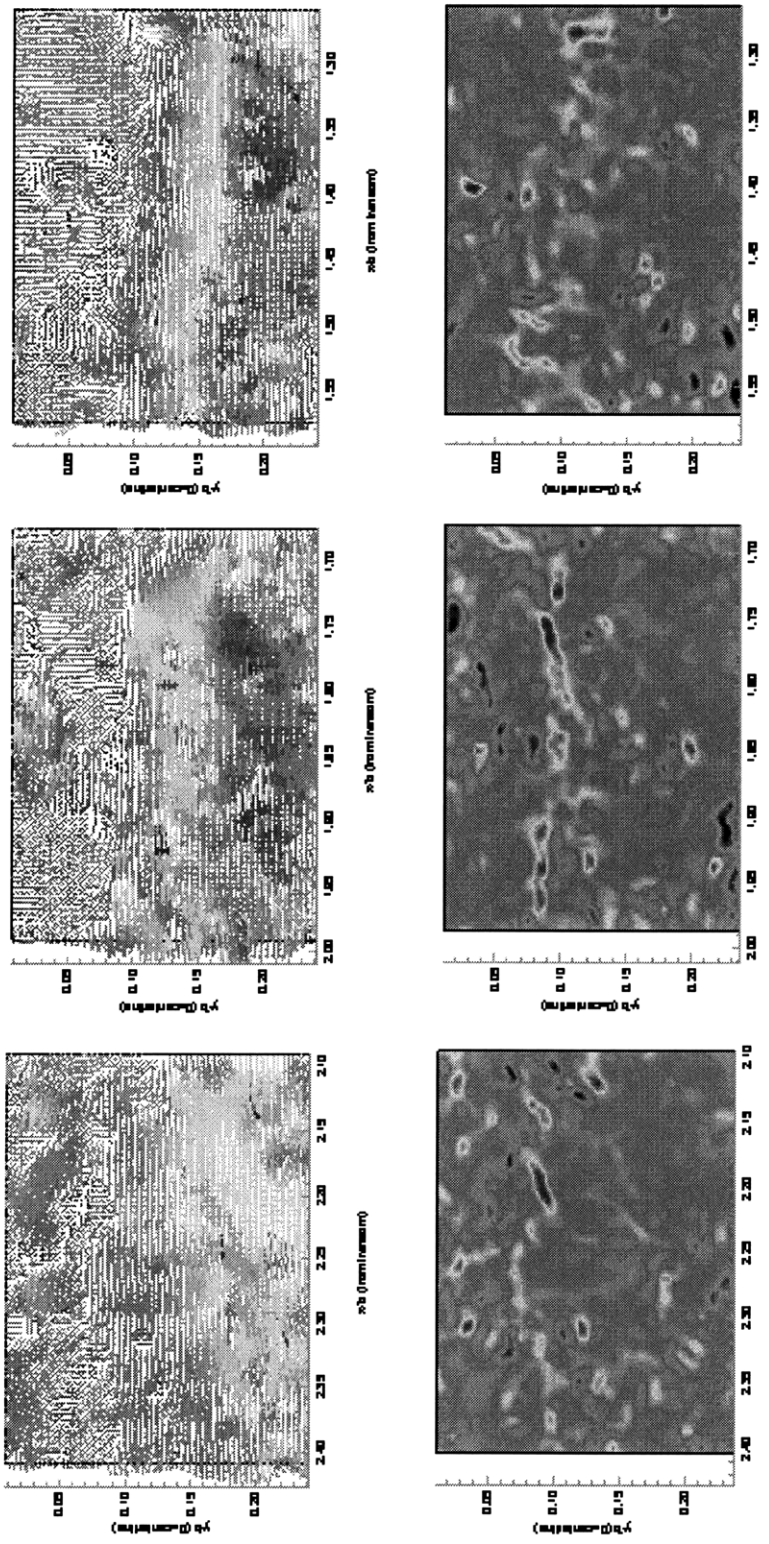

Figure 4-15: Velocity vectors and vorticity contours for three downstream wake locations (0.7m-1.25m). Model has moved from bottom to top of page.

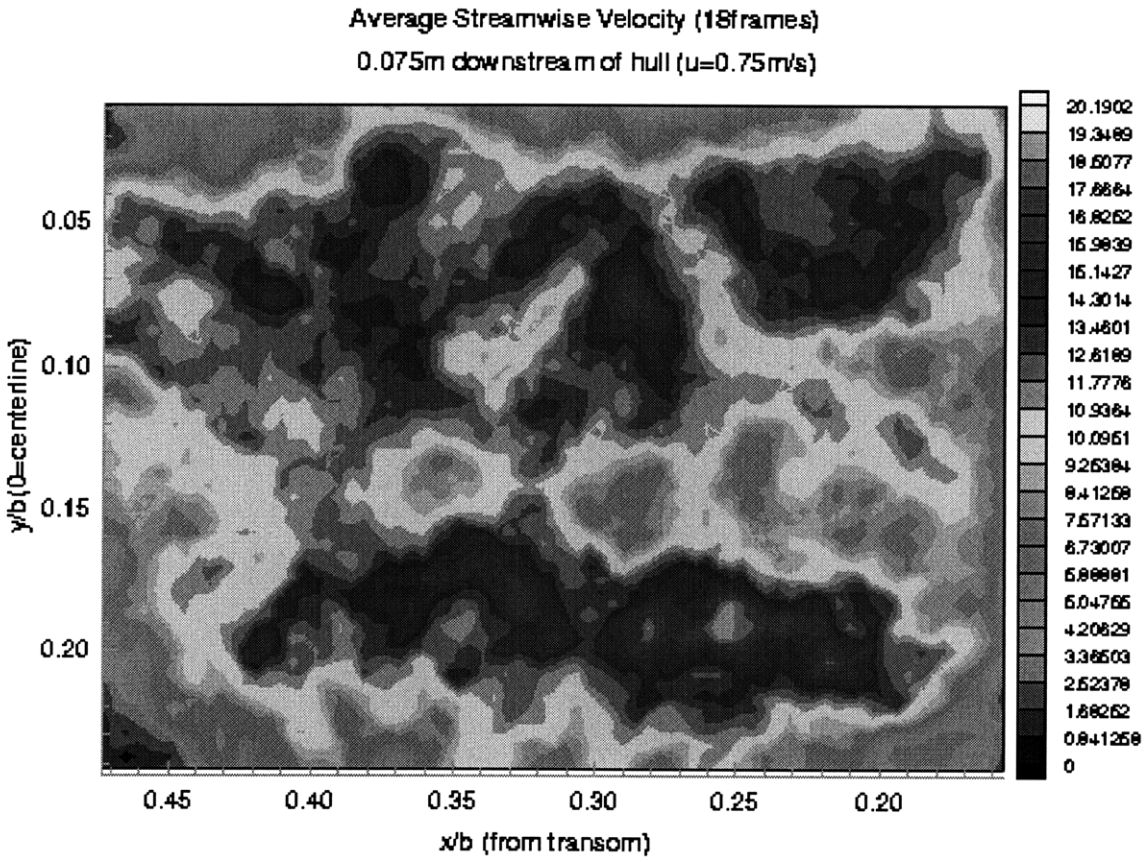

Figure 4-16: Average Streamwise Velocity from 18 DPIV fields 0.76m downstream of hull

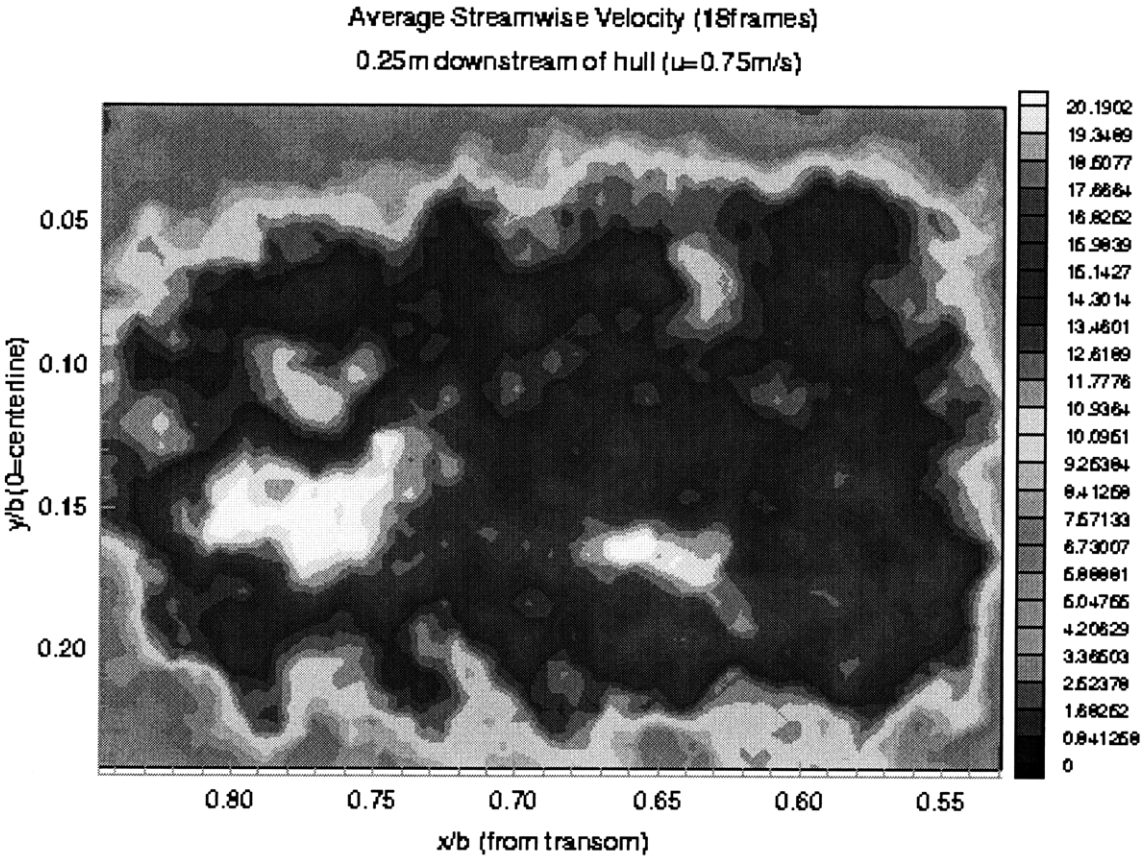

Figure 4-17: Average Streamwise Velocity from 18 DPIV fields 0.76m downstream of hull

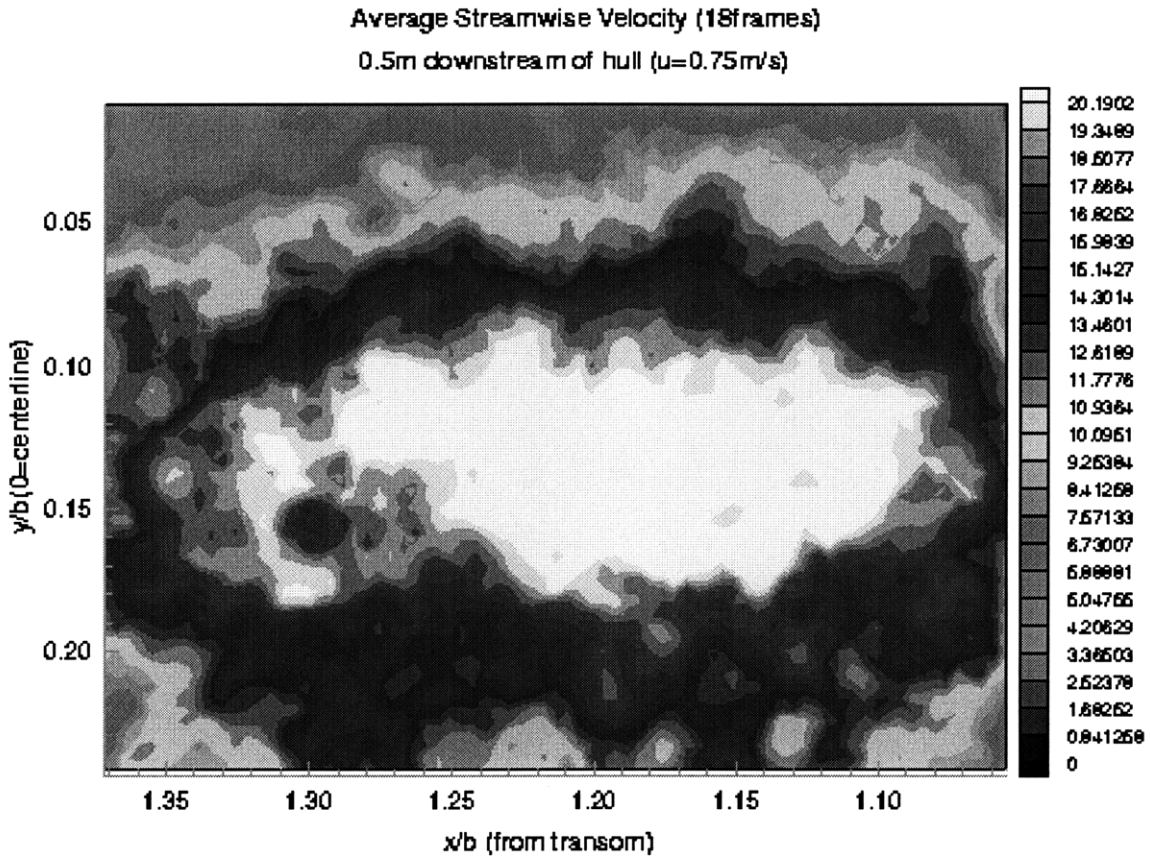

Figure 4-18: Average Streamwise Velocity from 18 DPIV fields 0.76m downstream of hull

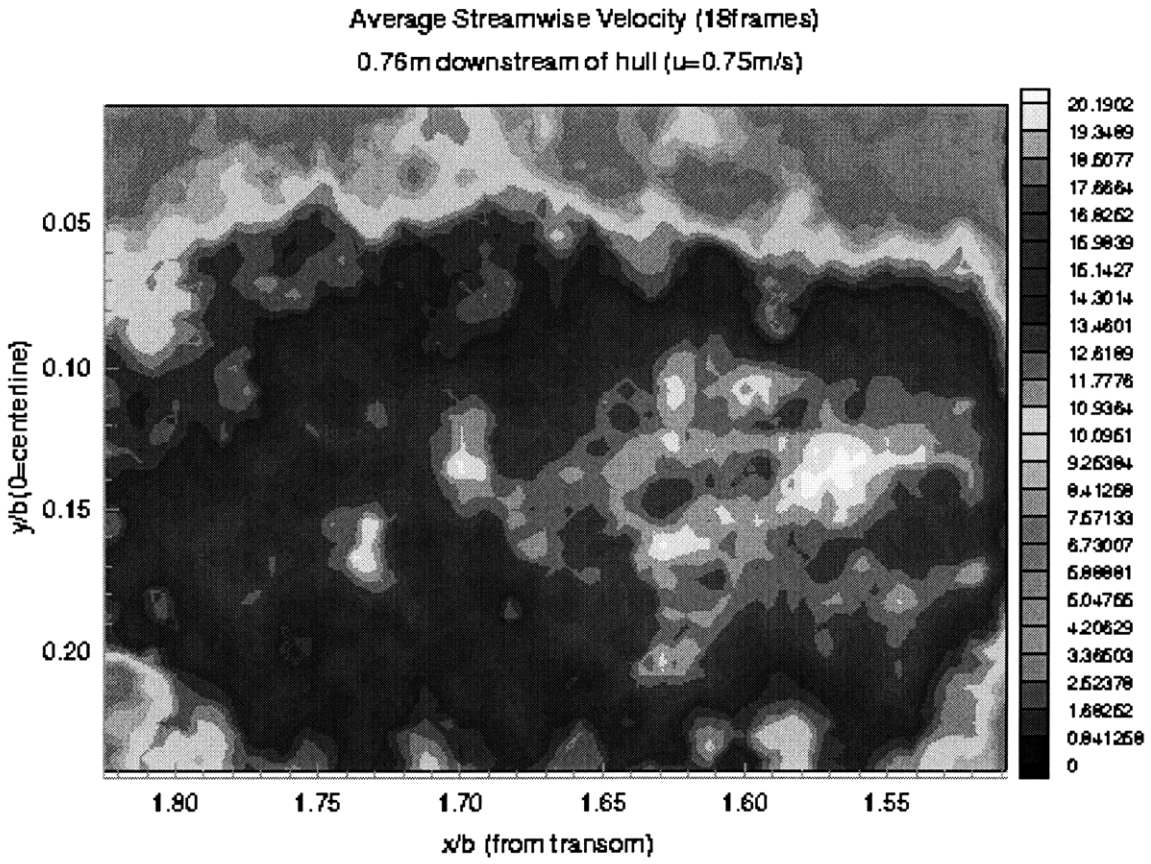

Figure 4-19: Average Streamwise Velocity from 18 DPIV fields 0.76m downstream of hull

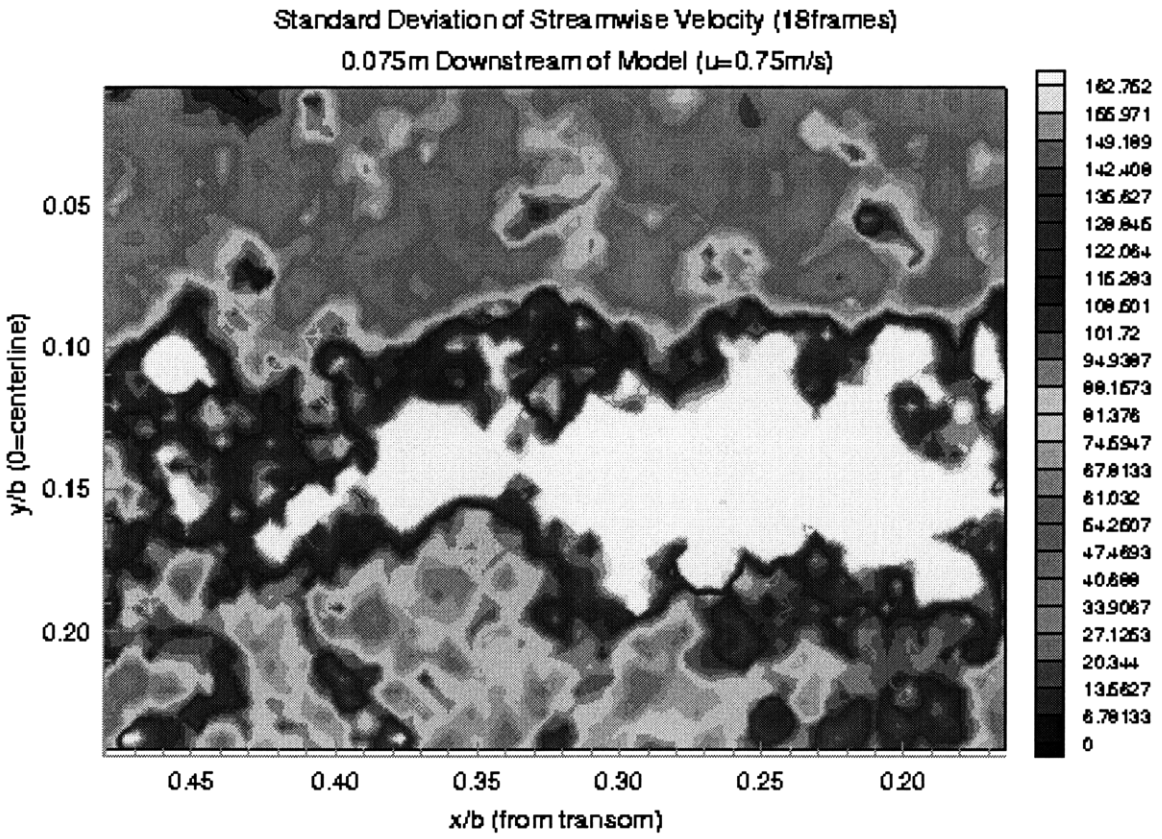

Figure 4-20: Standard Deviation from Mean Streamwise flow at 0.075m downstream

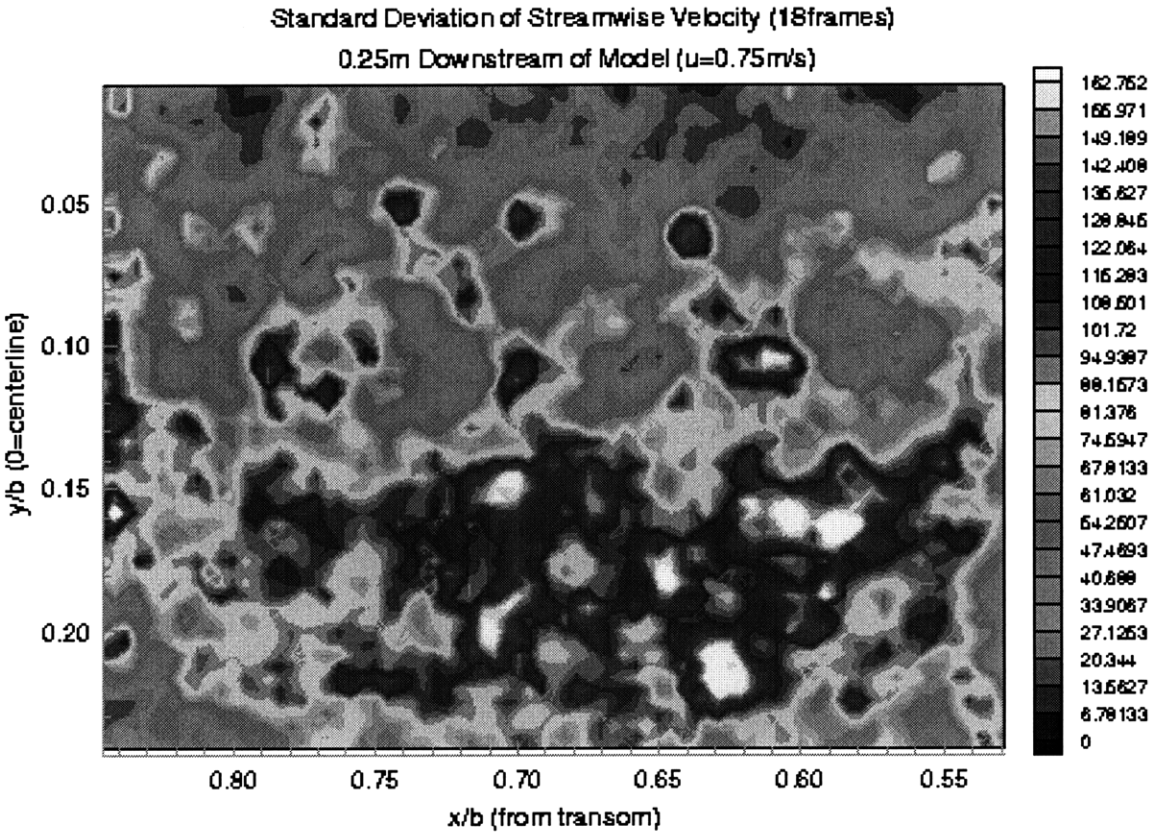

Figure 4-21: Standard Deviation from Mean Streamwise flow at 0.25m downstream

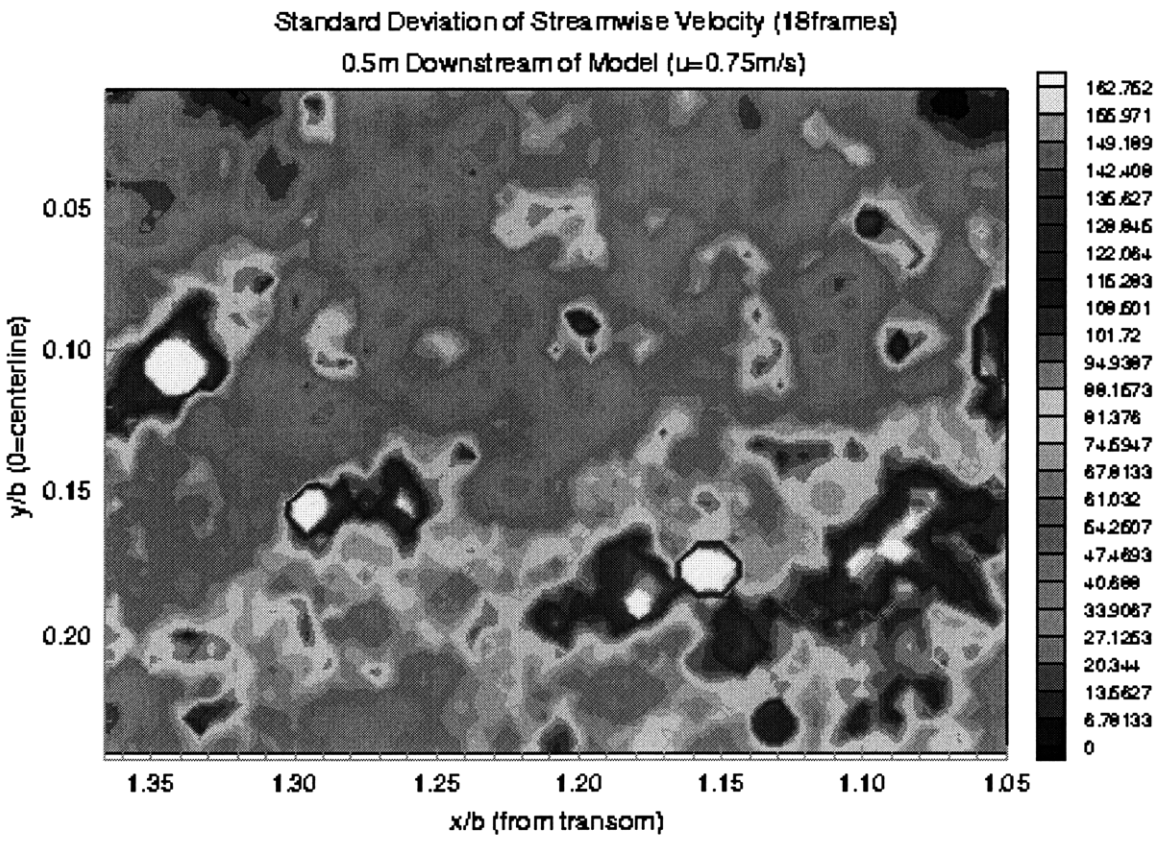

Figure 4-22: Standard Deviation from Mean Streamwise flow at 0.5m downstream

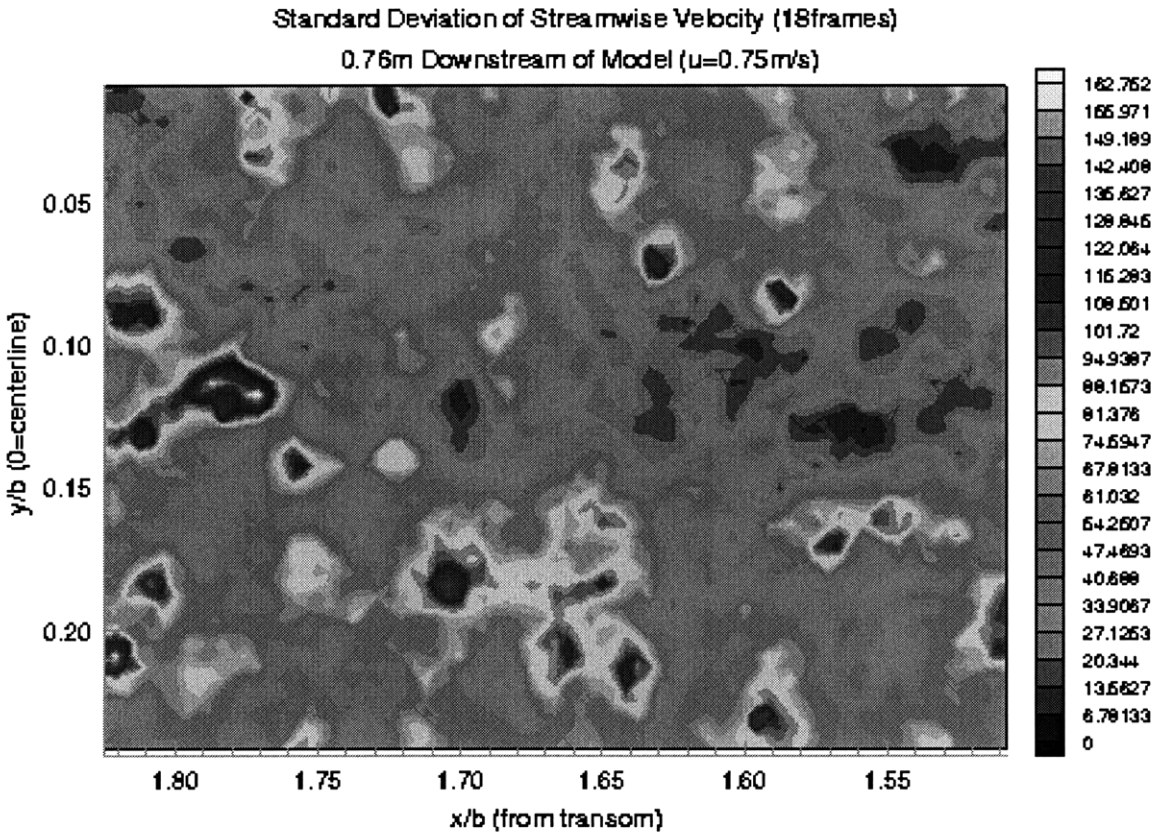

Figure 4-23: Standard Deviation from Mean Streamwise flow at 0.76m downstream

Chapter 5

Continued Visualization Experiments

The wake study described in Chapters 4 and 5 compared well with corresponding numerical simulations. Interest in targeting the causes of visualized wake manifestations, shifted focus in the 5514 towards the bow and free-surface interactions.

5.1 Photographs

The size of our towing facility, restricted the maximum achievable hull velocity and corresponding Reynolds and Froude Numbers. The hull was confined to run at speeds below 1.3m/s. A comparison of model to full-scale measurements is listed in table 5.1.

SHIP	v (m/s)	L (m)	d (m)	$\mathcal{R}e_L$	$\mathcal{R}e_d$	F_L	F_d
DDG51	15.5	141	9.7	$2.2\text{x}10^9$	$1.5\text{x}10^8$	0.417	1.59
5514	0.75	3.4	0.15	$2.5\text{x}10^6$	112500	0.129	0.617
5514	1.0	3.4	0.15	$3.4\text{x}10^6$	150000	0.173	0.825

Table 5.1: Relevant measurements for DDG51 and model 5514

Several experimental methods were proposed to investigate the free-surface shape near the bow of the 5514. These efforts were designed to validate numerical study

of the near-bow free-surface profile. Proposed methods included the use of whisker probes and grease pencils.

Whisker probes are thin, wire conductors used to make point measurements of run-up height based on the voltage conducted across the wire. While exhaustive implementation of these probes can accurately map a steady free-surface, they cannot be used very close to a body (such as the hull), or in the shadow of an overhang (such as the bow), nor can they resolve curling. A researcher at David Taylor supplemented whisker probe measurements by sitting on the bow of a model DDG-51 and tracing the free-surface connection with a pencil. These measurement techniques were time consuming, intrusive to the flow and low-resolution. To gain a broader representation of the bow wave with the capability to resolve intricacies such as curling and breaking, a digital camera was mounted to the towing carriage and photographs were taken at different speeds.

These photographs compared well with numerical representations at similar Froude Numbers [12]. A sample is shown in Figure 5-1, and a corresponding plot of a numerical comparison at Fr_d=1.14 is shown in Figure 5-2.

Both numerical and experimental models have difficulty achieving the velocities necessary to simulate full-scale flows. Complicated numerical methods must be employed to resolve the breaking and crashing wave formations, such as those at the bow of the DDG-51 pictured in Figure 5-3

5.2 Near-Bow Streak Videography

To pursue interest in below free-surface measurements, an investigation of near-bow flows with qualitative streak- videography was conducted. Desire to compare numerical simulations with empirical data of the flow near the sonar bulb of the 5514 prompted this first set of qualitative visualization experiments and subsequent attempts at quantitative methods.

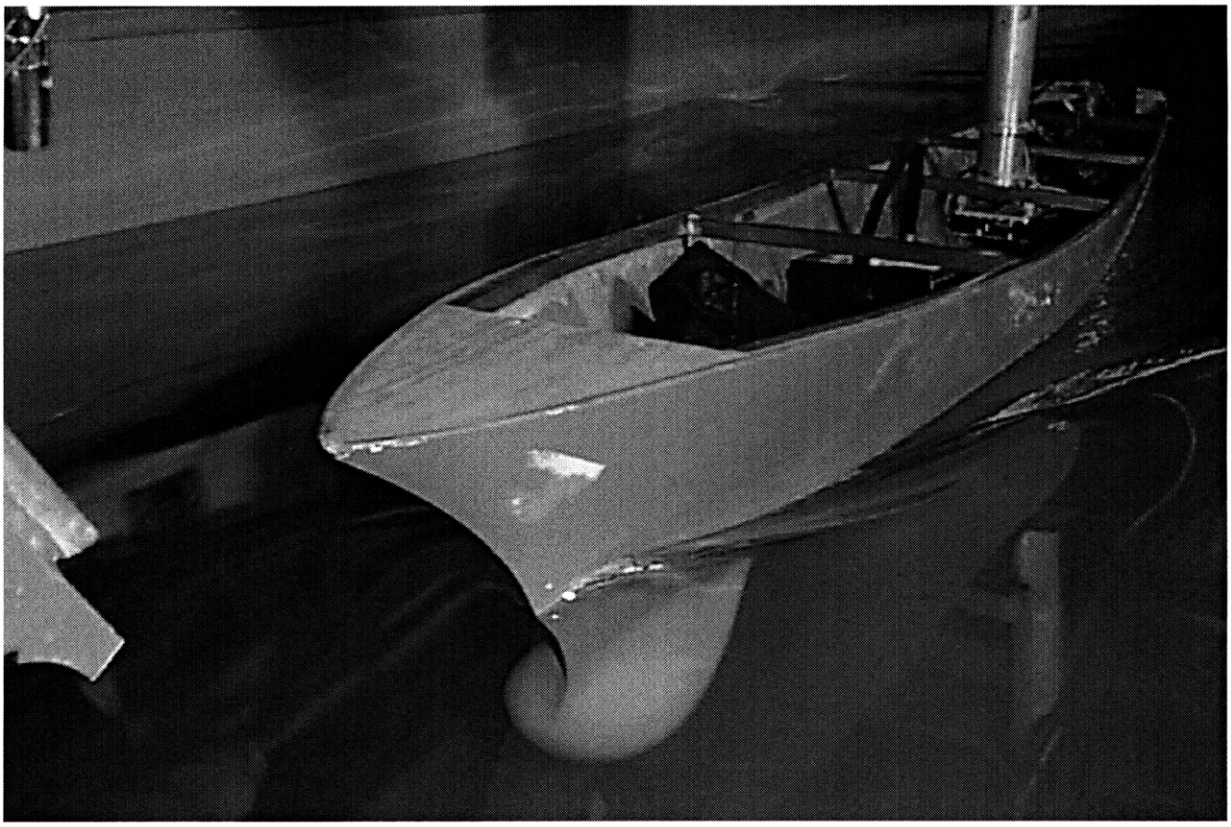

Figure 5-1: Photograph of the bow wave of the 5514 towed at 1.3m/s

5.2.1 Experimental set-up

The TI MC-1134 camera was secured in an underwater housing and mounted to the towing carriage aimed towards the bow, amid-ships. A red laser diode with line generating optics was mounted in an underwater housing aimed so that the laser plane was perpendicular to the free surface. (See Figure 5-4).

Approximately three meters of water was seeded with fluorescent particles and allowed to settle. The hull was then towed through the particle field with the camera focused on the laser plane. The images were recorded to the Sony LDV recorder mentioned in Chapter 3 and individual images were then selected and digitized for inclusion in this paper. Runs were conducted with the diode mounted in three different locations on the hull; (1) aimed at the middle of the bulb, (2) at the aft-section of the bulb and (3) just behind the bulb.

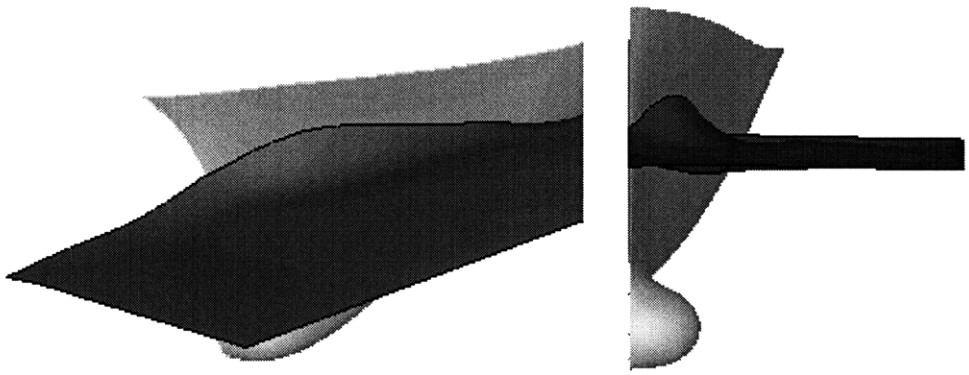

Figure 5-2: LES simulation of bow flow at similar Froude Number

5.2.2 Qualitative Results

Most of the tests were conducted at a tow speed of 0.75m/s. Very small circular structures were noted throughout the near-hull region. These structures seemed to congregate near the upper attachment point of the bulb to the hull. Because the camera and diode were moving through the water relatively fast compared to the capture rate of the camera and LDV, it was difficult to discern the three-dimensionality of these structures. Their existence, however, is evident in individual frames. In several sequences, it is possible to observe the evolution of a 3-D structure over a sequence of no more than 3 frames (0.09s or 7cm).

Figures 5-5 and 5-6 were taken from sequences filmed of the laser plane ~17cm from the static water-line bow at a tow-speed of 0.75m/s. The seed particles were allowed to settle after each run as well as following re-seeding and it is therefore believed that the circular structures visible in the still-images were formed by the moving model rather than the mixing particles. Sequencing began after steady forward motion had been achieved by the model. Figures 5-7 and 5-8 were taken at ~22cm from the bow at U=0.75m/s, and Figures 5-9 and 5-10 were taken 27cm from the bow. These pictures compare well with the LES simulations conducted by Leonard Imas [12] of near bow flow at similar Froude Number depicted in Figure 5-11.

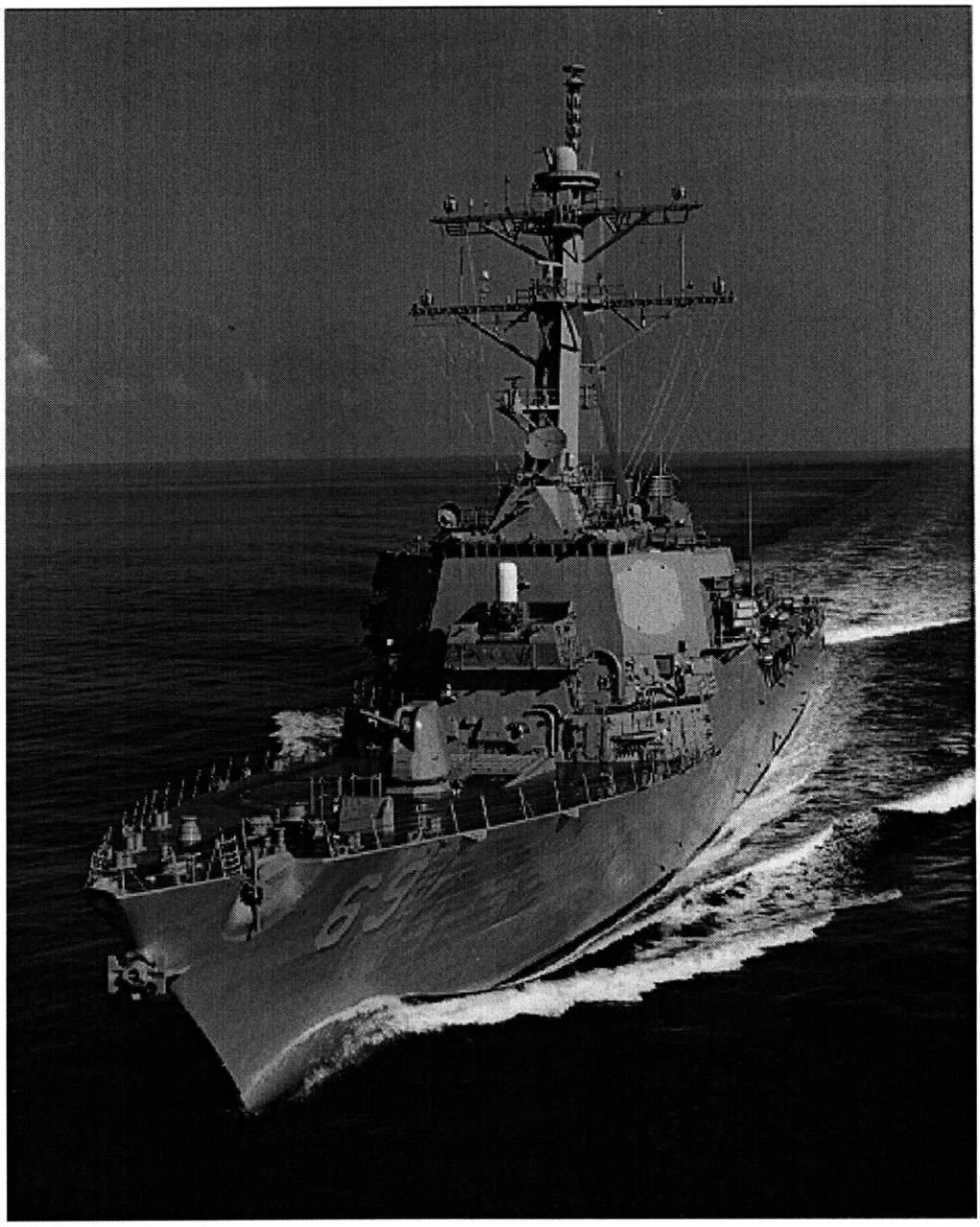

Figure 5-3: DDG-69 bow wave pictured at cruising speed from www.surfpac.navy.mil

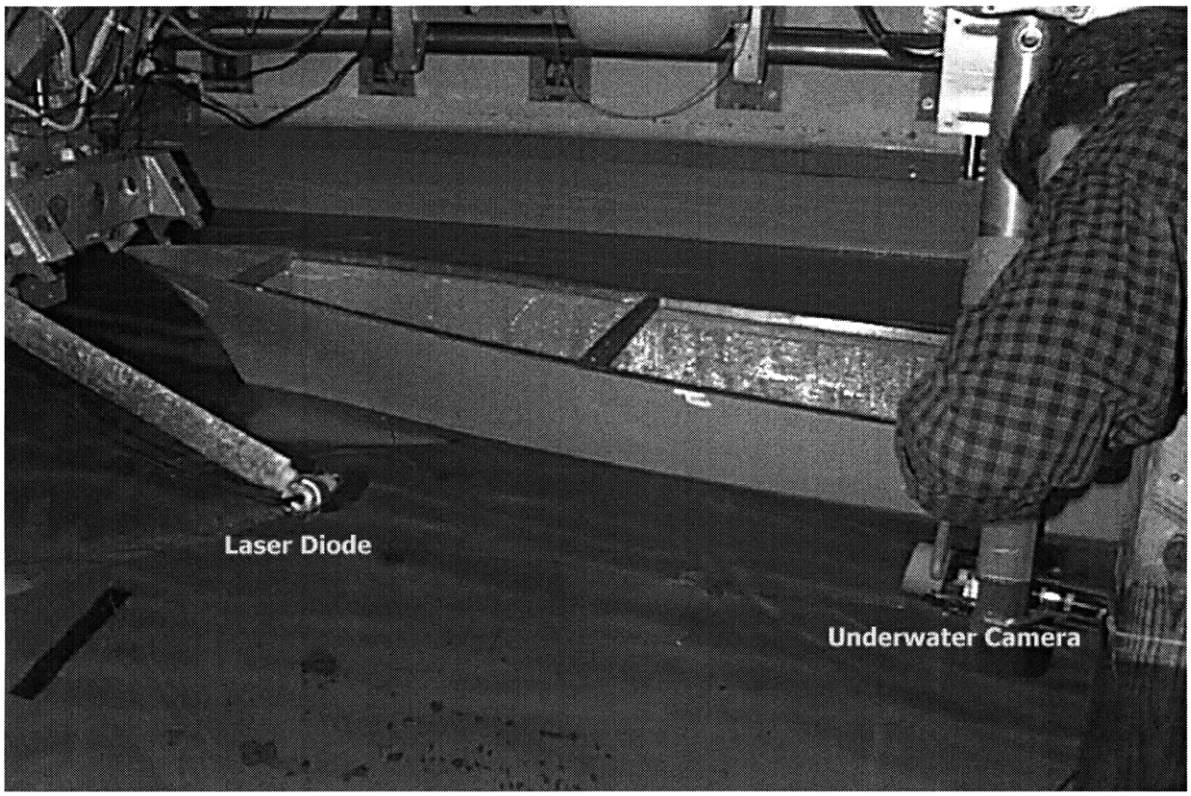

Figure 5-4: Laser Diode and underwater camera mounted to the 5514 for near-bow visualization

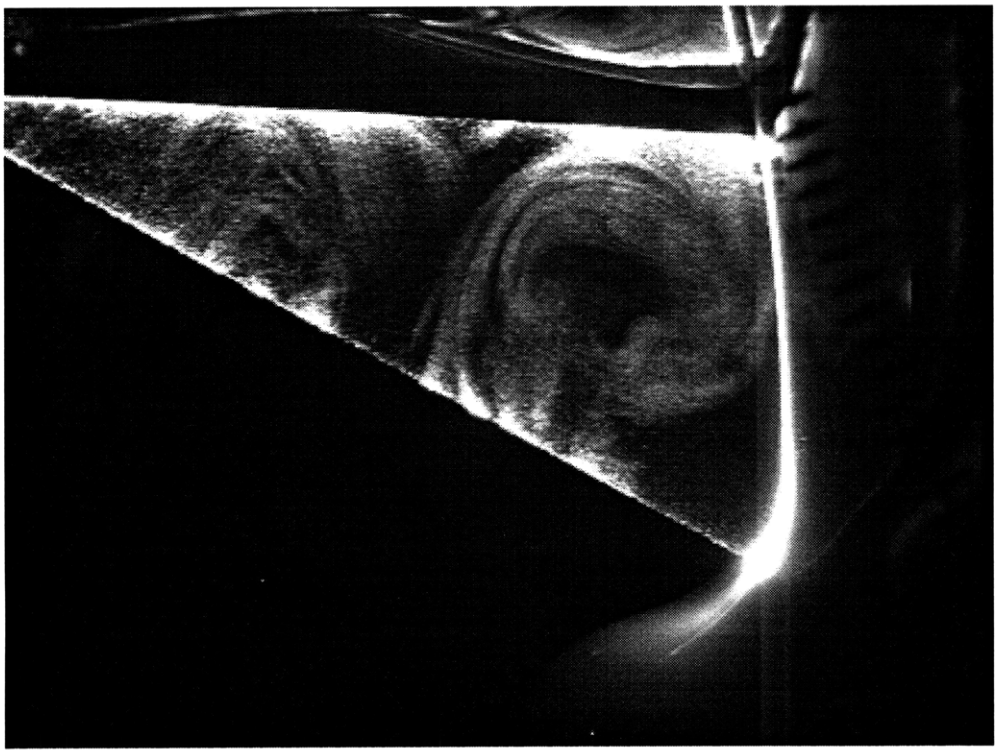

Figure 5-5: Near-bow streak videography at U=0.75m/s and x=17cm from waterline bow

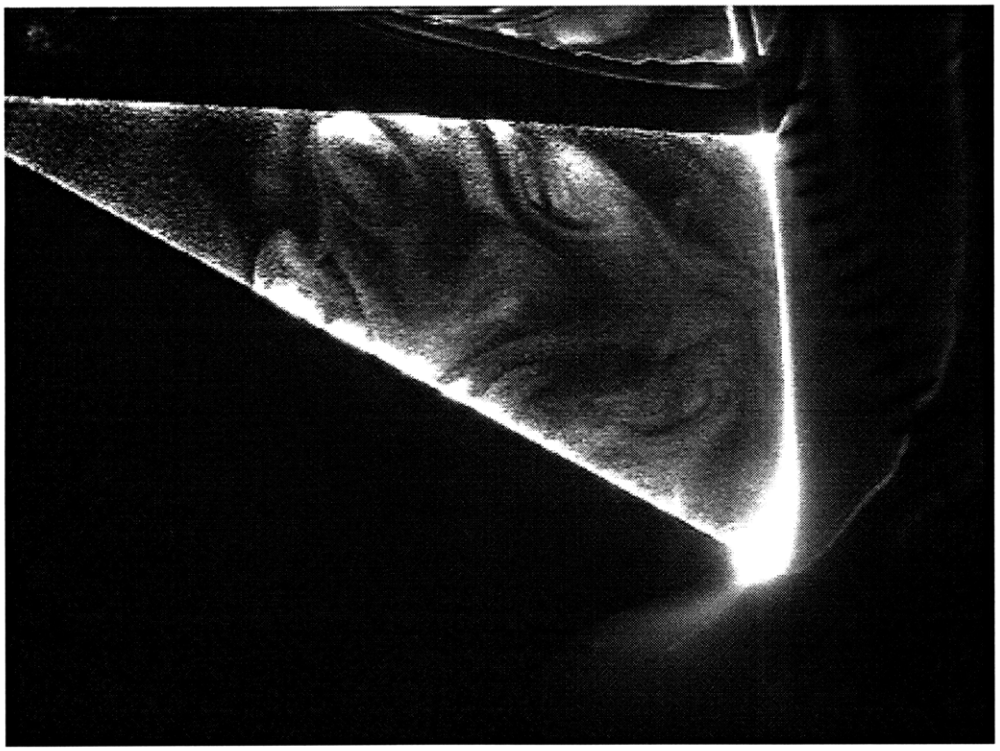

Figure 5-6: Near-bow streak videography at U=0.75m/s and x=17cm from waterline bow

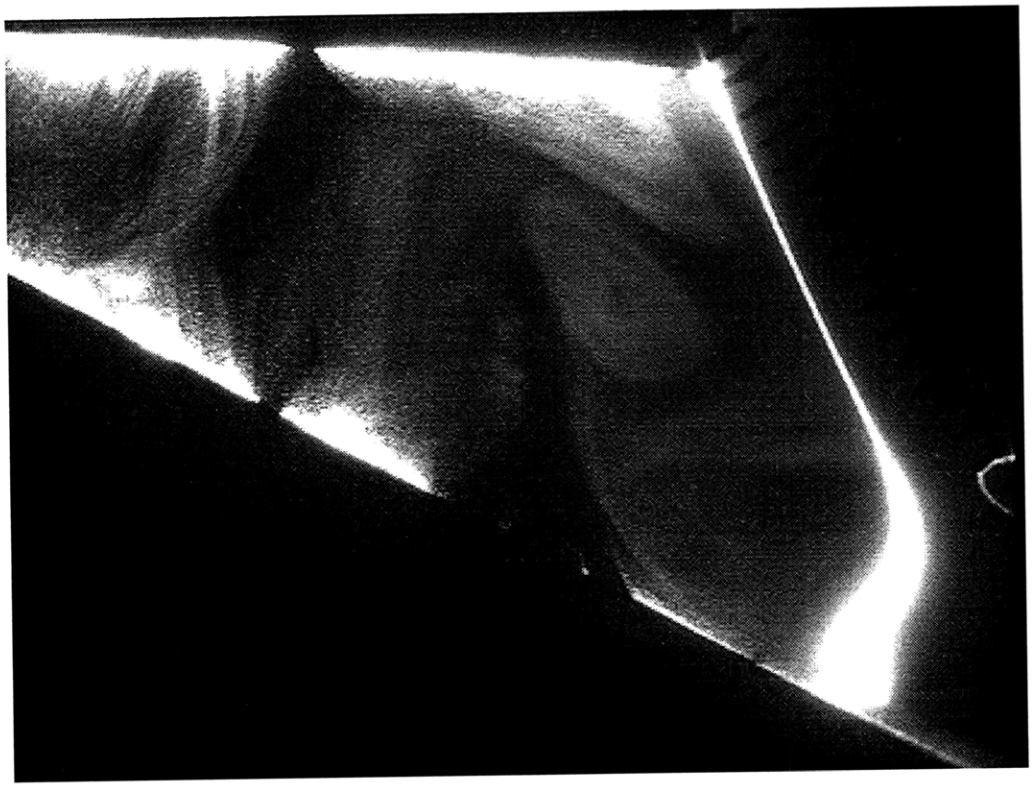

Figure 5-7: Near-bow streak videography at U=0.75m/s and x=22cm from waterline bow

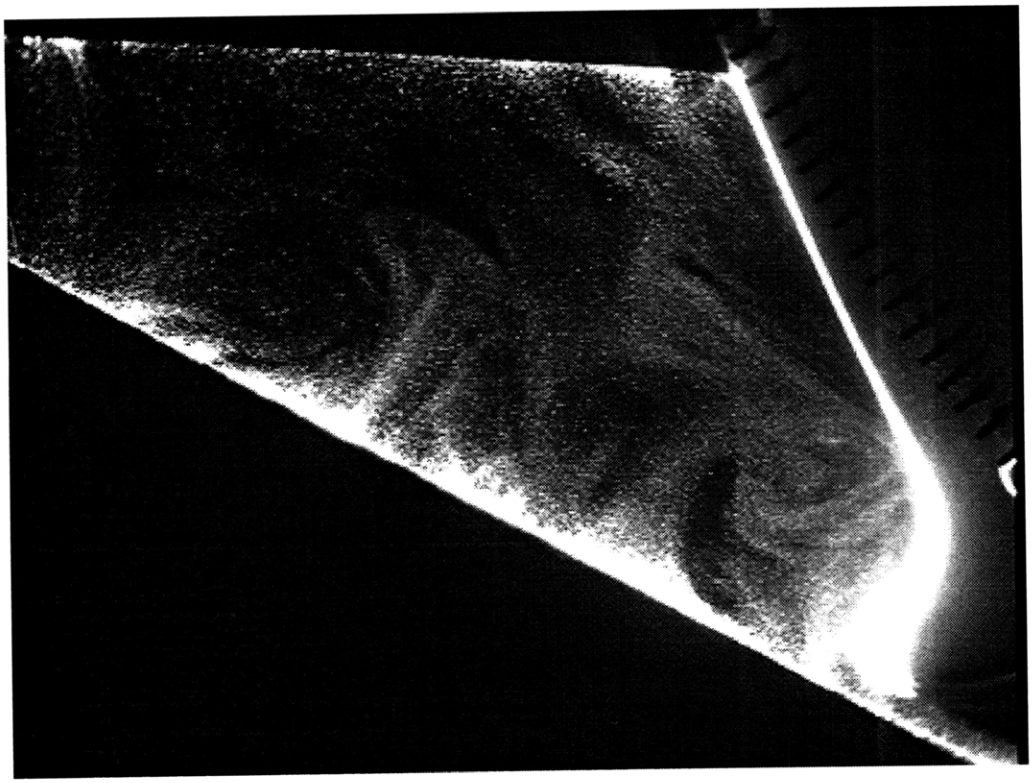

Figure 5-8: Near-bow streak videography at U=0.75m/s and x=22cm from waterline bow

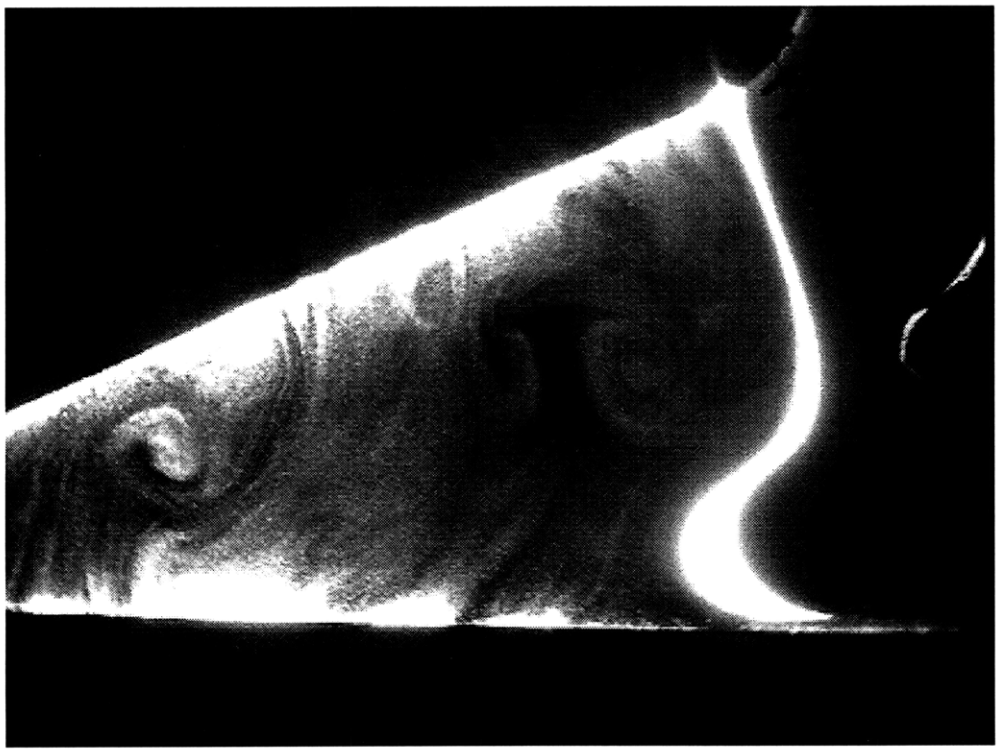

Figure 5-9: Near-bow streak videography at U=0.75m/s and x=27cm from waterline bow

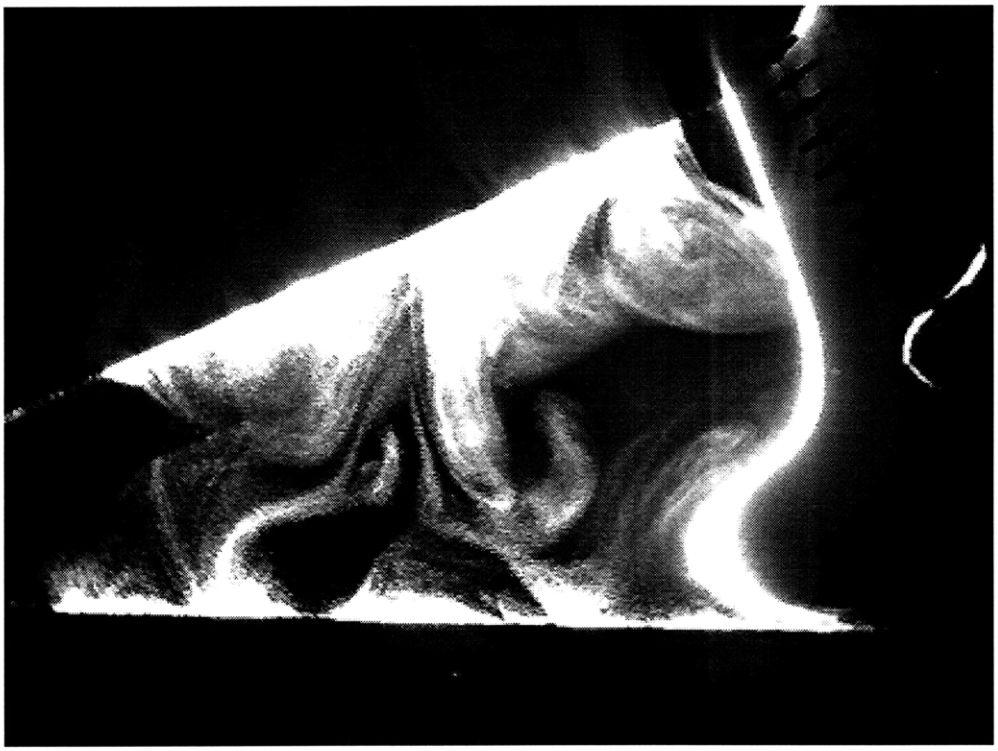

Figure 5-10: Near-bow streak videography at U=0.75m/s and x=17cm from waterline bow

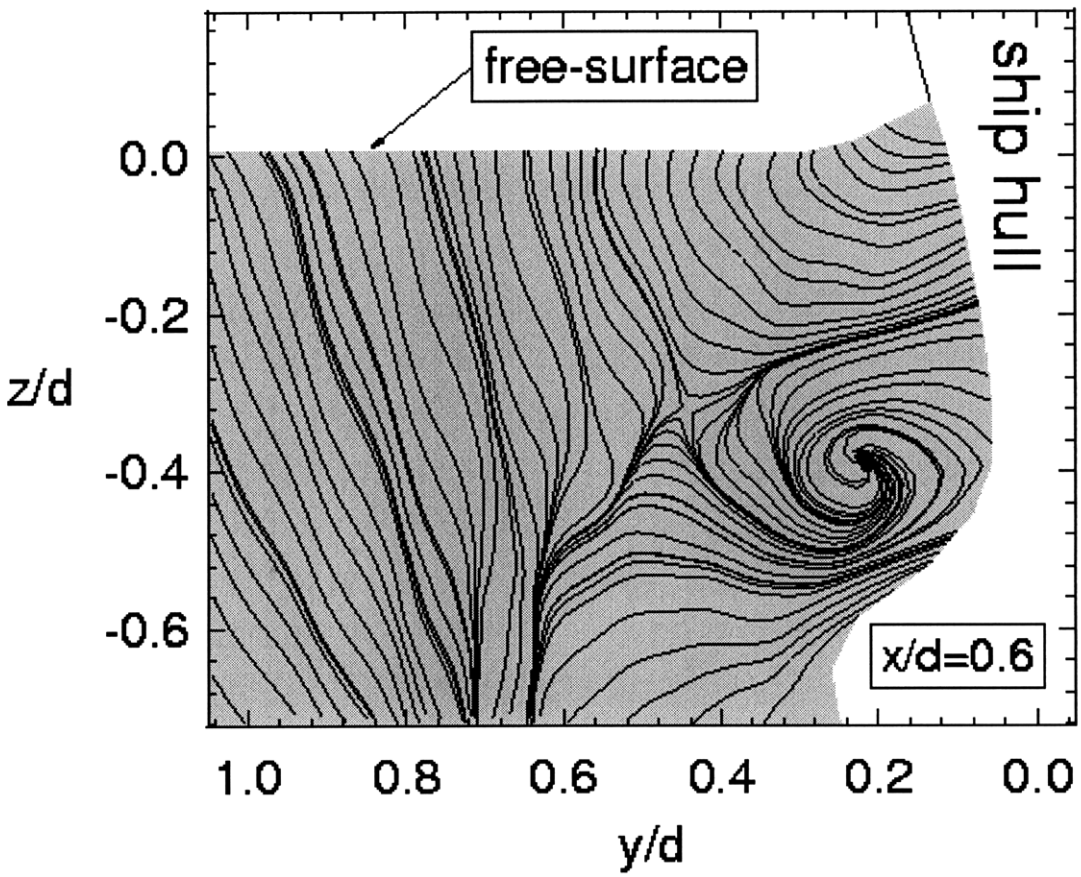

Figure 5-11: Streak lines from Numerical Simulation of flow in same region

5.3 Attempts at Near-Bow DPIV

To compliment qualitative visualization, several attempts at DPIV analysis of flows near the bow were also attempted. Because the PIV-400-30 cannot be mounted to the towing carriage and the diode laser used in the qualitative tests cannot be pulsed to create crisp particle images, the laser and camera had to be fixed while the 5514 came through the plane of the laser.

5.3.1 Experimental Set-up

The cylindrical optics system described in Section 4.2 was adapted to produce a vertical rather than horizontal DPIV laser plane. This was simply accomplished by changing the orientation of all the lenses (i.e. those lenses which were horizontal were made vertical and vise versa). The TI MC-1134 camera was secured on a vertical pillar underwater, aimed towards the bow of the 5514 and the laser plane (See Figure 5-12)

Light striking an water/air interface at an angle to the normal greater than θ_{crit} $\sim 42^o$, is totally internally reflected according to Snell's Law. This means that if the laser plane comes into the tank perfectly parallel to the free surface, there will be no doubling of intensity due to reflection, but that any disturbance to the slope of the free-surface will act like a mirror and cause streaking. This was indeed the case when the vertical laser plane was set up at the same height as the 5514. There was no problem with surface reflections when the water was still, but when the passing hull caused surface waves, each wave acted as an angled mirror and caused streaks of intensity gradients across the image plane.

This problem was solved by putting the optical bench on the floor and aiming the plane towards the surface. To eliminate reflections, the bench was angled such that the first point of contact of the laser plane and the surface was as close as possible to the waterline of the model at the bow. At this angle, no streaks were produced while the ship was in the plane, thereby minimizing correlation errors in the DPIV analysis.

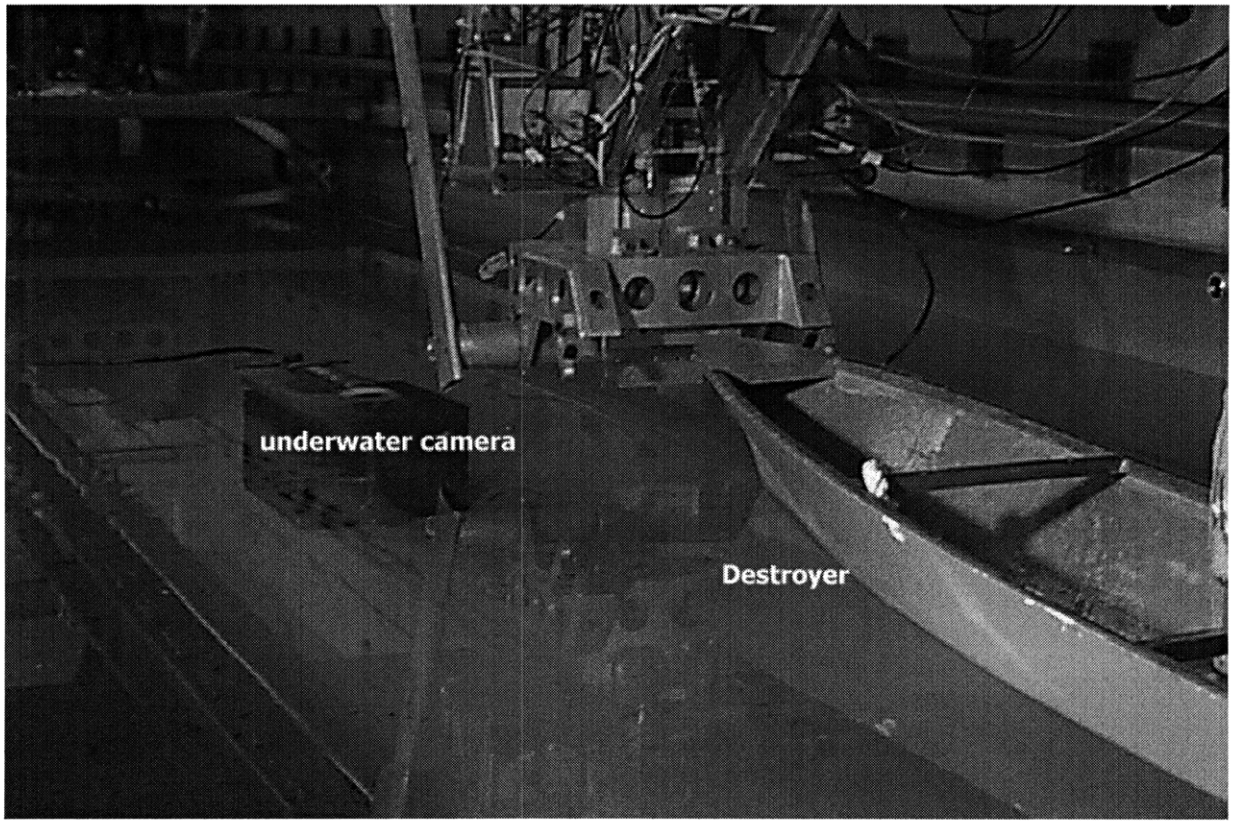

Figure 5-12: Underwater camera aimed at oncoming bow of 5514 for near-bow visualization

5.3.2 Reflection Problems

Unfortunately, however, the free-surface was not the only source of reflections in the near-bow DPIV plane. More severe reflections were caused by the hull itself. These reflections were subtle in the low-power laser diode experiments, but with the higher energy pulsed laser, they were so severe that CCD blooming occurred destroying the video signal.

At this point, instead of imaging the near-bow region, the experimental focus returned to the wake, where there were no complicating hull or surface reflections. With the same set-up, image sequences were taken of the image plane after the passing of the ship. Again, these were half-wake images with the camera positioned just to the side of the centerline of the model, centered at $\sim$0.2b.

5.4 DPIV of Wake Cross-sections

Although there are substantial through-plane particle motions in this set-up, these motions should be limited to the near hull region. The time difference between images in an image pair was reduced to 0.006s in hopes of capturing sequential images of the same particle field. The results were remarkably good as displacement data from DPIV analysis corresponds to areas where motion could be qualitatively recognized on playback of the video sequence.

Little activity was qualitatively noted in the wake for several frames after the complete passing of the ship. The most significant motion could be seen in the region approximately through which the sonar bulb had passed as well as in the viscidity of maximum beam. This is confirmed in the DPIV plots.

5.5 Conclusions

Qualitative near-bow studies compared remarkably well with numeric and theoretic predictions. Several prohibitive factors for near-bow qualitative studies have been identified and eliminated. Further select adaptations to the apparatus and subject will fascillitate detailed, quantitative visualization close to the bow of the 5514.

Further improvements in the wake study will come with further improvements in the experimental apparatus. To come closer to full-scale simulaitons, it may be advantageous to build a simple model of the bow which might be safetly towed at higher speeds. This section might be made of a transparent material such as plexiglass so that a laser might be mounted within the section removing the reflection problems caused by the hull.

Chapter 6

Modifications for Visualization on Live Fish

Fish of various shapes and sizes have the ability to control their motions in a fluid environment. This feature is difficult to achieve in man-made, marine vehicles and has motivated much research into the mechanisms of fish swimming over the past century. Fish accelerate, maneuver and hover using a wide range of complex motions, which include both fin and body movement. As with the ship wake study, theoretical, mechanical and numerical simulations of these motions benefit from comparisons with experiments on live fish. Logistical and biological constraints, however, complicate the use of DPIV methods of flow visualization. To facilitate quantitative investigation of the flow around live fish, the traditional DPIV system was modified as follows.

6.1 Problems with Old System

The DPIV system in the Ocean Engineering Towing Tank includes a high powered visible laser and fluorescent dyed-injected particles. It was designed for implementation on solid bodies towed through the laser and image planes. Attempts to use this system on live danios, seahorses and knifefish were completed with varying degrees of success and several common problems. These complications stemmed from the contrasts between live fish and typical DPIV subjects.

A common problem was that it was impossible to incite the animals to swim "naturally" through the illuminated plane and the field of view of the camera. The fish became quite agitated by the bright laser light and further spoked by attempts to bait or prod it into the image plane. Attempts to restrict the motion of the fish to the image window with walls or gates, disrupted the fluid flow and allowing the fish to swim on its own while filming for prolonged periods wasted costly, single-use recording media.

6.2 Modified System

A new system was built to minimize these complications and obtain fish-friendly quantitative flow profiles. The new set-up includes the following features, the highlights of which will be discussed subsequent sections:

- An Infra-red laser
- Lycopodium spores as particles
- Mu-Tech MV-1000 video digitizing board with MV-1200 daughter card
- NPC 200MHz Pentium Computer with Number 9 video card
- Texas Instruments MC-1134MOD high-resolution digital camera
- Berkeley Nucleonics 2-channel pulse generator timing box

6.2.1 Infra-Red Laser

Because the fish had been wary of the bright argon laser beam in earlier DPIV tests, it was replaced in the new apparatus with a lower intensity, invisible, Infra-red, diode laser laser. Diode lasers are easily pulsed with circuitry rather than mechanical shutters and the near IR beam is invisible to the human and fish eyes, but detectable by CCD arrays. In effect, a plane in the water could be imaged without the detection by the fish.

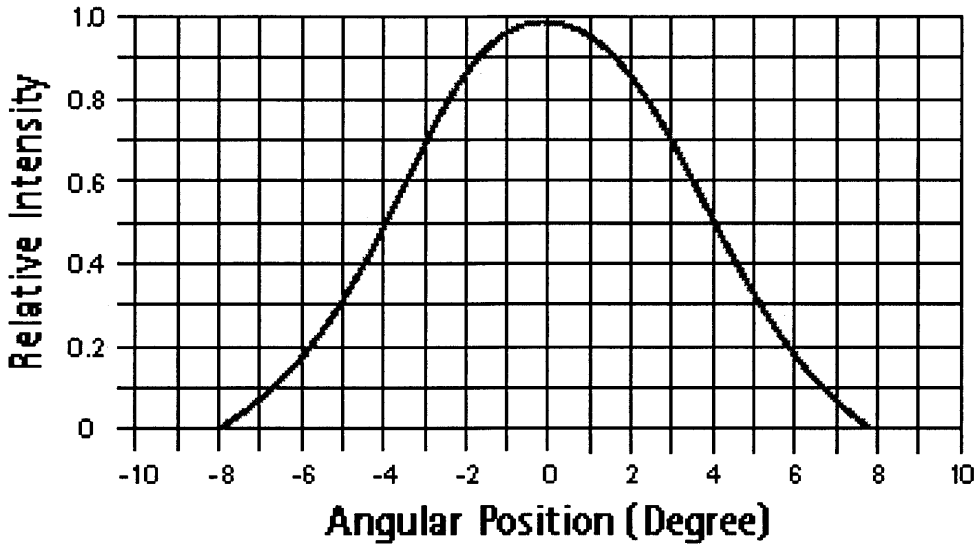

Figure 6-1: Typical Gaussian distribution of Intensity in laser plane

A 40mW, λ=808nm, diode laser with line generating optics to produce a 40^o fan angle was purchased from Power Technology, Inc. It was powered by a 12V source and included TTL input for modulation (active low). This laser supplied sufficient illumination for small tanks, but the fan angle proved too small and the diode was difficult to tune. Furthermore, the line generating optics maintain the Gaussian illumination profile of the beam which dropped off in intensity at the edges of the plane. See Figure 3.

6.2.2 Lycopodium spores

A search was conducted for non-toxic reflecting (rather than fluorescent) particles of appropriate size. Despite possibilities in microscopy, spectroscopy and plastics, lycopodium (mold) spores seemed best suited for this application. These particles come in dry form and were ordered from Ward's Scientific. They were inexpensive and expand to 60microns in diameter when soaked in water. Because the particles essentially became a closed volume of water when allowed to soak, they were nearly neutrally buoyant. They reflected Infra-Red well, and the contrast of particles in the laser plane was enhanced with a Kodak wratten gel-filter specified to pass the wavelength of the laser, but to reflect all other wavelengths.

6.2.3 Berkeley Nucleonics Pulse Generator

To pulse the diode laser with respect to the V-Drive from the camera, (like the gas lasers used in the ship model tests), a 2-channel pulse generator was purchased from Berkeley Nucleonics. The pulse generator can be programmed to output pulses of user defined length and strength at specified time intervals from an input signal. To alternate the delay from the beginning of a frame to the pulse of the laser and produce a frame-pair with minimal time difference (See Figure 3-7), a circuit was built to divide the V-Drive by 2 and pulse Channel 1 just before of 33ms (frame length) and channel 2 just after 33ms. Because the 2 channels had to drive the same input on the laser, a summing circuit was also built.

6.3 Preliminary Tests

Initial tests were conducted to prove that the CCD array could indeed image the near Infra-Red laser plane and that the plane was indeed invisible to the fish. Because the plane is invisible to experimenters and fish alike, a IR detecting card was used to align the plane.

It is particularly important to be careful when aligning IR lasers because they are as dangerous as visible lasers, although invisible.

The experimental set-up is pictured in Figure 6-2. Six grams of dry lycopodium spores were shaken with water in a small plastic container until the spores were saturated and held in suspension. A 20 gallon experimental fish tank was filled with approximately four inches of water. A rectangular glass pane, (nearly the same size as the fish tank) was elevated 0.5 inches from the bottom of the tank so that the fish was forced to swim above the plastic tank seal which is not transparent to the laser plane. In this arrangement the fish was confined to swim in a verticle space of approximately 3.5 inches and was allowed to swim freely throughout the experimental tank. The image area was approximately 4 inches by 3 inches in the center of the tank with at least three inches from any side of the image to any tank wall.

Unfortunately, the 40mW laser did not have sufficient power to modulate the

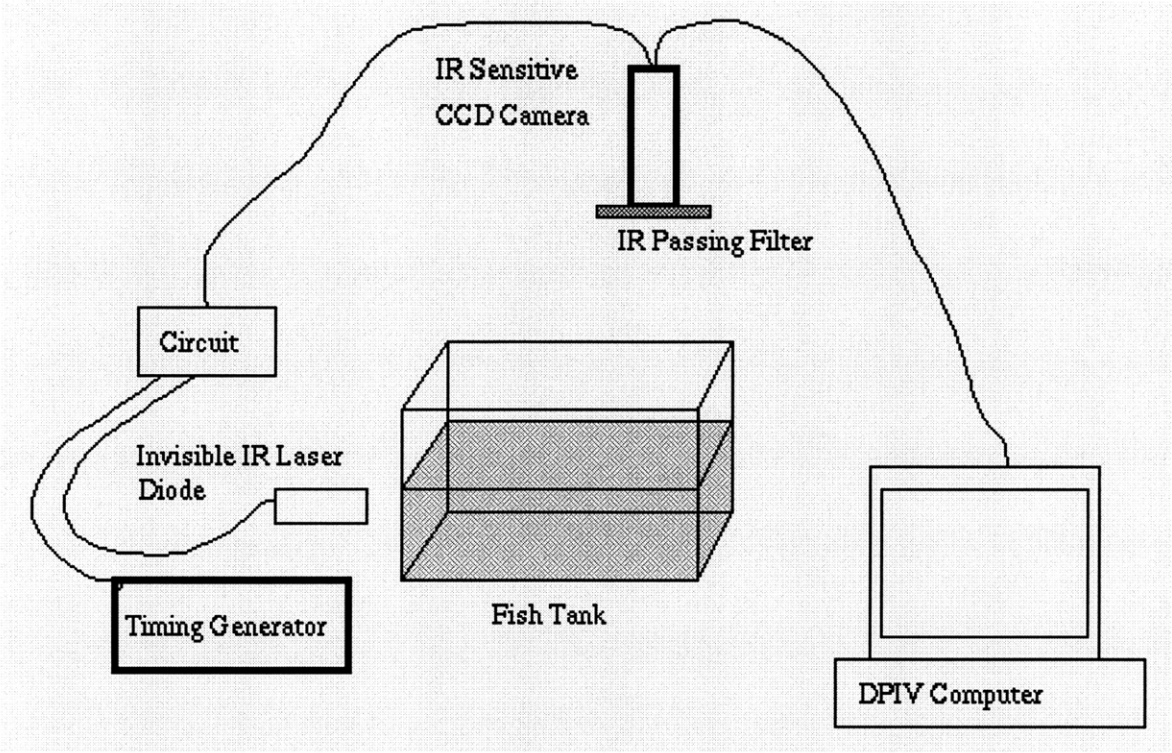

Figure 6-2: Experimental set-up for IR fish flow visualization

plane for DPIV experiments. With the laser turned on continuously, however, several sequences of qualitative streak visualization were obtained. One such sequence of the tail of a danio just out of a 90^o turn is shown in Figures 6-3 and 6-5.

6.4 New Diode Laser

Because the 40mW laser was not sufficiently powerful to illuminate the plane while pulsing, a new 2W IR diode laser was ordered from Lasiris. In addition to the power enhancements, this laser is also outfitted with line generating optics to produce a 60^o fan angle plane of illumination. These optics are designed to deliver equal intensity across the full width of the plane (rather than the Gaussian profile of the 40mW laser). The laser will also be pulsed with the BNC pulse generator and will hopefully fascillitate quantitative DPIV studies of the flow around fish.

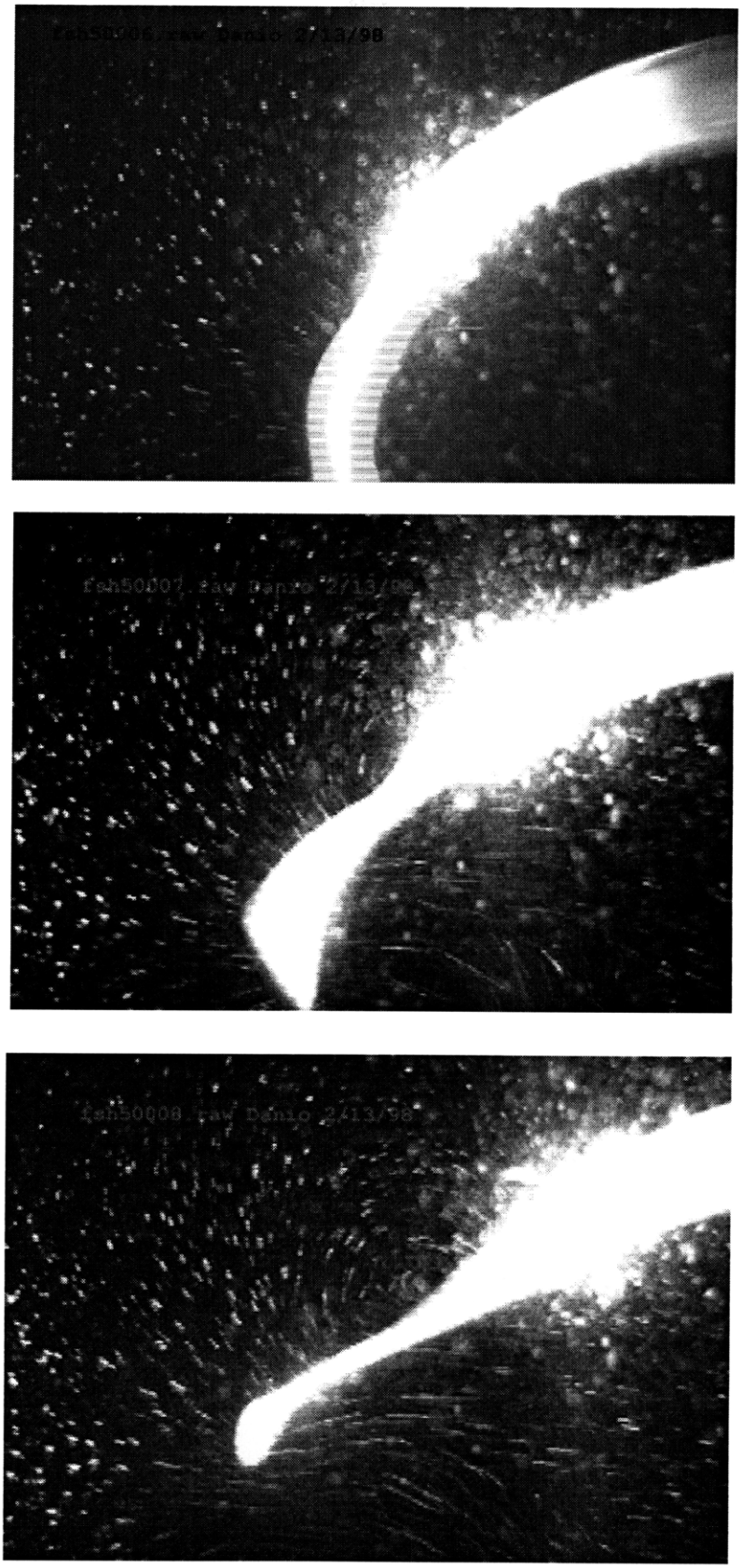

Figure 6-3: Three images in sequence of danio turning

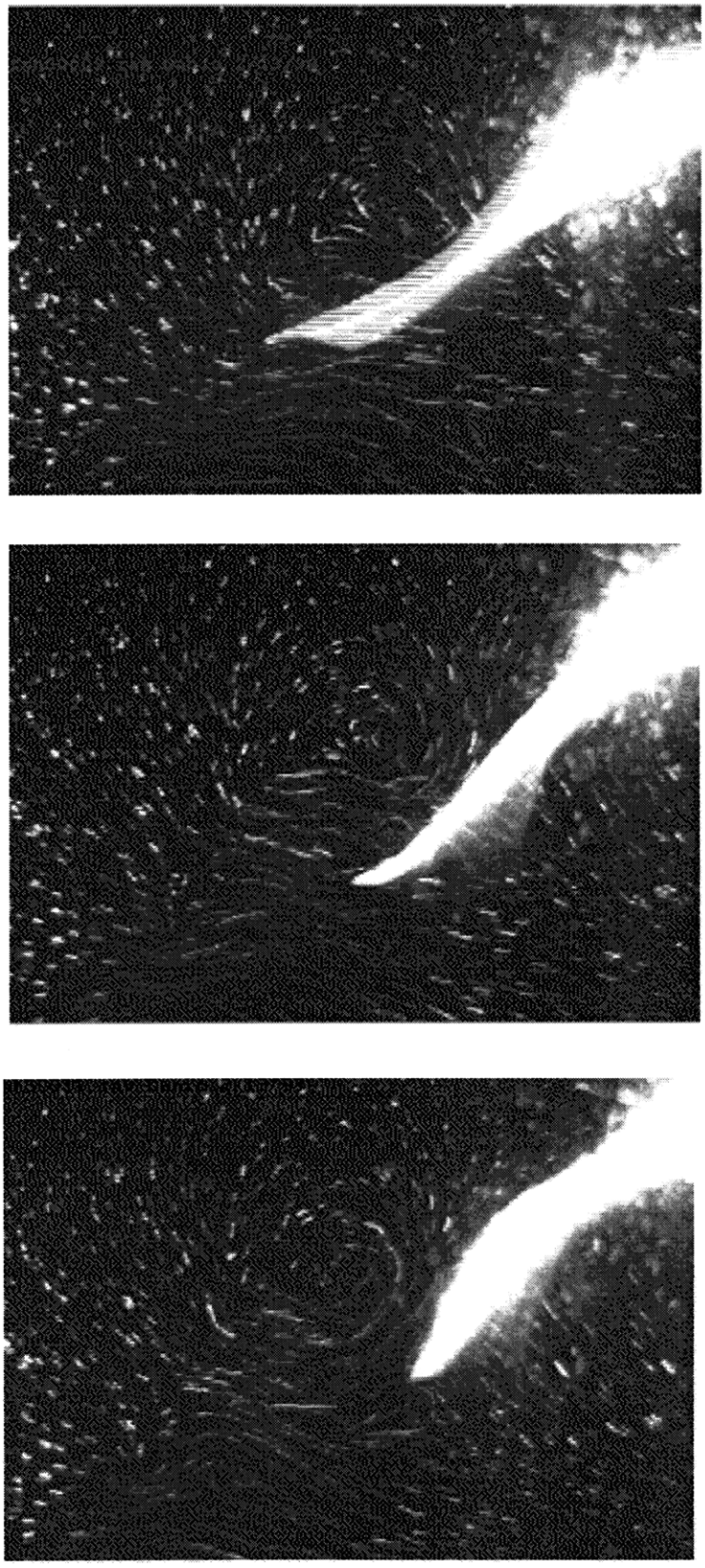

Figure 6-4: Three images in sequence of danio just after turn

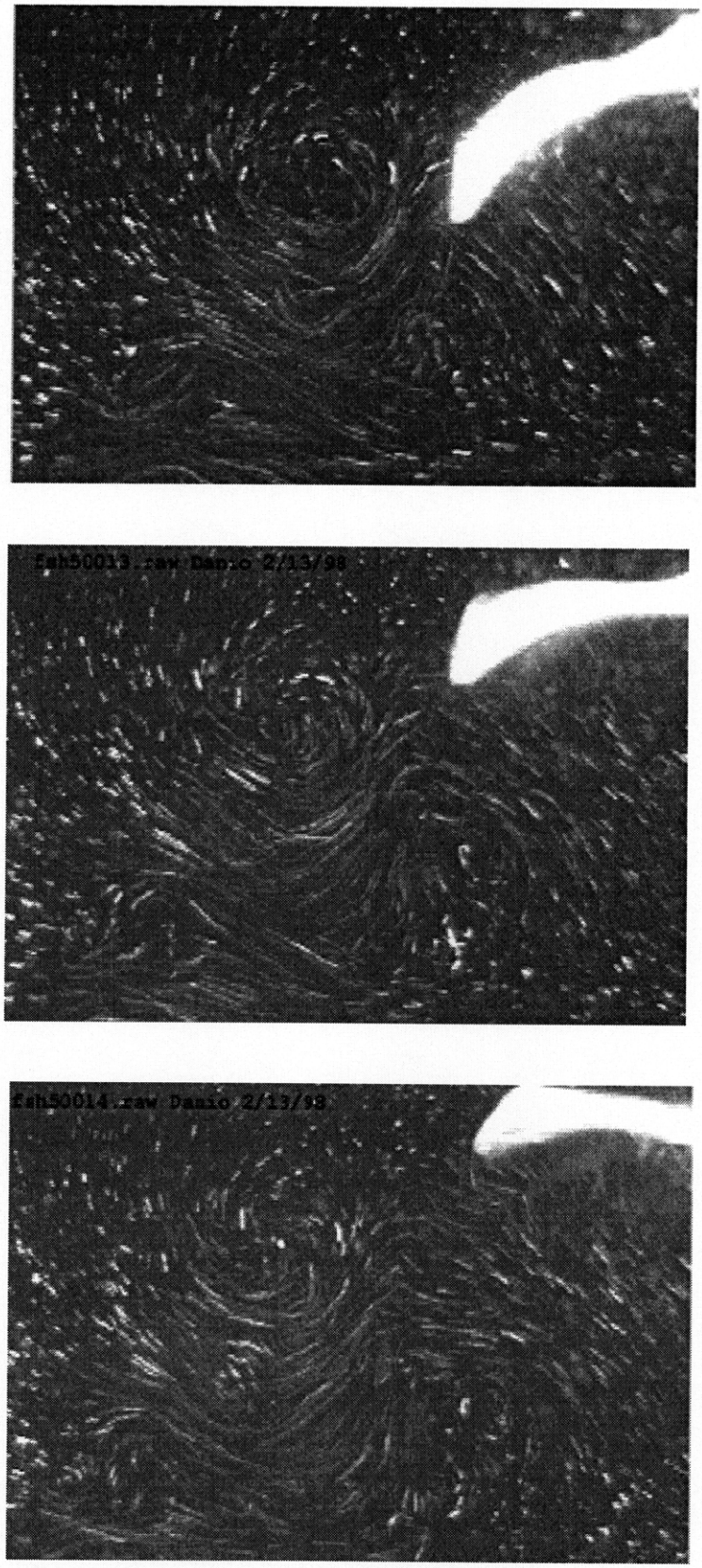

Figure 6-5: Next three images in sequence of danio

6.5 Recommendations

To further enhance the fish-friendly DPIV set-up, plans are in action to (1) build a translating camera/laser stand which can follow the fish, (2) re-write the driver software for the Mu-Tech board to take advantage of the full 1134x486 CCD resolution and (3) make the DPIV software modifiable to block out areas in the images and allow calculations closer to moving bodies in the images.

By securing the laser at a fixed distance equal to the focal length of the camera lens and mounting the laser and camera on a translational stand over the experimental fish tank, it will be possible to follow the fish in its maneuvers around the tank. This translational stage will have to have memory or knowledge of its position so that the movement of the stage can be removed from the particle motion during processing.

The Mu-Tech driver software is written in C++ and easily modified according to the Software Developers manual. According to the service staff at Mu-Tech, it is possible to modify the driver to accept 1134x486 images from the camera via the pixel clock out, v-drive and h-drive. In addition, the technicians at Mu-Tech claim that it is possible to make the sequencing application a re-circulating buffer. That is, rather than initiating the capture of a sequence at the beginning (before the action has taken place) make the memory buffer recirculating so that when an interesting event takes place, the experimenter can then go back and store it without wasting recording media and opportunities.

Finally, as there is much interest in fish maneuvering, it would be advantageous to have the ability to do DPIV as close as possible to the body of the fish. For processing images with the fish included with the particle field, one should be able to indicate where the fish is in Image 1 and Image 2 so that the algorithm does not look there for correlation of particle images. In order to make these specifications, DPIV source code will have to be available or written and modified.

These recommendations are would significantly enhance the performance of the current system. Thy are however, unnecessary for fully functional and beneficial use of the system. Initial attempts should focus on implementation of the existing apparatus

for the understanding of fluid flow around swimming fish and for the comparison and validation of numerical and mechanical models. These future modification would make an interesting project, but are not needed for fluid dynamic study.

Bibliography

[1] R. J. Adrian. Multi-point optical measurements of simultaneous vectors in unsteady flow—a review. *Int. J. Heat Fluid Flow*, 7:127–145, 1986.

[2] R. J. Adrian. Dynamic ranges of velocity and spatial resolution of particle image velocimetry. *Measurement Science and Technology*, 8:1393–1398, 1997.

[3] Ronald J. Adrian. Particle-imaging techniques for experimental fluid mechanics. *Annual Review of Fluid Mechanics*, 23:262–304, 1991.

[4] J.M. Anderson. *Vorticity Control for Efficient Propulsion.* PhD thesis, MIT, 1996.

[5] D. Barrett. The design of a flexible hull undersea vehicle propelled by an oscillating foil. Master's thesis, MIT, 1994.

[6] D. Barrett. *Propulsive Efficiency of a Flexible Hull Underwater Vehicle.* PhD thesis, MIT, 1996.

[7] James Taylor Czarnowski. Exploring the possibilitiy of placing traditional marine vessels under oscillationg foil propulsion. Master's thesis, MIT, 1997.

[8] Ronald R. Dong, J. Katz, and T. Huang. On the strtucture of bow waves on a ship model. *Journal of Fluid Mechanics*, 346:77–115, 1997.

[9] Joseph W. Goodman. *Introduction to Fourier Optics.* McGraw-Hill, New York, NY, 1968.

[10] J. Gray. Studies in animal locomotion vi. the propulsive powers of the dolphin. *J. Exp. Biology*, 7:192–199, 1936.

[11] H. Huang, D Dabiri, and M. Gharib. On errors of digital particle image velocimetry. *Measurement Science and Technology*, 8:1427–1440, 1997.

[12] Leonard Imas. *Hydrodynamics Involving a Free-Surface Body Juncture.* PhD thesis, MIT, 1998.

[13] A. K. Jain. *Fundamentals of Digital Image Processing.* Prentice-Hall, Engelwood Cliffs, NJ, 1989.

[14] Sean McKenna. Experimental investigation of low reynolds number ship wakes. Technical report, MIT, 1995.

[15] Sean McKenna. The influence of surface films on interfacial flow dynamics. Master's thesis, MIT/WHOI, 1997.

[16] A. Melling. Tracer particles and seeding for particle image velocimetry. *Measurement Science and Technology*, 8:1406–1416, 1997.

[17] Hideaki Miyata. Non-linear ship waves. *Advances in Applied Mechanics*, 24:215–288, 1984.

[18] E. M. Pogozelski, J. Katz, and T.T. Huang. The flow structure around a surface piercing strut. *Physics of Fluids*, 9:1387–1399, 1997.

[19] A. H. Techet. Vortical patterns behind tapered cylinders. Master's thesis, MIT, 1998.

[20] J. Westerweel. Fundamentals of digital particle image velocimetry. *Measurement Science and Technology*, 8:1379–1392, 1997.

[21] C. E. Willert. *The Interaction of Modulated Vortex pairs with a Free Surface.* PhD thesis, University of California, San Diego, 1992.

[22] C. E. Willert and M. Gharib. Digital particle image velocimetry. *Experiments in Fluids*, 10:181–193, 1991.

[23] Chiong C. Zhang. *Turblent Free-Surface Wakes Behind Towed Models–Experimental Measurements, Numerical Simulations and Stability Analsis.* PhD thesis, MIT, 1996.